Studies of Ablation Complications During the Treatment of Atrial Fibrillation

A Thesis
SUBMITTED TO THE FACULTY OF
UNIVERSITY OF MINNESOTA
BY

Stephen Quallich

IN PARTIAL FULFILLMENT OF THE REQUIREMENTS
FOR THE DEGREE OF
DOCTOR OF PHILOSOPHY

Paul Anthony Iaizzo

September 2015

Acknowledgements

There are a myriad of individuals I need to thank for helping to make this work possible. I have been privileged to work and collaborate with a number of inspiration colleagues. My sincere thanks to the following graduate students: Ryan Goff, Julianne Spencer, Steve Howard, Brian Howard, Lars Mattison, Megan Schmidt, Chris Rolfes, Mike Bateman, Mark Benscoter, and Ashish Singal. Even during the early mornings or late nights your positive attitudes and thoughtful feedback made my graduate experience enjoyable and an exceptional environment to be a part of. To the lab staff: Monica Mahre, Tinen Isles, Gary Williams, and Charles Soule thank you also for fostering this environment across graduate student generations and supporting the lab with your unique specialties. Furthermore, I need to thank the volunteers for working tirelessly in the background, which allows for the lab to run smoothly, especially Kevin Kriege, Dannah Reiter, and Mike Van Heel.

Paul Iaizzo you are truly a remarkable individual and mentor. The effort you expend teaching and inspiring innovative research is unparalleled. I value all of the experiences and guidance throughout the past 4 years you have imparted to me. Your passion and creativity rub off on everyone who works and interacts with you. The world needs more mentors with your energy to inspire.

Dedication

I dedicate this work to my family for providing their unwavering support in my scholastic and personal endeavors and always encouraging me to strive through each and every challenge. Thank you for instilling an intense curiosity in me so that I understood how and why things function along with a desire to help others.

Table of Contents

List of Tables

List of Figures

Section 1 Implications of Transseptal Punctures

The focus of this section of my thesis is assessing the biomechanical properties of the interatrial septum as it relates to transseptal punctures and navigation of catheters for ablation procedures. During a transseptal puncture procedure, incorrect device positioning may lead to serious complications, such as perforation of the aorta and/or cardiac tamponade. It is important to also consider that as a catheter crosses the septum there is a strain imposed on the tissue, and as such procedures continue, catheters are extensively manipulated to reach the desired anatomies, such as the mitral isthmus or pulmonary vein ostia: ultimately this may tear or shear the septal tissues. Noteworthy, during typical radiofrequency ablative procedures, with singular catheter tip electrodes, this issue is exacerbated due to the number of lesions necessary to electrically isolate the aberrant electrical signals. Furthermore, ablations targeting the right pulmonary vein antrum require an acute angle inflicting a substantial moment on the fossa ovalis, often eliciting septal damage. Even during catheter manipulation for more accessible anatomical structures, the fossa ovalis may undergoes extreme stresses and as a result iatrogenic atrial septal defects are induced. Importantly, these procedurally induced defects thus create a sufficient opening between the right and left heart, which can allow for the mixing of oxygenated and deoxygenated blood amongst other negative effects. With the direct visualization of this phenomenon using the Visible Heart® methodologies, one is able to directly observe their creations during radiofrequency and/or cryothermal ablation therapeutic procedures.

In order to better understand the responses of the septum to the transseptal puncture procedures and/or manipulation associated with subsequent catheter navigation, we aimed to identify the force limits that may be imposed on the septum so not to induce significant iatrogenic atrial septal defects. There exists tremendous growth in the field of ablative therapies for treating atrial fibrillation, with new technologies being readily developed. Given the common range of catheter sizes, 5-12 Fr, employed today for clinical radiofrequency and cryothermal ablation treatments, in work described within my

thesis these bounds were expanded so that future iterations of such devices would not be excluded. The following studies were designed and performed to comprehensively characterize the relative behaviors of the fossa ovalis during and following the transseptal punctures so that device designers and clinician may better understand the impacts of each crossing.

Tissue Properties of the Fossa Ovalis as They Relate to Transseptal Punctures: Translational Approach

Published in *Journal of Interventional Cardiology,* **28**(1), pp. 98-108, 2015.

Stephen A. Howard, PhD[1,3]; Stephen G. Quallich, BS[1,2];
Mark A. Benscoter, MS, MBA[1,3]; Bryce C. Holmgren, BS[1,2];
Christopher D. Rolfes, PhD[1,2]; Paul A. Iaizzo, PhD[1,2]

[1] Department of Biomedical Engineering, University of Minnesota, Minneapolis, MN
[2] Department of Surgery, University of Minnesota, Minneapolis, MN
[3] Medtronic Inc., Mounds View, MN

Funding Source*:* Medtronic, Inc. research contract (Mounds View, MN, USA); Medtronic had no involvement in study design, data collection/analysis/interpretation, or report writing.

Disclosures*:* Stephen Howard and Mark Benscoter were graduate students and also employed by Medtronic, Inc.; Paul Iaizzo has a research contract with Medtronic, Inc.

Preface

In order to gain access to perform cardiac ablation procedures for treating arrhythmias, transseptal punctures are routinely performed. With the continued growth and interest in such transcatheter procedures, more complex and difficult disease states can and are on the horizon for being treated. Along with these treatment strategies, it should be noted that the required catheter sizes have increased, thus adding additional strain to the fossa ovalis. It was recently reported that iatrogenic atrial septal defects persistence rates were 50% following transcatheter mitral valve repair using a 16 Fr catheter, and individuals

with iatrogenic atrial septal defects had increased mortality rates by a staggering 6 fold [1]. This highlights the need for a more comprehensive understanding of the clinical limits that may be imposed on the septum during cardiac procedures that utilize a transseptal puncture. In this study we specifically characterized the relative puncture forces and lateral tearing forces of the fossa ovalis induced by a range of catheter sizes. The data herein identified the relative consequences of performing a transseptal puncture and the bounds that the septum may endure prior to inducing injury.

I was responsible for assisting with the protocol development with the aid of Steve Howard and Cole (Bryce) Holmgren: specifically Cole and I harvested, prepared, and performed the lateral tear force experiments. In addition, I was also responsible for the data and statistical analyses along with contributing to the manuscript for the lateral tear portions. Steve Howard led the portion of the project composing puncture forces and Mark Benscoter, Chris Rolfes, and I all aided in performing these experiments. Furthermore, I presented the preliminary results of this study at the European Cardiac Arrhythmia Society (ECAS) in Munich, Germany in March 2014.

Summary

Objectives: This study focused on how catheter size affects transseptal puncture, what transseptal indication means, and whether the swine model is predictive for humans.

Background: Transseptal puncture is a common procedure that gains access to the left atrium, allowing percutaneous mitral valve repair, left atrial appendage closure, and left-sided ablations. The basic approach has not changed in many years, however the frequency of transseptal punctures and the size of devices are increasing with emerging treatments. This study focused on how catheter size affects transseptal puncture, what transseptal indication means, and if the swine model is predictive for humans.

Methods and Results: A broad range of devices (4F-18F) were advanced through atrial septa of swine hearts; some devices were inserted in both swine and human hearts using 10F catheters. Greater forces were required to puncture through the septa of human hearts compared to those of swine. Larger catheters used in swine hearts required greater force

to advance them through the septa, causing greater dilation of tissue and sometimes tearing the floor of the fossa ovalis; analyses indicated an exponential increase in size of the iatrogenic atrial septal defect. Specific tissue property testing of the septum primum showed that this tissue sheared at a lower exerted force in a superior to inferior direction.
Conclusions: Results may provide physicians with important knowledge about what to expect when treating a possible iatrogenic atrial septal defect or help them understand the consequences of transseptal punctures. Comparative data between swine and human atrial septal tissue properties provide critical insights between the species and offer clinicians and device designers important information relative to differences in tissue behaviors.

Introduction

Transseptal punctures (TSP) have been performed since the 1960s for a variety of clinical procedures [2]. The avascular fossa ovalis (FO) in the atrial septum provides an optimal location, as this tissue is thin and facilitates tenting to obtain access to the left side of the heart. It should be noted that other routes (e.g., through the arterial vasculature or transmyocardially) may elicit associated complications or be more difficult relative to a transseptal approach [3]. To perform a TSP, access to the right atrium is obtained through the venous system, then transseptal sheaths are advanced through the vasculature and into the right atrium. The placement of the sheath onto the FO is identified by watching for a characteristic “jump” of the dilator tip following retraction and dragging of the transseptal equipment inferiorly. After the FO has been located, the tenting can be generally visualized through fluoroscopy and, more commonly, echocardiography [4,5]. A physician will tend to look for the most optimal portion of the septum to puncture based on the type of left atrial procedure that needs to be conducted. Additionally in some patients, more than one puncture may be conducted to simultaneously advance different types of catheters into the left atrium. Nevertheless, the optimal placement of the puncture location is very important, as it will commonly affect the ultimate success or ease of a given clinical procedure [6].

The complication rates associated with transseptal punctures are cited to be as low as 0.74% of procedures intraoperatively [7]. Yet, the post-operative outcomes are considered separately and incidences of remnant interatrial shunts have been reported. For example, McGinty et al. presented a review indicating prevalence of iatrogenic atrial septal defects (IASDs) to be as high as 87% post procedure and, at an 18-month follow-up, incidences were reported as high as 15% [8]. Although the authors suggest that most of these created holes were resolved over time and the IASDs were not associated with clinical issues such as embolism, cyanosis, or right heart failure, they could still present issues especially if one assesses potential new procedures involving TSPs with larger sheaths [8].

As mentioned above, there are a number of procedures that require a TSP including left-sided cardiac ablations, percutaneous mitral valve repairs, mitral balloon valvulotomies, left atrial appendage closures, and certain ventricular assist device placements [3,9–18]. These procedures along with some newer and future procedures, including left ventricular endocardial pacing and percutaneous mitral and aortic valve implantation, could potentially bring about a greater prevalence of TSPs and thus higher incidences of potential complications [19–21]. As cardiology procedures have progressed, the range of sizes for transseptal devices has increased. To date, the smallest transseptal devices typically are 4F and range up to the largest reported of 22F [8,20]. This latter size range has prompted discussions regarding what the FO is capable of tolerating, a topic addressed in previous publications [8,12,14,22]. Yet, we consider here that a detailed study investigating the specific tissue properties of the FO and the impact of the various sized catheters on IASD formation is necessary to help understand clinical limits.

In addition to the puncture that is created in the FO, manipulation of catheters and tools across the septum may result in the tissues being stretched and/or torn, resulting in larger IASDs. A previous study relative to this topic was performed by Saitoh et al. with a mitral valve clip procedure under echocardiography [10]. The subsequent holes created and identified were elongated and elliptical (not circular), suggesting that the simple

puncture forces were not the only strains being placed on the septum, but rather some radial/shear forces applied by the catheter could potentially cause tears in an axial direction. Our present study was designed to provide additional insights relative to the tissue properties of the FO in relation to TSPs. Yet, by additionally utilizing both ex vivo swine and human hearts for a subset of our experiments, multiple variables could be studied and a relation to human cardiac anatomy can be specifically assessed [23–25].

Methods

Obtaining tissue and preparation

Swine hearts (n=48) were obtained fresh and were transported on ice and then dissected within 8 hours post excision. The right and left atria were opened to expose the interatrial septum while keeping intact the tissue surrounding and supporting the FO. The isolated cardiac tissues were warmed to 37°C using a circulating water bath. Images of the FO were taken pre- and post- puncture.

Human hearts were received as a donation for research to the University of Minnesota from organ donors whose hearts were deemed not viable for transplantation (via Lifesource, St. Paul, MN, USA). Table 1 provides brief medical histories of the donors including these cardiac conditions: one with atrial fibrillation, one with hypertension, and one with an unspecified "heart problem." Exclusion criteria for testing included lack of an intact atrial septum and other congenital abnormalities that would disallow the suction device to be implemented. These hearts were warmed with 37°C saline.

Table 1. Baseline characteristics of human hearts (n=7).

Demographic	Measurement
Male (%)	57.1
Age (years)	58.4±5.7
Weight (kg)	86.0±30

Catheter and fossa holder method

A suction device on a positionable arm provided circumferential adhesion surrounding the FO to hold the interatrial septum in a secure manor (Figure 1). The devices used in these experiments were composed of a dilator and sheath, and had internal diameters of 4, 8, 10, 12, 16 and 18 French, according to manufactures' specifications.

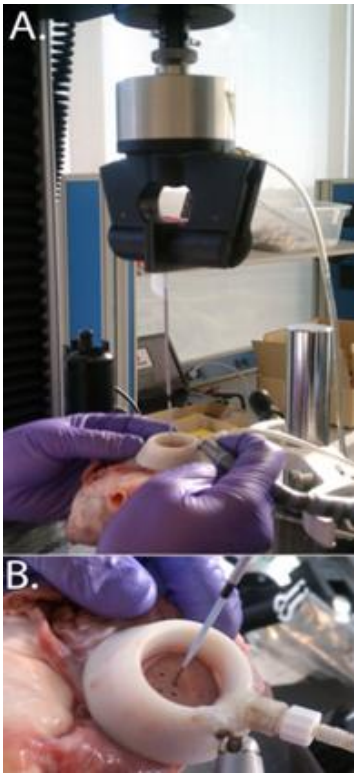

Figure 1. Radial adhering suction device for stabilization of the atrial septum for tissue puncturing. (A) Force testing machine with transseptal device attached and puncturing the atrial septum. (B) Close-up view of the atrial septum and stabilization device employed for puncturing.

Catheters were trimmed to a length of 15cm, and the dilator and sheath were bonded together with ultraviolet cure adhesive (Loctite, Henkel, Düsseldorf, Germany) at the cut end of the catheter. A Brockenbrough® (BRK, Medtronic, Inc., Fridley, MN, USA) transseptal needle, was cut 18cm from the tip and straightened to protrude from the dilator tip, as it would in clinical practice. The end of a Brockenbrough needle was separated from the main shaft and adhered into the tips of each of the dilators of those catheters with a stiff metal rod through the dilator to provide mechanical support for the

needle tip (Figure 2). The catheters were either clamped or inserted into a connector attached to a load cell for obtaining puncture forces.

Figure 2. Schematic of transseptal devices used for testing. The dilator was seated into the sheath and attached at the proximal end via adhesive. The center lumen was kept clear for a needle to be placed through it and protrude from the distal tip.

Tenting and puncture testing

A circumferential suction device was attached to the atrial septa of either swine or human hearts (Figure 1) to allow for continuous and repeatable fixation of the FO, as noted above. The device was locked into place with the FO in the center of the suction ring, and the FO was placed perpendicular to the trajectory of the transseptal catheter.

The forces required to puncture and tent the FO at various locations were obtained by using mechanical force tester (Instron, Norwood, MA, USA; Chatillon TCD225, Largo, FL, USA). The relative locations of tenting and punctures were defined in relation to the superior, inferior, anterior, and posterior orientations (Figure 3). The shortened catheters were affixed to the load cell so that their trajectory was normal to the floor of the FO. Following stabilization of the FO with the suction device, the catheters (without the needle protruding from the dilator) depressed the FO to a depth of 8mm for swine hearts and 12mm for human hearts at a rate of 254mm/min and then retracted to the starting position. The difference in the protocol between human and swine experiments was related to the identified differences in the tissue compliance between the swine and human tissues based on pilot studies of the tissue (data not shown). Then the catheters were driven through the FO with a transseptal needle protruding from the dilator at a rate of 254mm/min at various locations on the FO.

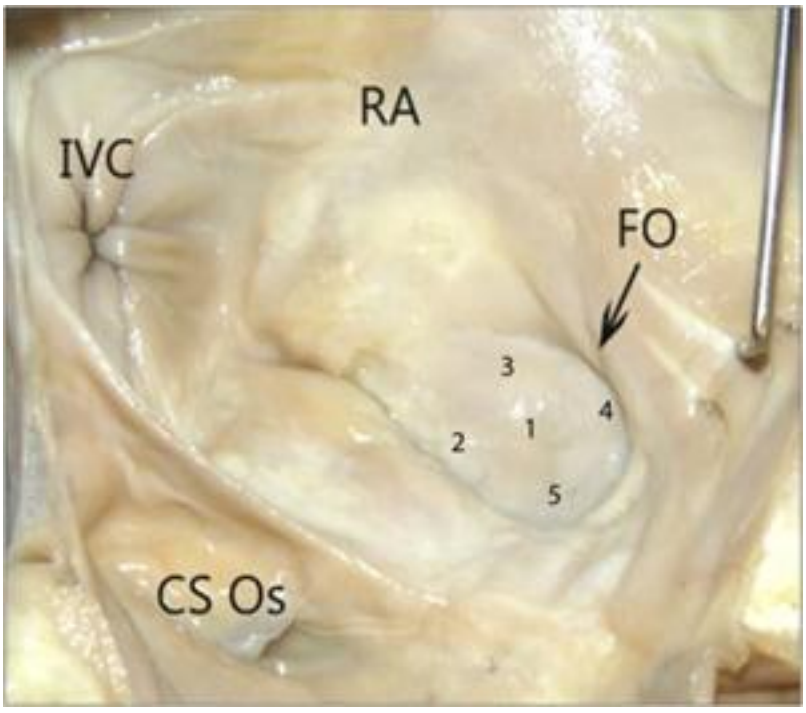

Figure 3. Location of the fossa ovalis (FO) in relation to other anatomy within the right atrium (RA): the inferior vena cava (IVC), and the coronary sinus ostium (CS Os). The numbers indicate various puncture locations: (1) center, (2) inferior, (3) posterior, (4) superior, and (5) anterior.

Initial analyses of the force versus distance relationships indicated that the largest forces required for transseptal puncture were when the tips of the needles, tips of the dilators, dilations of the septum, and tips of the sheaths were going through the septum (Figure 4). The forces and distances were recorded by the system for each of these events for the various puncture locations. Following the punctures, the remnant holes were measured.

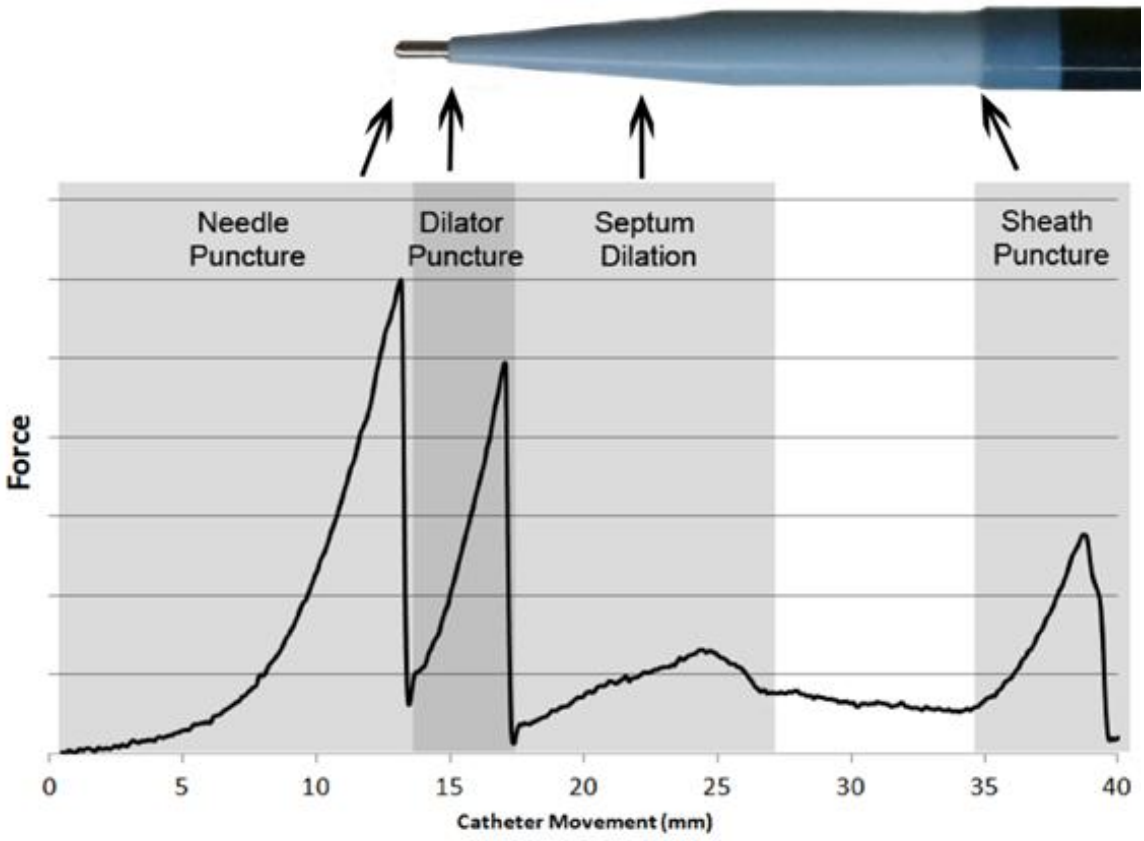

Figure 4. Characteristic force verses distance graph during fossa ovalis puncturing. Note the distinctive peaks during each transition of the dilator and sheath; upon reaching a new layer, the force increases due to the need for fossa ovalis expansions.

Fossa shear force analyses

Additional swine hearts were obtained ranging from 400-650g in size (n=70). The atrial septum including approximately 5mm of tissue surrounding the floor of the FO was excised from each heart. Samples were randomized to size and direction groups, and the inferior or posterior portion of the musculature surrounding the FO floor was cut off (Figure 5 A). The FO was punctured with a transseptal Brockenbrough® needle and then a 4F, 12F, or 18F sheath was advanced through the septum. In all cases, the sheath and dilator were maintained in a perpendicular position relative to the floor of the FO via a custom fixture (Figure 5 B). While the side of the FO opposite the cut side was anchored, the sheath was pulled away from the base at a rate of 100mm/min causing it to rip

through the FO, employing a mechanical force tester. These atrial septa were ripped towards the cut section of the septum in either a superior or posterior direction. The average sheath ripping forces were defined as the average forces while the septum primum was ripping. To illustrate, Figure 5 C shows that the 10-19mm extension portion for this sample was defined as the average ripping force, while the peak sheath ripping force was the highest force recorded. Fossa ovalis dimensions, average ripping force, and peak sheath ripping force were also recorded.

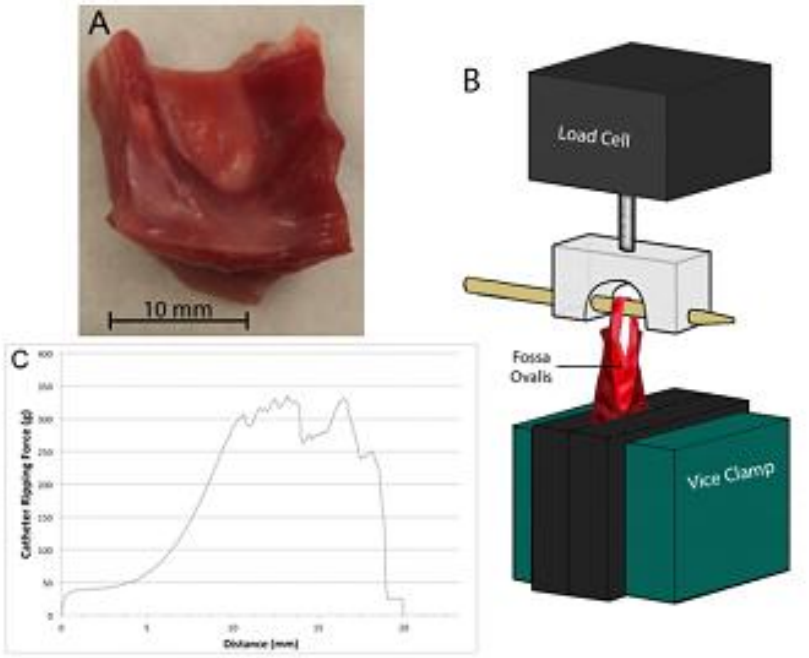

Figure 5. Schematic representation of the fossa ripping test setup. The muscular tissue adjacent to the septum primum (posterior rim of the fossa ovalis for posterior pulls and superior rim for inferior pulls) was cut off to allow the sheath to fully disengage from the atrial septum without consequence from the muscular portion of the atrium surrounding the floor of the fossa ovalis (A). The fossa ovalis was ripped by a catheter which was inserted through the floor of the fossa ovalis in the mechanical force tester (B). An example of the resultant force versus extension plot is shown in (C).

Statistical analyses

All data are represented as the mean±SE unless otherwise noted. Student's T-tests were used for one-to-one comparison and ANOVA was employed for multi-group comparisons. Significance was determined with a p-value<0.05.

Results

Tenting studies

The initial tenting experiments showed that the average forces required to tent and extend the septum primum by 8mm were greater for the human hearts compared to swine (199±30gf vs. 135±5gf respectively, p<0.001). By breaking down the data to assess the relative effects of location on the tenting forces, only one statistically significant difference was identified in the inferior portion of the FO, where the human tenting was significantly higher (145g±65g, n=40, vs. 292g±213g, n=8; p<0.01). The remainder of the species comparisons for each location were not significantly different (Figure 6). Yet, if one combines all tenting data per species, the swine hearts were shown to require significantly less force to tent the fossa regardless of the location (swine 138±5g n=180 vs. human 199±30g, n=23, p<0.001).

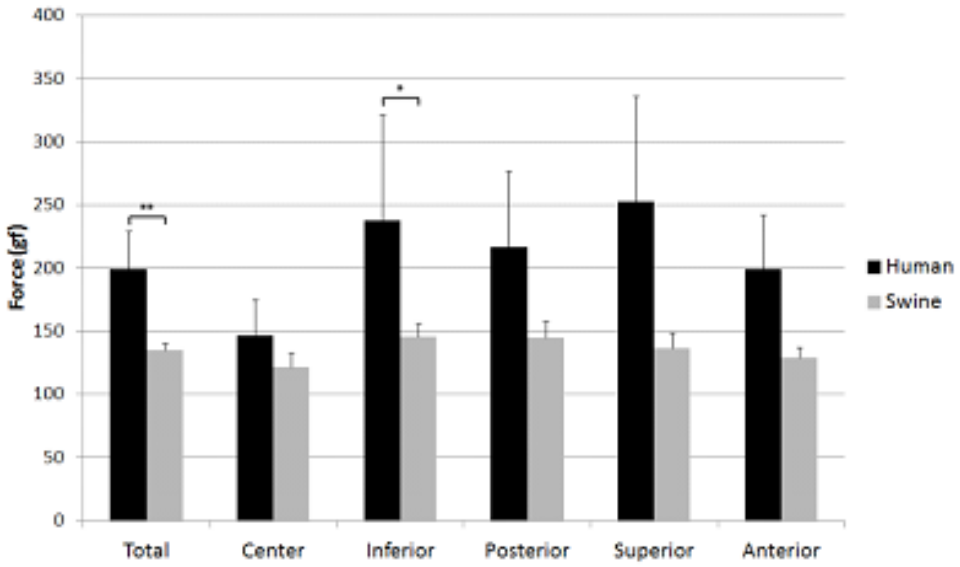

Figure 6. Forces required to tent the fossa ovalis by 8mm. Experiments were performed on excised human (n=8) and swine (n=40) hearts. (*=p<0.01, **=p<0.001)

Puncture forces: human vs. swine comparisons

Human heart specimens were punctured only with the 10F catheter for comparison to the swine hearts. These punctures produced characteristic force versus distance plots, where the forces for the needle, tips of the dilator, and the sheaths to pass across the septum were easily observable as transient peak forces (Figure 4). The other force recorded of interest was the maximum force seen during the dilation phase of the septum (i.e., when the tapered portion of the dilator passed through the FO).

When comparing the 10F catheter data between swine and human samples, the results showed a higher force required for each portion of the catheter (Figure 7). The greatest difference between species was observed for the data between the peak forces of the tip of the dilator, requiring 240% greater forces for the human hearts. It should be noted that significant differences were found when comparing the average forces required to pass the various potions of the catheter through the septum for the tip of the dilator, dilation, and the sheath ($p<0.01$ for each; Figure 7).

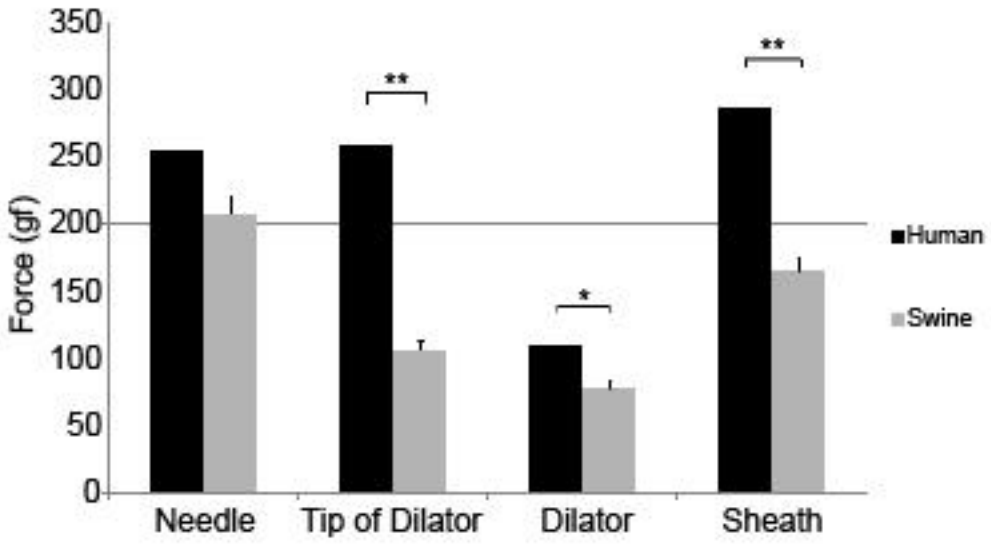

Figure 7. Average peak forces required to pass various portions of 10F sheath through the septum primum in isolated septa of human and swine hearts. Significant differences were found

between these two species when comparing the tip of the dilator, dilation, and sheath forces (*=p<0.01, **=p<0.001)

Puncture forces: sheath size comparisons

The variability in the needle punctures alone resulted in an average puncture force of 201±75gf (±SD) with the 176 punctures that were performed with the Brockenbrough® needle. To account for these variations in tissue performance, the subsequent portions of the sheath were normalized to the needle puncture forces. This was done to help determine the relative relationship between sheath sizes and resultant forces required to traverse the atrial septum. Subsequently, it was found that there was a direct correlation between catheter size and the forces required to pass through the septum. ANOVAs were performed for each of the sheath sections and we found significant differences within each group with p-values<0.001 (Figure 8). The other notable trend observed was that the dilation forces were significantly less for each of the sheath sizes compared to both the passing of the tips of the dilator and/or the shaft of each sheath (p<0.02 in all instances).

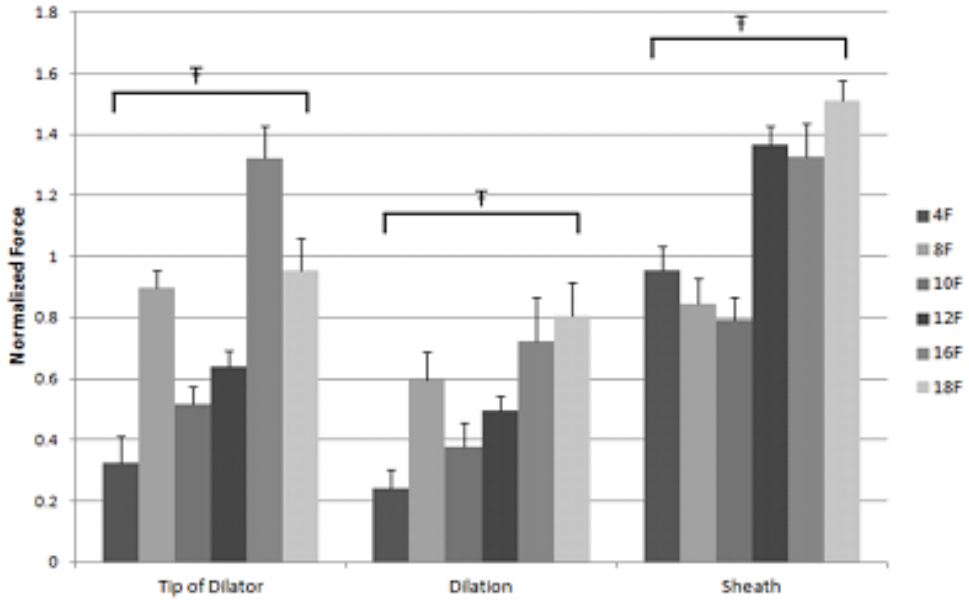

Figure 8. Relative forces required to traverse the atrial septum with various portions of a transseptal sheath of difference sizes. (Ŧ=p<0.001 based on ANOVA)

Following the punctures, images were taken of the resultant holes formed in the atrial septa. The minimum and maximum lengths were determined and plotted in relation to the outer diameter of the sheath. There was a positive correlation between the resultant hole sizes and the sheath sizes, as would be predicted. These data identified an exponential increase in resultant hole sizes (Figure 9).

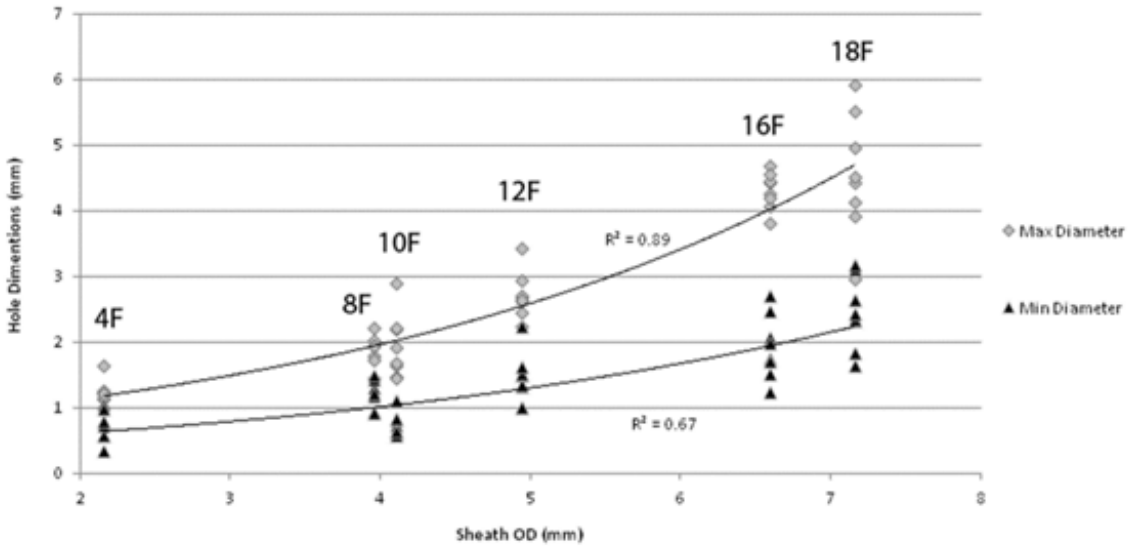

Figure 9. Minimum and maximum diameters of induced iatrogenic atrial septal defects, following transseptal punctures employing various sized catheters.

Septal ripping forces

A summary of septum ripping by utilizing different sheath sizes is presented in

Table **2**. The chosen direction of induced FO ripping had a significant impact on the resultant average tearing force and peak tearing force ($p<0.05$). Superior-to-inferior induced rips required an average tearing force of 301±26gf, while those elicited in the anterior-to-posterior direction required 363±41gf (

Table **3**). Also, larger forces were required to rip the septa with larger sized sheaths (Figure 10). The averages of the mean sheath tearing forces were 258±20, 362±25, and 555±56gf for the 4F, 12F, and 18F sheaths respectively; there were significant differences between the sheath sizes and sheath tearing forces between the 18F and 4/12F

groups ($p<0.001$). Heart weight, animal weight, FO thickness, and width (superior-to-inferior) did not statistically differ between any of the groups ($p>0.05$).

Table 2. Summary of fossa ovalis dimensions and sheath tearing forces listed by sheath size.

	4 F (n=15)	12 F (n=20)	18 F (n=15)	p-value
Fossa ovalis thickness (mm)	1.1±0.1	1.2±0.1	1.1±0.1	0.727
Superior/inferior width (mm)	16.5±1.1	14.3±0.7	15.7±1.2	0.241
Anterior/posterior width (mm)	10.7±0.9	7.7±0.6	9.2±0.7	0.005
Average tearing force (gf)	258±20	301±26	555±56	p<0.001
Peak tearing force (gf)	344±26	417±37	704±72	p<0.001
Heart weight (g)	487±10	464±13	451±10	0.563

*Values are reported as mean±SE

Table 3. Directional differences in septal tearing forces using a 12F sheath.

	Superior-to-Inferior (n=20)	Anterior-to-Posterior (n=20)	p-value
Fossa ovalis thickness (mm)	1.2±0.1	1.1±0.1	0.717
Superior/inferior width (mm)	14.3±0.7	14.8±1.1	0.569
Anterior/posterior width (mm)	7.7±0.6	7.9±0.7	0.480
Average tearing force (gf)	301±26	424±41	0.012
Peak tearing force (gf)	417±37	551±60	0.033
Heart weight (g)	464±13	452±18	0.844

*Values are reported as mean±SE

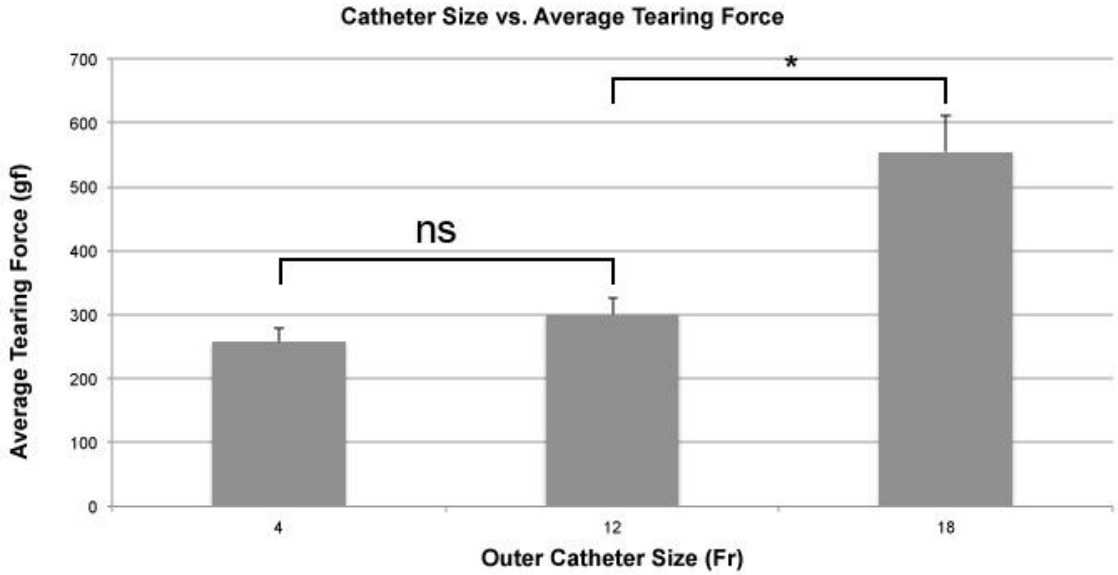

Figure 10. Catheter size versus average tearing force. Tearing forces of the fossa ovalis increased with the usage of a larger diameter sheath, but did not significantly differ between the 4F and 12F sheaths (p>0.05). Error bars depict mean±SE. *p-value<0.001

Discussion

There are a number of different procedures requiring TSP including left-sided cardiac ablations, percutaneous mitral valve repairs, mitral balloon valvulotomies, left atrial appendage closures, and certain ventricular assist device placements [3,9–18]. In many cases, the tissue of the FO is punctured and manipulated with large size devices. This study described a series of translational experiments that were performed to better understand the biomedical impacts of procedures that require the transseptal delivery of catheter systems through the atrial septum.

The results of this study showed that a swine model is helpful to determine the forces required for eliciting tenting and punctures, and that the forces measured were less than those seen in humans (121±11gf vs. 146±26gf, $p<0.001$). Further, it is important to note that in both human and swine hearts, with the exception of potentially trying to tent the muscular septum, the relative septal location at which one chose to puncture was not

material to the amount of force that may be required to produce tenting. The devices used in this study showed that, on average, the needle tented the septum 9.3±.3mm in humans and 9.8±.14mm in swine hearts (p=0.2), prior to ultimately perforating the septum. These outcomes demonstrate the ability of the swine model to serve as a proxy for humans.

In addition, the risk of cardiac tamponade continues to be a concern when conducting the TSP. Using the outcomes from this study, in an a heart ranging from approximately 30mm to 50mm in diameter [26–28], the needle will strain the FO approximately 25% of the distance into the left atrium before perforating and thus protruding into the left atrium. One should also keep in mind that this does not take into consideration that there is a slightly lateral but also superior trajectory on the needle when deployed through most TSP devices. These factors could potentially explain clinical incidents of left atrial perforation and resultant tamponade [13].

Within the puncture data, the relative variability was notably similar between the swine and human tissue groups; the standard deviation was 33% of the mean for human punctures and 37% for swine. Further, these values correlated to 75gf for the swine hearts and 90gf for human specimens, when assessing the Brockenbrough® needle puncture forces alone. Importantly, since the same needle was used, this variation was most likely due to the differences in cardiac anatomy or slight changes in tissue thickness. Furthermore, larger catheters resulted in greater forces required to cross the septum; similarly, it was observed visually that as catheter size increased so did the remnant holes that were created. These remnant holes may contribute to the ability for post-procedure healing. It has been reported that most IASDs close in patients over time, but in some individuals this can take up to year[7].

An observation was made that subsequent stretching of these tissues required lower forces in swine, especially in the case of the dilator tips and dilation shafts. However, this is not necessarily the case for human tissue. Notably, the dilator tips deployed in the human septum required more than twice the force relative to swine tissue. This can be

interpreted to indicate that there are clear distinctive differences between the atrial anatomies of these two species, which could potentially relate to the tissue structure or composition. Yet, it should be noted that another potential source of variability in our data could be associated with varied disease states and cardiac morphologies that were present within the donated human hearts.

While medical device developers are striving to use the smallest types of delivery systems possible, catheter sizes in the realm of overall TSPs are getting larger due to their more complicated nature, e.g., with percutaneous mitral repair systems like the Abbott Mitra Clip being placed through a 22F catheter. Similarly, there is a major industry push to develop transcatheter mitral valve replacement systems that will be delivered via TSP; for comparison, the current transcatheter aortic valve systems utilize delivery catheter sizes ranging from 18F to 24F [29]. Needless to say, new mitral valve delivery catheters would probably be similar in size (if not larger) due to the difference in mitral and aortic valve circumferential areas. Thus when these technologies are deployed in humans, the clinician should have a good understanding of how the septum will react to the TSP [10,30]. In clinical use, navigating transseptal catheters within the left atrium typically requires sheath manipulation and risks FO tearing. Although procedures are trending toward larger sheath use, the incidence of FO tearing may be lower due to the larger sheer forces in larger sized catheters (Figure 10). Further studies will need to specifically investigate FO tearing in order to fully characterize septal damages sustained by various clinical procedures.

Study limitations

The availability of human hearts for such studies is rare as one would expect, thus the majority of described experiments were performed with swine hearts. The use of swine hearts provided a method to test multiple catheter types, and we were able to relate these results to a subset of comparative human tissue trials.

The true mimicking of physiological conditions imposes other issues related to force application on the catheter to puncture the atrial septum while accurately recording the displacement and the load. Using a consistent and repeatable suction device to hold the septum allows for a more controlled study with respect to load and displacement. Along with the consistency, the rate at which the tissue was pulled or punctured was kept consistent as a way to reduce the variables in the experimental setup.

Conclusion

These translational in vitro studies of fresh heart specimens, both human and swine, provide a unique perspective on the challenges of conducting a transseptal procedure and present compelling data for further discussion on the device size constraints as more devices are constructed. In these uniquely designed experiments, we specifically observed that swine can serve as a reasonable model to mimic the human condition. In addition, advancements that are tested in the swine model can serve as a more rigorous application due to the more delicate nature of the swine anatomy.

Comparisons of Transseptal Puncture and Tearing Forces Employing 12, 16, 18, and 23 Fr Delivery Systems Using Traditional or Radiofrequency Puncture Techniques

Submitted to *Journal of Interventional Cardiology,* 2015, in review.

Mark A. Benscoter, MS[1,3]; Stephen G. Quallich, BS[1];
Megan M. Schmidt, BS[1]; Lars M. Mattison, BS[1]; Paul A. Iaizzo, PhD[2]

[1] Department of Biomedical Engineering, University of Minnesota (Minneapolis, MN)
[2] Department of Surgery, University of Minnesota (Minneapolis, MN)
[3] Mayo Clinic, Rochester, MN

Funding: Research contract with Medtronic, Inc., Minneapolis, MN

Preface

As previously mentioned, transseptal punctures usage has been increasing in recent years with the advent of technological advancement and/or numerous novel minimally invasive cardiac procedures. In this study, our aim was to distinguish if performing the transseptal puncture with an array of needle types could reduce the relative required forces needed to cross the septum and/or to minimize damage to the fossa ovalis during catheter manipulation. Specifically, we developed a transseptal puncture system to compare against the two currently employed clinical systems that are routinely utilized. Using methodologies I helped previously developed within our laboratory [31], Mark Benscoter, Megan Schmidt, Lars Mattison, and I together harvested, prepared, and performed the herein described puncture and lateral tear force experiments. I was the lead investigator for the septal tearing component of the project and completed the data and

statistical analyses as well as contributed to the manuscript for those sections. Mark and Megan shared these same responsibilities for the punctures portion of this experimental paradigm. I also presented preliminary results of this study at the Transcatheter Cardiovascular Therapeutics (TCT) conference in Washington, DC in September of 2014.

Summary

Objectives: Quantitatively compare catheter delivery systems of different sizes, with and without RF needles, for performing atrial transseptal crossing. Investigate puncture force required to cross the septum and potential anatomic damage of the fossa ovalis (FO).

Background: Left atrial access is required for transcatheter therapeutic approaches, such as mitral valve repair/replacement, left atrial appendage closure/ligation, and left heart endocardial ablation. Advancements in device designs have changed how catheter delivery systems perform transseptal punctures, including variations in sheath size and use of RF energy instead of mechanical force for device delivery. Questions exist regarding the ability of the FO and associated structures to withstand the biomechanical impact of transseptal puncture force.

Methods: We analyzed the puncture and tear force of FOs from 167 swine hearts after transseptal punctures using: conventional curved transseptal needles (TN), RF transseptal needles (RFTN), or 5-Fr RF electrodes tipped with small segment of a TN (ETN). Four delivery systems were assessed (12-, 16-, 18-, 23-Fr).

Results: Mean puncture force for the dilator and sheath was significantly different for the 3 methods for 12-, 18-, and 23-Fr sizes ($P<0.05$). Comparing needles, normalized mean puncture force of the TN (100±54.6 grams) was significantly different from ETN (64.9±32.9 grams)($P=0.01$). Comparing delivery systems, normalized mean puncture force of the 12-Fr system (100±36.7 grams) was significantly different from the 23-Fr system (157.6±66.2 grams)($P=0.005$). The FO withstood greater peak tearing forces with a 23-Fr ETN, compared with all other sizes ($P=0.01$).

Conclusions: These results are invaluable for clinicians and engineers designing new transseptal medical devices to prevent anatomic damage.

Keywords: Atrial fibrillation; atrial fibrillation ablation; transseptal catheterization; transseptal puncture; left atrial access

Abbreviations

ETN=radiofrequency electrode with the tip of a transseptal needle

FO=fossa ovalis

RF=radiofrequency

RFTN=radiofrequency transseptal needle

TN=transseptal needle

Introduction

Ongoing development of new devices for cardiac therapies continues to rely on performing transseptal punctures to access the left atrium, a technique originally developed by Ross et al. and Cope et al. in 1959 [32,33]. But the increasing size of devices and their subsequent manipulation because of increasing procedural complexity are, more and more, challenging the limits of the fossa ovalis (FO), particularly its ability to stretch without tearing (Figure 11).

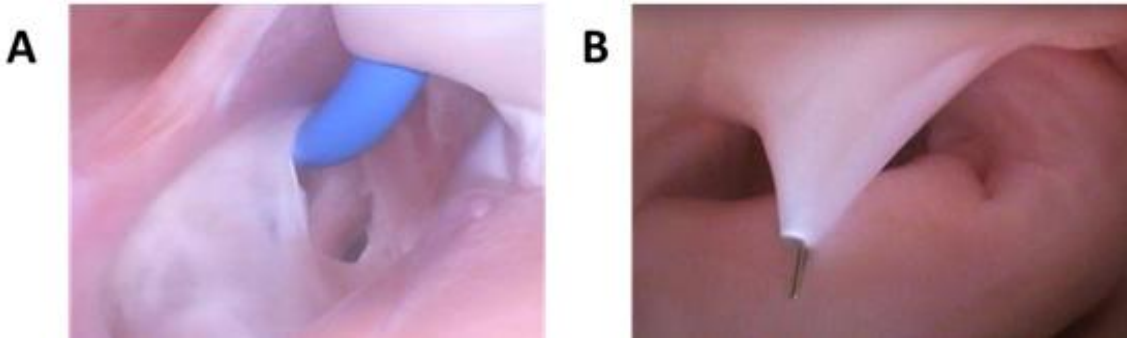

Figure 11. (A) Swine heart's torn fossa ovalis with a sheath through the opening made by a transseptal puncture, as viewed from the left atrium. (B) Human fossa ovalis puncture, as viewed from the left atrium.

To successfully treat cardiac diseases, it is essential to have access to the anatomy in a way that is least likely to incur injury. Crossing the septum through the FO has a major

impact on device delivery into the left heart and on the ability to reach key anatomic locations, such as the mitral isthmus, the mitral valve, and the pulmonary veins. The use of cryogenic balloon ablation therapies and transcatheter mitral valve repair and replacement devices requires 12- to 24-Fr delivery systems. Ideally, systems for accomplishing transseptal punctures would allow the tissue to dilate and be manipulated without tearing.

Recent advancements in device designs have prompted changes in how catheter delivery systems perform transseptal punctures, including variations in sheath size (12-, 16-, 18-, and 23-Fr) and the use of radiofrequency (RF) energy rather than mechanical force. RF-based needles, intended to reduce the risk of cardiac tamponade, use RF energy delivered through the tip of the transseptal needle, typically at 10 watts for a period of 1 to 10 seconds [34–38].

In our study, the primary objective was to quantitatively compare catheter delivery systems using different sheath sizes (12-, 16-, 18-, and 23-Fr), with or without RF, for performing atrial transseptal crossing. Specifically, our focus was on the puncture force required to cross the septum and its impact on anatomic damage (tearing) of the FO. We reviewed the puncture force and dilation strain of traditional and RF-based transseptal puncture systems, analyzed the impact of large-diameter delivery systems, and assessed a RF device using 4 different delivery system sizes.

Methods

Study population

Fresh swine hearts (n=167) were obtained from Glencoe Family Farms (Glencoe, MN, USA), the University of Minnesota's Large Animal Veterinary Department (St. Paul, MN, USA), and the Visible Heart® Laboratory (Minneapolis, MN, USA). Hearts were dissected within 24 hours after they were excised. We first visualized the FO through the inferior vena cava, and then opened the right and left atria to expose the interatrial septum. Next, we removed the septal tissue, taking care to keep intact all tissue

surrounding and supporting the FO. Each specimen included at least 5 mm of adjoining atrial septal tissue.

Puncture devices

To perform transseptal punctures of the FO, 3 devices were utilized: (1) conventional curved transseptal needle (TN) (Brockenbrough® Medical, Medtronic, Inc., Minneapolis, MN, USA) with a dilator and sheath; (2) NRG® RF transseptal needle (RFTN) (Baylis Medical Company, Montreal, QC, Canada) with a dilator and sheath; and (3) 5-Fr RF electrode with the tip of a TN (ETN) along with a dilator and sheath (Figure 12). We used the 5-Fr ETN to understand whether an initial puncture with a larger RF tool would have an effect on the subsequent force for the dilator and sheath, particularly in the 18- and 23-Fr sheath sizes.

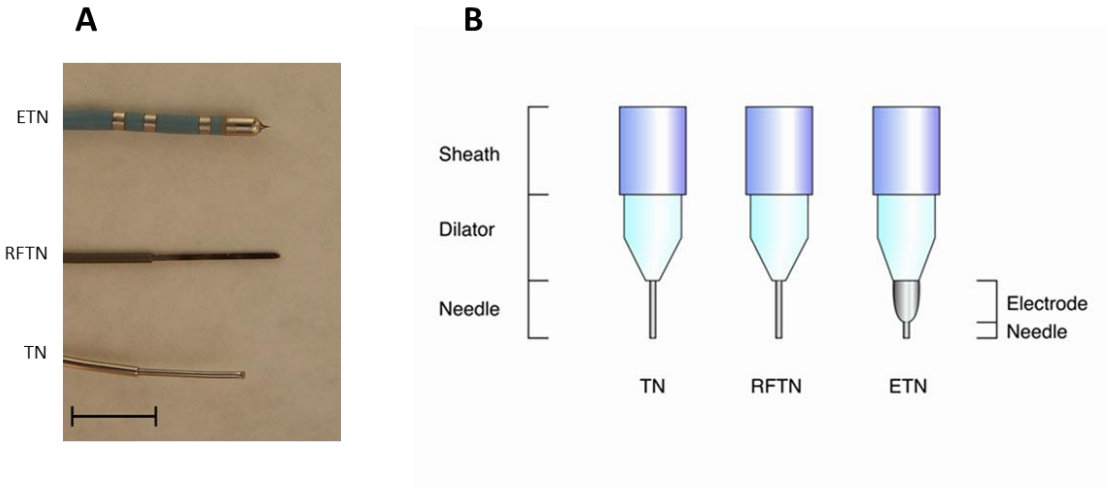

Figure 12. (A) Three transseptal puncture devices used in this study including (top to bottom): 5-Fr RF electrode with the tip of a transseptal needle (ETN), radiofrequency transseptal needle (RFTN), and a conventional curved transseptal needle (TN) (scale bar=1 cm). (B) Components of the three devices (purple=sheath, green=dilator).

Each delivery system was comprised 3 parts: sheath, dilator, and needle. For dilator dimensions, we defined the distal diameter as the diameter of the opening at the tip of the dilator, taper length as the distance from the tip of the dilator to the end of the tapered section of the dilator on the shaft of the dilator, and shaft diameter as the diameter of the

shaft of the dilator at the end of the tapered section (Table 4). For sheath dimensions, the outer diameter was measured (Table 5).

Table 4. Dilator dimensions for each delivery system

	12-Fr TN & RFTN	12-Fr ETN	16-Fr TN & RFTN	16-Fr ETN	18-Fr TN & RFTN	18-Fr ETN	23-Fr TN & RFTN	23-Fr ETN
Distal diameter (mm)	1.63	2.43	1.57	1.97	1.5	1.95	2.21	2.42
Taper length (mm)	14.02	10.14	65.04	49.5	56.12	59.58	64.15	68.77
Shaft diameter (mm)	3.56	3.5	5.36	5.32	5.82	5.8	7.57	7.59

ETN=5-Fr RF electrode with the tip of a transseptal needle; RFTN=radiofrequency transseptal needle; TN=transseptal needle

Table 5. Sheath dimensions for each delivery system

	Sheath size			
	12-Fr	16-Fr	18-Fr	23-Fr
Outer diameter (mm)	4.84	5.86	6.83	8.60

Force testing

For all force measurements, both the puncture device and the septal tearing method used the same load cell for force measurements. To measure the puncture and tearing force of the FO, we used the Chatillon TSD110 Digital Force Tester™ (Chatillon, Largo, FL, USA). We mounted the specimens as described by Howard et al. [31]. After tissue mounting, we activated the tester with data logging to complete either FO puncturing or septal tearing. To determine maximum puncture force, maximum tearing force, and mean tearing force, we used MATLAB (MathWorks, Natick, MA, USA) assessing the stress-strain curve.

FO puncturing

To confirm the puncture location, we directly visualized the FO (Figure 13B). The selected needle or electrode was inserted into the dilator until it extended approximately 2 cm past the tip of the dilator, then it was placed in close proximity against the FO, perpendicular to the center of the FO. The needle or electrode was extended past the tip of the dilator and placed against the FO. Then, the septum was mounted in preparation for puncture (Figure 13A). The system was advanced at a rate of 254 mm/min upon the FO until the needle, dilator, and sheath fully crossed the FO. The remaining pieces of the delivery system were advanced across the FO, with all 3 devices, once the septum was punctured.

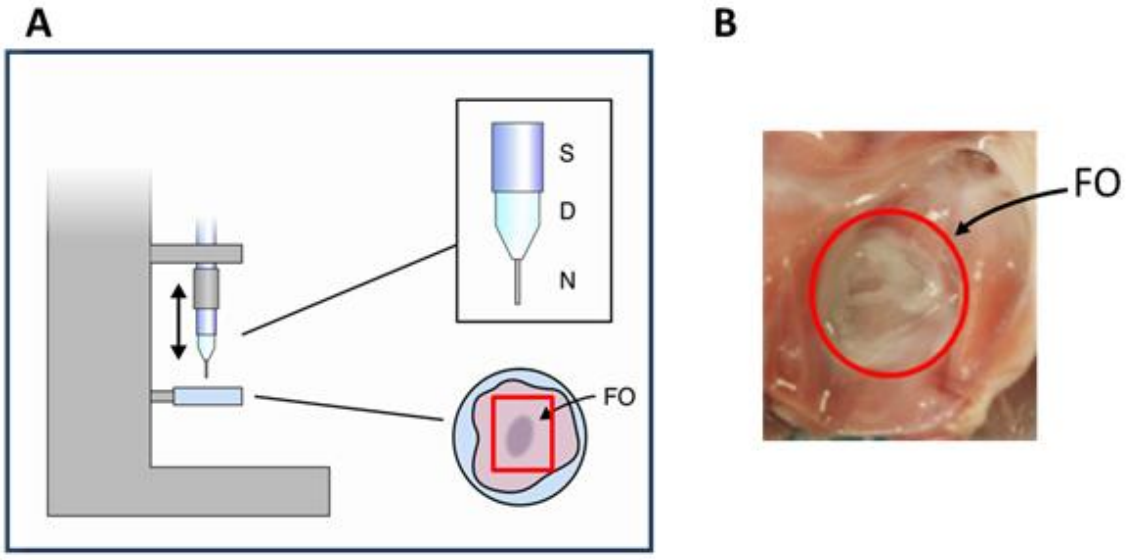

Figure 13. (A) Setup for transseptal punctures, with the device positioned to be inserted through the fossa ovalis (FO) mounted on a plate; all 3 components—sheath (S), dilator (D), and needle (N)—were oriented perpendicular to the specimen. (B) Septal tissue prepared for puncture (red oval shows the FO).

The approach was similar with the RFTN. The RFTN was connected to the RF generator (Baylis Medical Company), and RF energy was delivered using 10 watts while the entire system was advancing toward the fossa at a rate of 254 mm/min. The rate of movement was set to match the same rate as the conventional curved TN, in an attempt to mimic

current clinical practice. Energy delivery was initiated before contact with the tissue and terminated after puncture.

With the ETN, a 5-Fr electrode using RF energy was delivered using 30 watts with the Medtronic Atakr® (Medtronic, Inc.) generator. The ETN was connected to the RF generator and advanced at a rate of 127 mm/min until puncture was achieved. Note that, with the ETN, the rate was reduced by half, in order to allow time for the RF energy to affect the tissue. The photo and diagram in Figure 13 were each derived using a Chatillon TSD110 Digital Force Tester™ (which moved the system and recorded forces). The tissue specimen was bonded to the holding apparatus using Loctite adhesive (Henkel Corporation, Westlake, OH, USA).

Contained within the dilator of the ETN was a 5-Fr electrode with a TN tip at the distal end, which enabled contact with the tissue. The outer diameter of the dilator and the inner diameter of the sheath were similar to prevent a gap at the interface of each. In addition, the dilator had a tapered tip to allow for easy advancement across the septum, reducing the risks of tearing the FO. The dilator tip of the ETN was placed against the tissue to induce a mild degree of tenting. The device was advanced, while energy was delivered to the tip, to perform the puncture. The internal lumen of the dilator remained unobstructed, to allow for the needle and electrode to pass through the lumen and extend beyond the tip of the dilator. The amount of needle extension beyond the tip of the dilator was predetermined, given a restriction in the internal diameter of the dilator at the tip. The 5-Fr electrode was placed on the tip of a flexible Pebax® shaft (Arkema, Colombes, France) and then inserted through the inner lumen of the dilator. The catheters were attached using a custom fixture to a load cell for obtaining continuous puncture forces.

Septal tearing

For septal tearing experiments, we used 86 swine hearts (weight: 175 to 625 grams). For each specimen, we excised the FO and surrounding tissue, then punctured each FO with 1

of 3 devices (TN, RFTN, or ETN). Next, we advanced the dilator and sheath (12-, 16-, 18-, or 23-Fr) through the specimen.

Once the puncture was performed, we mounted the specimen on the fixture such that no force was being placed against the specimen, as described by Howard et al. [31]. The delivery system was maintained in a perpendicular position relative to the FO via a custom fixture. To remove any excess septal tissue, we made a cut superior to the FO, thereby ensuring that only FO tissue would tear during each test while leaving the surrounding septal tissue unaffected. For each test, we used a TSD110 Digital Force Tester™ to pull the sheath away from the base, tearing through the tissue at a rate of 100 mm/min. The atrial septa were ripped in an inferior to superior direction. Once the sheath was no longer in contact with tissue, the test was terminated. We defined sheath tearing force as the mean force while the septum primum was tearing, and adapted our FO tearing method from Howard et al. [31]. For this study, we recorded all FO dimensions, as well as mean and peak sheath tearing force.

Statistical analysis

Each experiment included randomized specimens of the variables, along with *t* tests and *P* values (set at <0.05), to determine statistically significant differences between means. To examine the influence of change in variation, we normalized the puncture force data, using a needle type and sheath size as a reference point. To examine the relationship between the anatomy and puncture devices, we used analysis of variance (ANOVA) with a resulting R^2value. For all analyses, we used Minitab version 12 (Minitab Inc., State College, PA, USA).

Results

In our comparison of the needle subgroups, we found that sheath size affected the force to cross the septum and FO resistance to tearing. In addition, the use of RF energy changed the force necessary to cross the FO. To the best of our knowledge, this study is the first to show how a larger puncture device can acutely affect performance of transseptal

punctures, sometimes doing so as well as, or even better than, more traditional methods (Figure 14).

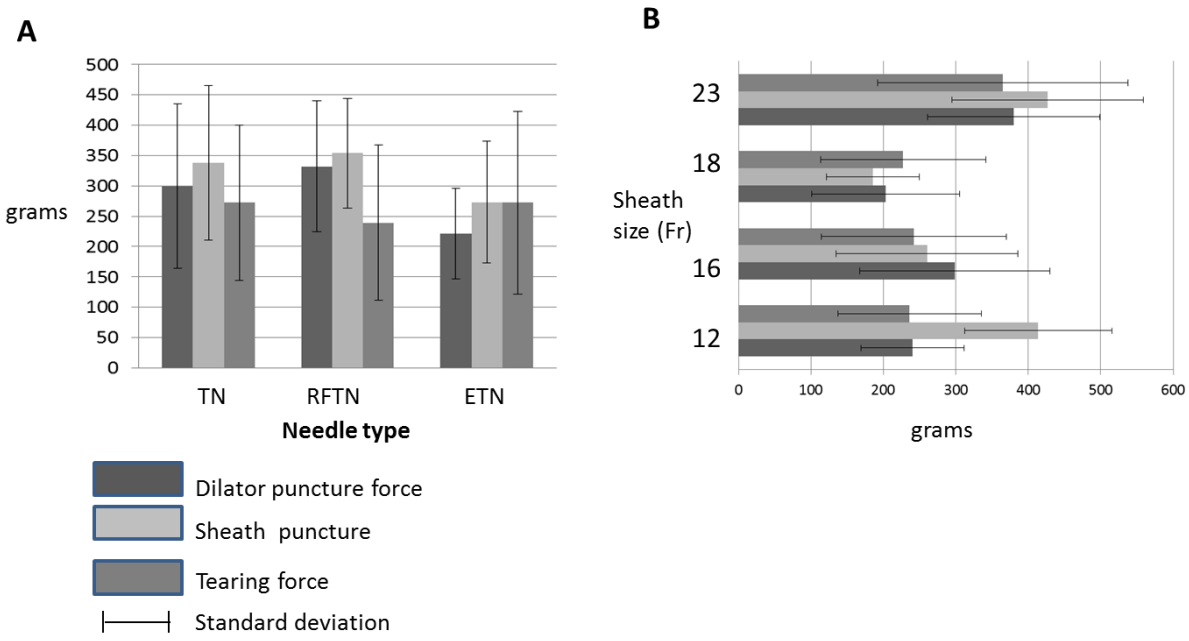

Figure 14. (A) Force data (in grams) for all tearing and puncturing by needle type: transseptal needle (TN), radiofrequency TN (RFTN), or 5-Fr RF electrode with the tip of a TN (ETN). (B) Force data (in grams) for all tearing and puncturing by sheath size: 12-, 16-, 18-, or 23-Fr.

To analyze the results, we first divided all data points into subgroups by needle type (TN, RFTN, and ETN). For those 3 subgroups, we calculated the mean and standard deviation (SD) for the dilator (TN, 299.5±135.3; RFTN, 332.1±107.6; and ETN, 221.1±74.7 grams), sheath size (TN, 337.8±126.9; RFTN, 353.9±90.2; and ETN, 272.9±100.4 grams), and tearing force (TN, 272±128; RFTN, 239±128; and ETN, 272±151 grams) independent of sheath size (Figure 14A). Next, we divided all data points into subgroups by sheath size (12-, 16-, 18-, and 23-Fr). For these 4 subgroups, we calculated the mean and SD for the dilator (12-Fr, 240.4±71.3; 16-Fr, 298.8±131.3; 18-Fr, 202.7±102.01; and 23-Fr, 379.8±118.9 grams), sheath size (12-Fr, 413.7±101.4; 16-Fr, 260.2±125.5; 18-Fr, 185.4±64.3; and 23-Fr, 426.9±132.1 grams), and tearing force (12-Fr, 236±9; 16-Fr, 242±128; 18-Fr, 227±114; and 23-Fr, 365±173 grams) independent of needle type (Figure 14B).

FO puncturing

Our study produced a total of 81 FO punctures from 81 specimens. We first analyzed puncture force across all sheath sizes by the 3 components (needle, dilator, sheath) of the delivery system (Figure 15A). Then we calculated the mean and SD of each of the 3 devices across all sheath sizes (TN, 300.7±163.1; RFTN, 207.6±139.4; and ETN, 181.8±93.5)(Figure 15B). The puncture force for the 2 RF-based methods (RFTN, ETN) was significantly less than for the TN (RFTN vs. TN, P=0.03; ETN vs. TN, P = 0.004). Finally, we examined the puncture force of each paired dilator/sheath combination. In our analysis of all 81 specimens, we found no relationship between the dilator and sheath puncture force (R^2=0.29)(Figure 15C).

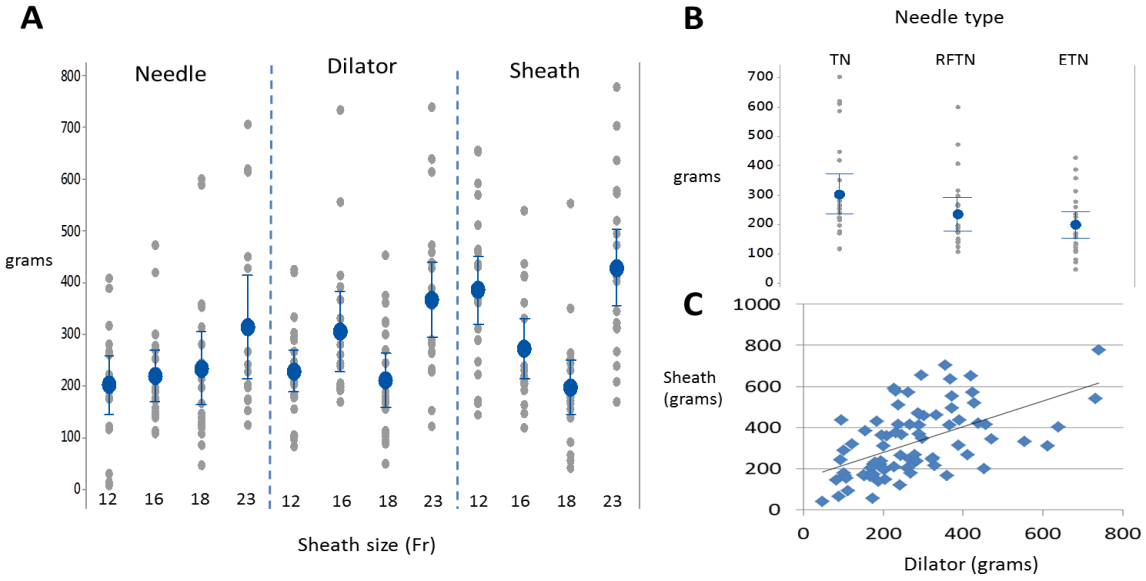

Figure 15. (A) Mean puncture force and standard deviation (in grams) for the needle, dilator, and sheath by sheath size (for all specimens). (B) Mean puncture force and standard deviation (in grams) by needle type: transseptal needle (TN), radiofrequency TN (RFTN), or 5-Fr RF electrode with the tip of a TN (ETN) (for all specimens). (C) Relationship between dilator and sheath puncture forces with an overall R^2 of 0.29.

Next, we grouped all data points by sheath size (12-, 16-, 18-, and 23-Fr) and then placed them in subgroups by needle type (TN, RFTN, and ETN)(Figure 16). To determine any significant differences in the amount of force to cross the FO, we compared each of our delivery systems against the 12-Fr system, which is used extensively in transseptal applications. Using the TN, we found significant differences between the 12- and 18-Fr

sheaths (*P*=0.001) and between the 12- and 23-Fr dilators (*P*=0.003). Using the RFTN, all of the sheath forces were significantly different from the 12-Fr (16-Fr, *P*=0.003; 18-Fr, *P*=0.001; and 23-Fr, *P*=0.004). Using the ETN, we found significant differences between the 12- and 18-Fr sheaths (*P*=0.001) and between the 12- and 23-Fr dilators (*P*=0.05).

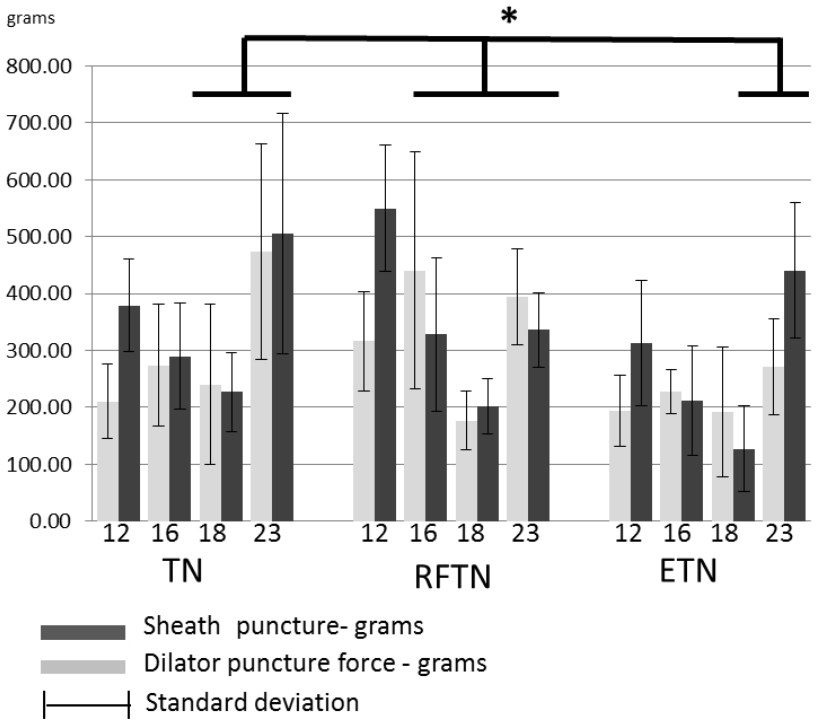

Figure 16. Mean puncture force and standard deviation (in grams) by needle type and sheath size. * *P*≤0.05

Given the specimen variation associated with inherent FO tissue properties, we performed an additional analysis; data were normalized to account for this variation. First, we normalized the puncture methods, using TN as the reference. By doing so, the mean force to cross the FO was not significantly different from the TN when using the RFTN (*P*=0.11), but the mean force was significantly different when using the ETN (*P*=0.01)(Figure 17A).

Second, we normalized sheath sizes. Using the 12-Fr as the reference point, we found that the force to cross the FO when using a 23-Fr sheath was significantly different

(*P*=0.005). However, we found no significant differences when using either the 16-Fr (*P*=0.09) or the 18-Fr sheath (*P*=0.30)(Figure 17B).

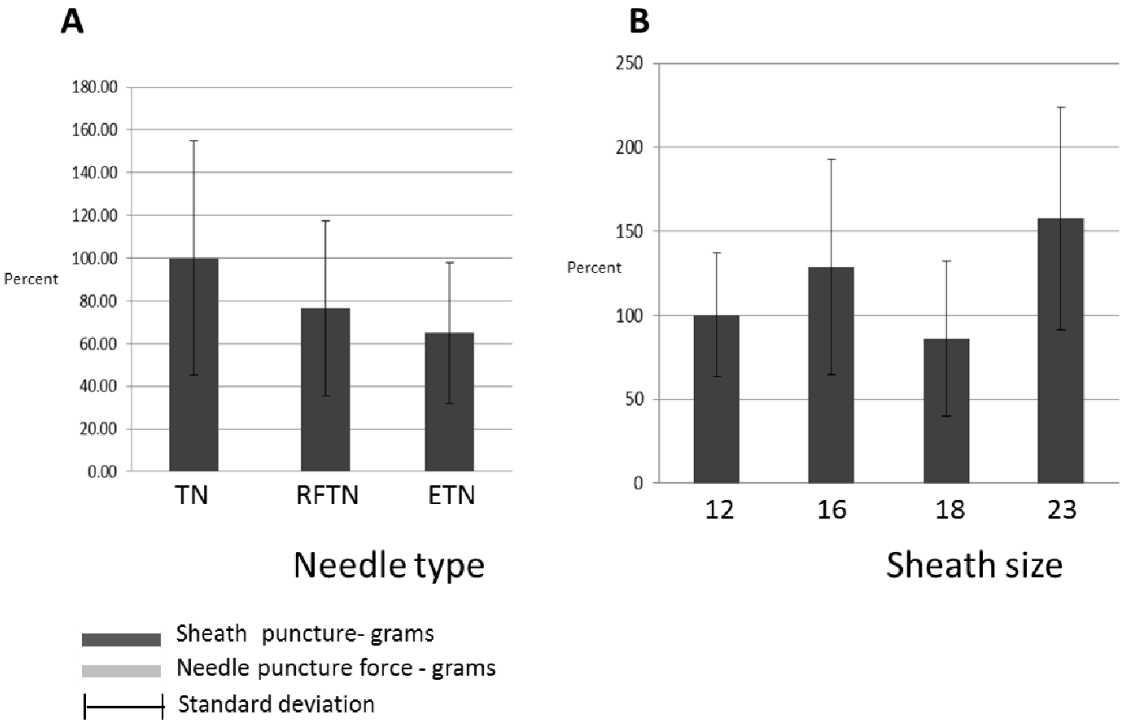

Figure 17. (A) Puncture force (in grams), with data normalized against the transseptal needle (TN) and 12-Fr size, *by needle type*: TN, radiofrequency TN (RFTN), or 5-Fr RF electrode with the tip of a TN (ETN). (B) Transseptal crossing force (in grams) *by sheath size*: 12-, 16-, 18-, or 23-Fr.

Septal tearing

The baseline septal tearing characteristics by needle type (Table 6) and sheath size (Table 7) are summarized. The anatomic measurements of the FO, by sheath size and needle type, are presented in Table 8. The baseline FO characteristics by needle type (Table 9) and by sheath size (Table 10) are also provided in tabular form. We found a statistically significant difference between the tearing force of the 23-Fr sheath as compared with the 12-, 16-, or 18-Fr sheaths (Figure 15). However, needle type had no statistically significant impact on tearing initiation distances or on mean or peak tearing forces (*P*>0.05).

Table 6. Baseline tearing characteristics by needle type

	TN	RFTN	ETN	

	(n=26)	(n=28)	(n=32)	*P*
Tearing initiation distance (mm)	7.5±3.2	6.8±3.1	5.8±2.7	0.068
Mean tearing force (gf)	272±128	239±128	272±151	0.55
Peak tearing force (gf)	360±173	306±161	372±208	0.33

ETN=5-Fr RF electrode with the tip of a transseptal needle; RFTN=radiofrequency transseptal needle; TN=transseptal needle

Table 7. Baseline tearing characteristics by sheath size

	12-Fr (n=23)	16-Fr (n=23)	18-Fr (n=21)	23-Fr (n=19)	*P*
Tearing initiation distance (mm)	6.7±2.7	6.0±2.4	7.0±3.7	6.4±3.1	0.72
Mean tearing force (gf)	236±99	242±128	227±114	365±173	0.002
Peak tearing force (gf)	308±138	312±157	296±139	515±233	<0.001

Table 8. Anatomic measurements of the fossa ovalis

	TN	RFTN	ETN	*P*
12-Fr				
SI length (mm)	13.5±2.8	11.6±3.7	15.7±4.1	0.56
AP length (mm)	7.2±2.6	7.8±2.4	7.07±2.05	0.89
Thickness (mm)	0.39±0.3	0.5±0.1	0.32±0.1	0.14
16-Fr				
SI length (mm)	12.9±3.5	15.3±2.9	13.7±4.6	0.47
AP length (mm)	8.6±4.9	7.1±5.3	7.7±2.2	0.89
Thickness (mm)	0.5±0.1	0.6±0.3	0.5±0.1	0.75
18-Fr				
SI length (mm)	15.3±3.3	14.5±4.4	13.9±2.1	0.87
AP length (mm)	8.3±3.4	7.9±2.6	8.3±2	0.94
Thickness (mm)	0.4±0.1	0.6±0.3	0.3±0.1	0.11

23-Fr				
SI length (mm)	12.4±4.5	13.5±1.3	17.0±7.1	0.45
AP length (mm)	6.9±3.3	8.2±1.8	10.1±5.6	0.42
Thickness (mm)	0.4±0.1	0.4±0.1	0.29±0.26	0.25

AP=anterior/posterior length; ETN=5-Fr RF electrode with the tip of a transseptal needle; RFTN=radiofrequency transseptal needle; SI=superior/inferior length; TN=transseptal needle.

Table 9. Baseline fossa ovalis characteristics by needle type

	TN (n=26)	RFTN (n=28)	ETN (n=32)	*P*
SI length (mm)	11.8±2.3	14.4±4.5	13.2±2.5	0.01
AP length (mm)	5.8±2.2	8.6±4.5	7.8±2.0	<0.001
Thickness (mm)	0.8±0.5	0.9±0.7	0.9±0.3	0.58
Heart weight (grams)	387±81	415±110	376±74	0.22

AP=anterior/posterior length; ETN=5-Fr RF electrode with the tip of a transseptal needle; RFTN=radiofrequency transseptal needle; SI=superior/inferior length; TN=transseptal needle.

Table 10. Baseline fossa ovalis characteristics by sheath size

	12-Fr (n=23)	16-Fr (n=23)	18-Fr (n=21)	23-Fr (n=19)	*P*
SI length (mm)	13.3±3.2	12.6±2.7	12.7±3.6	14.2±3.6	0.37
AP length (mm)	7.7±3.6	7.3±3.0	7.3±2.2	7.8±3.0	0.92
Thickness (mm)	0.8±0.4	1.0±0.6	0.9±0.5	0.8±0.5	0.49
Heart weight (grams)	379±109	408±80	391±89	389±79	0.75

AP=anterior/posterior length; SI=superior/inferior length.

Anatomy for puncture

The variation in anatomy among our specimens affected both the FO puncturing process and the septal tearing forces.

FO puncturing

Overall, we found only a narrow variation in the FO thickness of our specimens (0.46±0.07 mm). We found no statistically significant relationship between FO thickness and the type of device used (R^2 for TN, 0.001; ETN, 0.005; and RFTN, 0.11). In addition, we analyzed the relationships between sheath size (12-, 16-, 18-, or 23-Fr) and FO anatomic measurement by needle type, but found no statistically significant differences (Table 5).

Septal tearing

We collected anatomic measurements for all of the specimens used for tearing, to determine any relationship between anatomy and tearing resistance, but found none. We found a statistically significant difference when each method of puncture was compared against the superior/inferior length (P=0.01) the anterior/posterior length (P<0.001)(Table 6). No other statistically significant differences were found. Although samples were randomized, there was a significant difference between anterior/poster and superior/inferior width for the needle groups (P<0.05)

Discussion

Our 4 main findings were as follows: (1) In the case of 16- and 23-Fr sheath systems, the force required to cross the FO is higher than for a 12-Fr system; (2) when comparing the 3 types of devices, the ETN significantly differed from the TN, but the RFTN did not; (3) with the 23-Fr sheath size, the FO's tearing resistance was significantly higher than the other sizes; and (4) between the 12-, 16-, and 18-Fr sheath sizes, the FO's resistance to tearing did not significantly differ.

FO puncturing

When comparing the TN with the RFTN, the TN resulted in lower transseptal crossing forces of the dilator and sheath with the smaller 12- and 16-Fr systems, and the RFTN resulted in lower transseptal crossing forces with the 18- and 23-Fr systems. The use of the larger ETN resulted in lower mean transseptal crossing forces with the 12-, 16-, and 18-Fr systems. It is possible that the RF lesion created by the ETN enabled the dilator and sheath to cross with greater ease, an occurrence also observed with the RFTN.

The dimensions of the dilators and sheaths might contribute to differences in force by delivery system size. The variation in forces by delivery system size and by needle type may be due to the unique design of each dilator. Additional work is necessary to optimize dilator tip design. Our data (normalized against the 12-Fr system) showed no significant differences in mean puncture forces with the 16- and 18-Fr systems. The lack of differences in normalized mean puncture force may be due to design elements such as tip contour or tolerance differences between each component of the delivery system.

Furthermore, when comparing all needle types by sheath size, FO thickness had no significant impact. However, the difference in FO thickness with the ETN subgroup was significantly smaller than with the other 2 devices ($P<0.05$). Our additional analysis comparing FO thickness and puncture force (grams) revealed, with all 3 needle types, the lack of a strong correlation between FO thickness and puncture force. Thus, the variable of FO thickness could be a confounding factor. In future studies, a broader selection of same-size devices is warranted, in order to explore the variation from device to device within a particular size.

It is important to note that during transseptal punctures with the 5-Fr electrode needle (i.e., with the ETN), in some specimens, we observed steam pops when using a power setting of 30 watts. The use of RF energy might cause the tissue temperature to increase, resulting in dielectric breakdown and vaporization of the fluid, damage to the adjacent tissue, and release of the contents as a steam pop. In our observations, the amount of power applied exceeded the amount required to cause rupture, and resulted in fluid

vaporization near the tip of the catheter. With the optimization of applied power and temperature settings, it may be possible to control the energy delivery and eliminate this phenomenon; the literature suggests that tuning ablation parameters can minimize steam pop occurrences [39].

These results indicate that additional studies of a larger RF-based device might yield improvements in reducing the amount of force required to perform transseptal punctures. The lack of a significant difference between the normalized mean puncture force of the TN and RFTN could be associated with the amount of power delivered or with insufficient time exposure of the tissue subjected to the RF (given the effects of mechanical force of the needle against the tissue). Anatomic variation of FO size and thickness may contribute to variation in the forces for FO puncturing and septal tearing. Using the TN as a baseline, we found that either the ETN or RFTN led to comparable or better results—evidence that all 3 devices perform similarly. A chronic study is required with several months of follow-up to examine the post-procedure recovery of the FO and to investigate the post-procedure healing of punctures performed by both mechanical and RF methods.

Septal tearing

We observed significant differences in septal tearing properties by sheath size; our results correspond with previous investigations [31]. It appears that a critical sheath diameter exists at which tearing forces dramatically increase (Figure 18). As new procedures continue the trend toward larger catheter sizes to reduce septal tearing, the initial puncture holes created are still of concern. Yet, the clinical implications of iatrogenic atrial septal defects remain to be clinically determined. It is important to note that some physicians are already using closure devices to treat these defects [40].

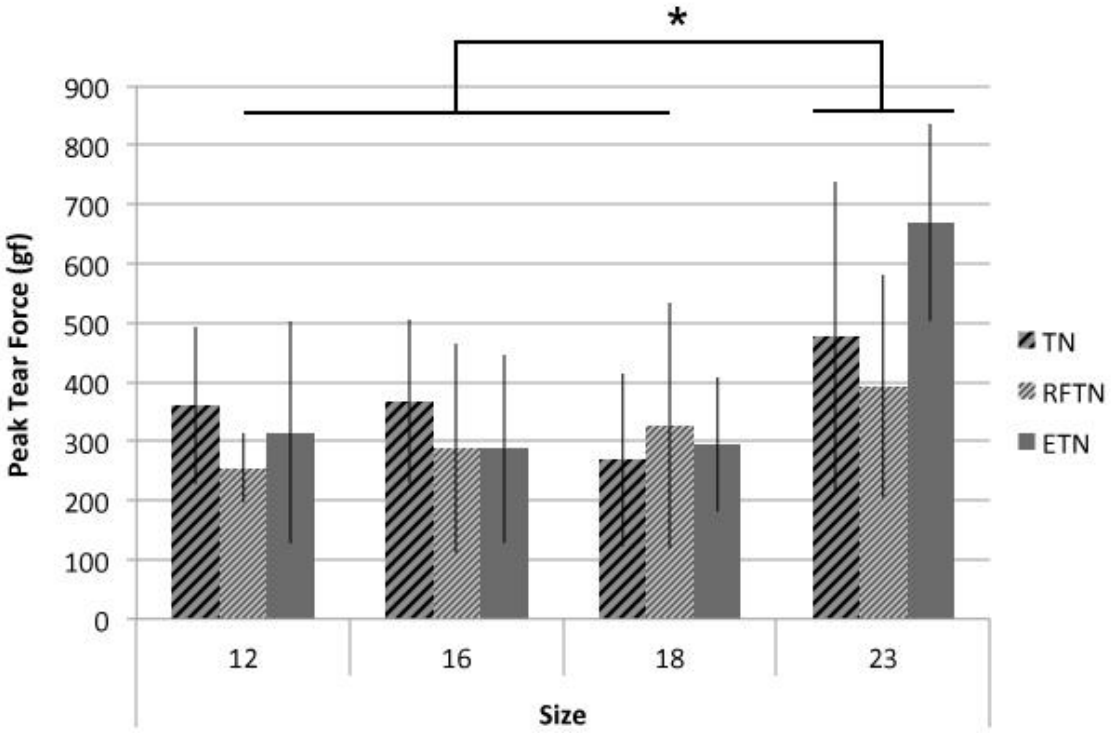

Figure 18. Peak septal tearing forces by sheath size: 12-, 16-, 18-, or 23-Fr. The only significant difference occurred when using the 23-Fr sheath, as compared with the other 3 sizes. *P<0.001

Regardless of the needle type (TN, RFTN, or ETN), we found no statistically significant differences in the tearing forces with the 12-, 16-, and 18-Fr systems. This finding suggests that, on an acute scale, no single technology has demonstrated a clear reduction in iatrogenic atrial septal defect size. Someday, technologies may facilitate tissue remodeling resulting in better closure. Future investigations are needed to determine whether or not transseptal punctures aided by RF will generate better natural closure in the long term.

Additional work is needed to better understand the ETN and to account for variations in anatomic differences. Opportunities also abound to further investigate different iterations of the ETN that may perform better than the one used in this study.

Study limitations

In our analyses of the septal tearing tests, we assumed that the surrounding anatomy of the FO had little impact on the observed forces. Depending on the pertinent anatomy targeted in the procedure, catheter torquing might be amplified, resulting in changes in tearing forces. An in vivo study or a biomechanical model examining this behavior would aid in identifying the importance of other factors relative to septal tearing.

In addition, our study focused on transseptal elements at the time of puncture. Additional work is needed to study the residual hole that is formed, including a safety study to examine FO healing. Although our study found no statistically significant difference by needle type and FO thickness, additional work is needed to study the interactions between device size and anatomic variation in FO thickness and size. Finally, the ability to perform similar studies on fresh tissue isolated from human hearts would be ideal; such studies are ongoing in our laboratory, but it will take time to acquire the necessary specimens.

Conclusion

Using a range of devices and catheter sizes, we investigated the relative puncture and tearing forces required to perform transseptal punctures and FO tearing. Normalized mean puncture forces using the TN and RFTN were not significantly different.

Additional studies aimed at reducing septal puncturing and tearing forces are needed, optimizing designs by refining not only the shapes and sizes of delivery systems but also the power utilized. Solutions must be found to improve the safety of transseptal punctures.

Acknowledgments

This work was done in collaboration with all listed co-authors along with the editing support of Dr. Mary Knatterud.

Section 2 Effects of Radiofrequency and Cryothermal Ablations on Cardiac Tissues

This section of my thesis focuses on investigations related to complications that may primarily arise during the applications of radiofrequency or cryothermal ablations. Complication rates as high as 4-6% has been reported for such cardiac ablation procedures [41,42], and this leaves extensive opportunities for future improvements relative to the safeties and/or efficacies of such procedures. To focus even further our investigations concentrated on complications that are initiated on an acute time scale. For example, following the transseptal puncture necessary for radiofrequency ablation procedures to be performed on the left side of the heart, catheters often need to be maneuvered extensively to reach various target locations. Typically, the clinician must carefully position lesions and connect these focal lesions to ensure that aberrant electrical signals are isolated. Mapping catheters connected to electrical mapping systems and fluoroscopy aid electrophysiologists in guiding catheters to their desired locations. Unfortunately, these visualization techniques have a number of limitations when one hopes to minimize associated complications with such applied procedures: one cannot directly visualize the ongoing response of catheter manipulation of the septal anatomical structures.

Furthermore, in an effort to ensure transmural lesion generation, clinicians will often attempt to increase contact forces to catalyze proper lesions. These applied forces may in turn add additional strain to the fossa ovalis, which is transeptally supporting the catheters and thus this may even increase the risks for eliciting cardiac tamponade due to subsequent cardiac perforations. Additionally, during procedures utilizing radiofrequency energy delivery, there are risks for the elicitation of steam pops; these explosive events are dependent on an array of not well-understood parameters, many of which correlate with the creation of transmural lesions. Interestingly to date, the cryothermal tolerances of cardiac tissues had lacked characterization: yet over-delivery of this energy may cause

phrenic nerve injury while its under-delivery hinders the development of transmural lesions. Nevertheless still today, identifying the optimal clinical dose delivery remains a challenge for both commonly employed ablation modalities. However, a better understanding of the biomechanical changes associated with these ablation modalities is essential knowledge needed in order to reduce the occurrence of complications. Delivering the appropriate ablative dose with minimal adverse effects is nontrivial, and in the following translational studies was performed to investigate a large number of associated factors and their roles in reducing the incidence of such complications.

Optimal Contact Forces to Minimize Cardiac Perforations Before, During and/or Following Radiofrequency or Cryothermal Ablations

Published in *Heart Rhythm*, **12**(2), pp. 291-296, 2015.

Stephen G. Quallich, BS[1,2]; Michael Van Heel, BS[3]; Paul A. Iaizzo, PhD[1,2]

[1] Department of Biomedical Engineering, University of Minnesota, Minneapolis, MN
[2] Department of Surgery, University of Minnesota, Minneapolis, MN
[3] Department of Mechanical Engineering, University of Minnesota, Minneapolis, MN

Conflicts of Interest: Research contract with Medtronic, Inc.
Financial Support: This study was funded, in part, by Medtronic, Inc. (Minneapolis, MN, USA)

Preface

During cardiac ablation procedures, the atria may undergo forces that occasionally exceed their physical limits, and when these boundaries are surpassed perforation may occur and as a consequence life threatening cardiac tamponade may arise. While maneuvering catheters and applying required ablative energies there are risks for inducing perforations. This is especially important to consider during radiofrequency ablative procedures, where often higher contact forces are used to ensure the generation of transmural lesions. It has been reported that radiofrequency therapies require less contact force to perforate the atrial wall. This study provides invaluable data for both clinicians and device designers so to compare the contact forces required to perforate ablated swine and human atrial tissues. Both radiofrequency and cryothermally ablative procedures were performed across a range of employed catheter sizes: the obtained date

helps to better define the boundaries of acceptable contact forces that may be applied clinically before complications occur.

I was responsible for the study design, data and statistical analyses and the initial draft of the manuscript. Mike Van Heel aided in the collection of swine experimental data. The preliminary findings of this study were presented at the American College of Cardiology (ACC) in Washington, DC in March 2014. Ongoing research is being conducted in the Visible Heart Lab to further assess the contact forces required for perforations in human hearts that had been prior diagnosed to elicit atrial fibrillation.

Summary

Background: Catheter perforations remain a major clinical concern during ablation procedures for treating atrial arrhythmias, and may lead to life-threatening cardiac tamponade. Radiofrequency (RF) ablation alters the biomechanical properties of cardiac tissue, ultimately allowing for perforation to occur more readily. Studies on the effects cryoablation has on perforation force, as well as defining the perforation force of human tissue are limited.

Objective: Investigate the required force to elicit perforation of cardiac atrial tissue following or during ablation procedures.

Methods: Effects of RF and cryothermal ablation on catheter perforation forces for both swine (n=83 animals, 530 treatments) and human (n=8 specimens, 136 treatments) cardiac tissue were investigated.

Results: Overall average forces resulting in perforation of healthy unablated tissue were 406±170g for swine and 591±240g for humans. Post-RF ablation applications considerably reduced these forces to 246±118g for swine and 362±185g for humans ($p<0.001$); treatments with cryoablation did not significantly alter forces required to induce perforations. Decreasing catheter sizes resulted in a reduction in forces required to perforate the atrial wall ($p<0.001$). Catheter perforations occurred over an array of contact forces with a minimum of 38g being observed.

Conclusion: We consider that the swine model likely underestimates the required perforation forces relative to those of human tissues. We provided novel insights related to the comparative effects of RF and cryothermal ablations on the potential for inducing undesired punctures, with RF ablation reducing perforation force significantly. These data are insightful for physicians performing ablation procedures as well as medical device designers.

Key Words: catheter ablation, cardiac tamponade, arrhythmia, cardiac perforation, RF ablation, cryoablation

Glossary of Abbreviations:
AF=atrial fibrillation
RF=radiofrequency

Introduction

Today, atrial fibrillation (AF) affects over 5.1 million people in the United States and, as the population continues to age, the incidence is expected to increase at least 2.5 fold by 2050 [43,44]. Recently, a complication rate of 4-6% was reported for catheter ablation procedures performed to treat AF [41,42]. These complications can be prompted by a number of factors, ranging from induced septal defects following transseptal punctures to perforation of the atria. More specifically, cardiac tamponade has been reported to occur in 1.3% of ablation procedures [41]. It is considered that complications may arise throughout these procedures due to a number of factors, such as transseptal punctures, adverse catheter maneuvers, or excessive contact forces during energy applications.

Perforation of the atrial wall during ablation procedures, which may lead to pericardial effusions and/or life-threatening cardiac tamponade, has only recently gained attention. Cardiac perforation is most common in AF procedures and occurs less frequently in other cardiac procedures [45]. It is suggested that perforations may result from employing high power usages and/or contact forces to ensure the creation of transmural lesions via

radiofrequency (RF) energies. Unfortunately, there are no comprehensive studies reported in the literature investigating the causes of cardiac tamponade during ablation procedures. Yet, it is important to note that even procedures like transseptal punctures are associated with a complication rate as high as 0.79% and cardiac perforation with tamponade in 0.11% of cases [7]. Further, it is known that mechanical perforations with diagnostic catheters have also been associated with cardiac tamponade. Interestingly, the presentation of pericardial effusion in RF and cryothermal ablation procedures is not significantly different [46]. Furthermore, patients with AF have been reported to have thinner atrial walls; this likely elicits circumstances that allow for perforations to occur even more readily [47]. Other important factors to consider during these clinical procedures include movements of the heart throughout the cardiac cycle as well as those due to respiration, as these can alter the applications of desired contact forces and provide added challenges for clinicians [48].

Additionally, it is regarded that the biomechanical properties are altered during the heating and cooling of tissues. For example, loss of pulmonary vein compliance and the denaturation of collagen occurs at temperatures of 60-65°C, yet elastin remains unchanged until reaching temperatures of 80°C [49]. During cryoablation structural proteins remain intact, although realignments occur due to ice crystal formations [50]. Therefore, better understanding of the required contact forces for proper lesion formation, while minimizing ruptures, may lead to reduced occurrences of cardiac tamponade. The studies we present here provide novel insights related to the biomechanical effects of RF and cryothermal ablations relative to the potential to induce punctures of cardiac atrial tissues. These studies could be considered as translational since we compared results for both isolated viable swine and human atrial samples.

Methods

Sample Preparation

Human heart specimens (n=8) were obtained from non-viable organ transplant donors through our local organ procurement organization LifeSource (St. Paul, MN, USA)

(Table 11): note these tissues were considered as viable, since these specimens were typically acquired and tested within 6-12 hours following explantation. It should also be noted that all non-AF heart had a non-dilated atrial pathology. Healthy 7 to 9-month-old Yorkshire Cross swine cardiac specimens (n=83; animal weight 75-110 kg; heart weight 400-650g) were acquired from the University of Minnesota Meat Sciences Laboratory and the Visible Heart Lab (waste tissue from unrelated experiments) and stored in saline prior to testing. Fresh atrial samples from the free wall (atrial appendage and atrial roof) were carefully dissected out.

Table 11.Human heart demographics

Heart #	Age (Yr)	Weight (kg)	Heart Weight	Gender	Cause of Death	Cardiac History
1	45	96	537	M	Cerebral vascular accident	Hypertension, Alcoholism
2	34	86	422	M	Cerebral vascular accident	None
3	62	73	456	F	Cerebral vascular accident	Hypothyroidism, Hyperlipidemia
4	52	74	401	F	Cerebral vascular accident	None
5	81	75	504	F	N/A	Atrial fibrillation, Mitral regurgitation
6	67	82	330	M	Bladder cancer	None
7	69	77	456	M	Chronic obstructive pulmonary disease	None
8	67	59	496	F	Chronic obstructive pulmonary disease	None

Atrial samples (n=666) were randomized to the following study groups: 1) no treatment, 2) RF ablation with a non-irrigated RF Marinr catheter (Medtronic, Minneapolis, MN) for 1 minute at 30 W with a temperature limit of 65°C, 3) RF ablation using the same parameters as #2, with induced perforation during the last 5 seconds of applied ablation, or 4) focal cryoablation with a Freezer MAX catheter (Medtronic) for 2 minutes (Figure 19). Cryoablated samples were permitted a sufficient amount of time for ice to thaw prior to the induced perforations. All samples were carefully anchored and submerged in saline before each ablative modality was applied. Each catheter was subsequently advanced at a rate of 500 mm/min with a mechanical force tester (Chatillon, Largo, FL, USA) until perforation occurred. An array of catheter sizes (5, 7, and 8 Fr) was also investigated in these experiments.

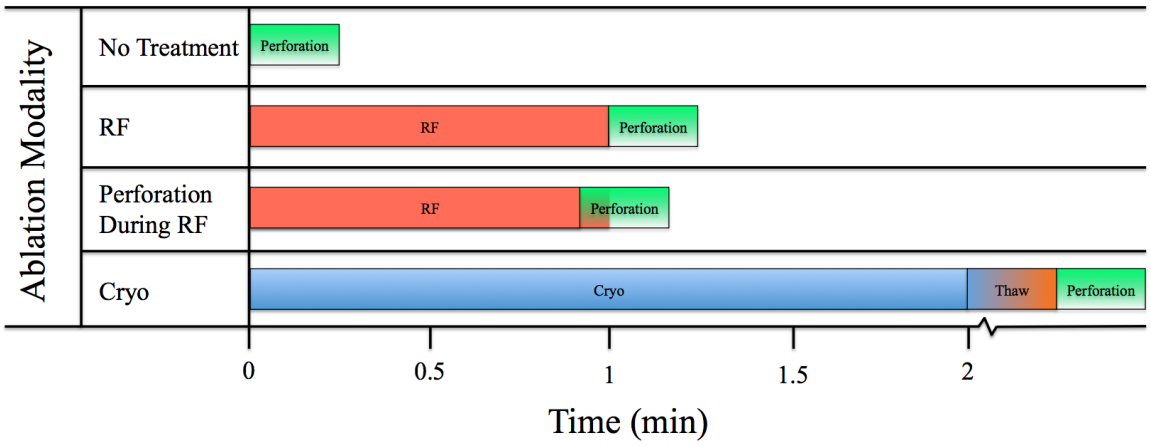

Figure 19. Graphical depiction of the treatment groups in relation to the application of ablation and the induction of catheter perforation. Cryo=cryoablation treatment; RF=radiofrequency treatment.

Data Analysis

The maximum force readings corresponding to the perforation forces were analyzed with Minitab (State College, PA, USA). All force values were reported as mean ± standard deviation. Student's *t*-test for one-to-one comparisons or analysis of variance (ANOVA) for the various study groups were used to compare normally distributed data. P-values ≤0.05 were considered significant.

Results

Catheter perforation forces for the right and left atrium were significantly different for the prepared human and swine tissue samples for all ablation groups investigated ($p<0.001$). Importantly, the required perforation forces for the RF-ablated samples were almost 2 fold less than those required for the cryoablated or untreated samples, as shown in Figure 20 ($p<0.001$). In other words, the cryoablation procedures appeared to have little or no effect on perforation forces when compared to the control (no treatment) group ($p=0.43$). The effects of perforation during RF ablations were minimal and not statistically significant compared to the other RF ablation group ($p=0.27$).

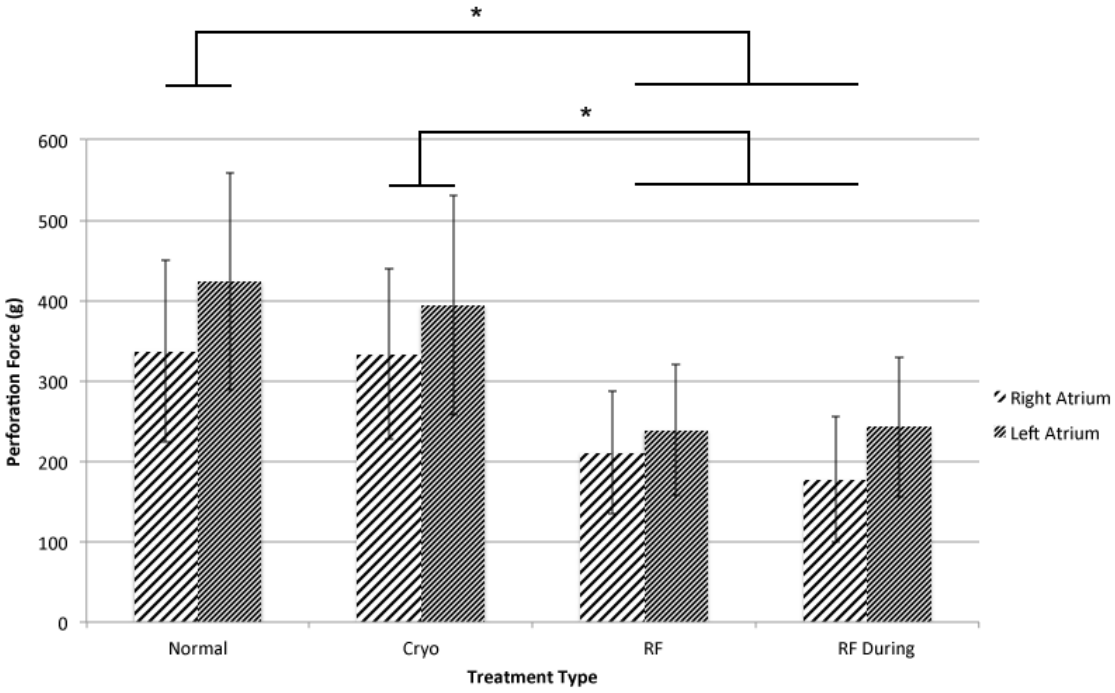

Figure 20. The perforation force for swine right and left atrium compared across different ablation modalities (*p<0.001). Perforation of the right atrium required substantially less force compared to the left atrium. Also, perforation following either radiofrequency (RF) ablation group entailed significantly less force than the cryoablated (Cryo) or the untreated (Normal) samples. Error bars represent STD.

A noteworthy observation was that catheter size was highly correlated with the likelihood to perforate the myocardium following or during an ablation. Smaller catheters required

lower forces to induce ruptures than larger ones for all ablation modalities and tissue types ($p<0.05$, Table 12); ablation modality effects with RF reducing perforation forces were also confirmed within each catheter size. Additionally, human atrial perforation forces were significantly different than those for the swine tissues (Table 13). Here we observed that the minimum forces to perforate ablated and healthy human atrium were 38 g and 57 g, respectively (Table 14). Similar minimum perforation forces of 63 g and 96 g for ablated and healthy swine atrium were also observed. It should be noted that the human atrial samples used in this experiment were from individuals without known histories of AF for all but one individual.

Table 12. Comparison of perforation force sorted by catheter size, tissue type, and ablation modality

		Ablation Modality	Perforation Force (g) 5 Fr	7 Fr	8 Fr	P-value
Tissue Type	RA	N	293±91	337±120	425±115	<0.001
		Cryo	318±124	333±106	412±141	0.033
		RF	214±76	209±79	294±134	<0.001
	LA	N	345±115	421±120	691±148	<0.001
		Cryo	451±109	394±106	699±155	<0.001
		RF	246±76	237±78	426±172	<0.001

RA=right atrium; LA=left atrium; N=no treatment; Cryo=cryoablation treatment; RF=radiofrequency ablation treatment

Table 13.Comparison of perforation forces between swine and human tissue sorted by ablation modality and tissue type

		Ablation Modality	Perforation Force (g) Swine	Human	P-value
Tissue Type	RA	N	337±120	545±238	<0.001
		Cryo	333±106	595±183	<0.001
		RF	192±78	386±186	<0.001

	LA	N	421±137	692±218	<0.001
		Cryo	394±136	668±278	<0.001
		RF	237±79	445±235	<0.001

RA=right atrium; LA=left atrium; N=no treatment; Cryo=cryoablation treatment; RF=radiofrequency ablation treatment

Table 14. Minimum perforation forces of swine and human tissue sorted by ablation modality and tissue type

		Ablation Modality	Perforation Force (g)	
			Swine	Human
Tissue Type	RA	N	96	57
		Cryo	104	98
		RF	63	38
	LA	N	187	149
		Cryo	131	258
		RF	67	62

RA=right atrium; LA=left atrium; N=no treatment; Cryo=cryoablation treatment; RF=radiofrequency ablation treatment

Discussion

Here we describe novel results from an in situ experiment designed to investigate the required force to elicit perforation of cardiac atrial tissue following or during ablation procedures. We employed a translational approach in which we studied both viable swine and human specimens. Perforation forces following or during RF ablation and in the control/no treatment group were similar to those reported in the literature, with RF ablation reducing the forces required to elicit perforation significantly [51,52]. In these previous studies, an individual user manually advanced the catheter until perforation occurred, whereas in this present study we employed a uniaxial testing machine to

automate the advancement of the catheter at a constant speed. In other words, in our testing methodology, the goal was to remove variations due to the operator. Interestingly, we observed that the minimum perforation forces were 63 g for RF atrial ablated swine tissue versus 96 g for healthy non-ablated tissue, while Shah et al. reported values of 40 g and 131 g respectively for swine atrial tissue [51].

To our knowledge, comparison studies relative to perforation forces following RF or cryothermal ablations have not yet been reported in the literature. Cryoablation did not alter perforation forces compared to untreated fresh tissue for both the swine and human tissue samples. It is important to note that we utilized fresh, viable tissue samples in these investigations. It was previously reported that frozen tissue samples typically are altered in the low stress state, with possible differences in other portions of the stress-strain curve [53]. Thus, any changes observed exist at the onset of force application and dissipate substantially as the applied force increases. It has been reported that freezing (the application of cryoablation) does not change the ultimate tensile strength or, if so, minimally [54,55]. This suggests that the forces required to perforate would be similar to those of native unablated tissue, which hold true for the results we present here.

RF ablation is considered to cause the denaturation of collagen as well as cell membrane disruption. Specifically, at high temperatures (60-65°C) collagen breakdown occurs [56]. It is also suspected that while physicians attempt to create transmural atrial lesions, heat will build up in the myocardium. Typically, an ablation console will only provide data on the catheter tip temperatures, and these are not representative of tissue temperatures. One can consider that thermal energy builds up transmurally within the myocardium, since the endocardial surface and catheter tip will be convectively cooled by the flow of blood through the heart. While ablating tissue to a minimum of 50°C to ensure the creation of a myocardial scar for a successful isolation procedure, (reaching temperatures of 60°C) the transition zone for collagen breakdown is not unforeseeable. A breakdown of collagen in the ablated myocardium will weaken it, explaining the reduction in the perforation force following RF ablation.

Catheter size is not often considered during ablation procedures, yet it is an important factor influencing the incidence of cardiac perforation. We found that utilizing a larger size catheter significantly reduces the risk of perforation. Even enlarging the catheter size by a single French often increases the required force for perforation. It is important to note that given the aggressive ablation parameters used, transmural lesions were observed for all catheter sizes. Thus, lesion size likely had minimal effect on the observed perforation forces since it encompassed a much greater volume than the catheters. Therefore, with similar tissue damage a smaller catheter will perforate more easily. This finding is intuitive when considered from a mechanic's perspective of the relationship between applied force, surface area, and resultant pressure. Implementing this knowledge regarding catheter size and punctures relatives to clinical procedures may reduce the occurrence of cardiac tamponade. Further research investigating the effects of catheter size on perforation force is needed to determine if these results can be extrapolated to larger than 8 Fr catheters.

Physicians quite often apply contact forces that exceed the lower limit perforation forces we described here, which increases the likelihood of complications. For example, Kuck et al. observed that during AF procedures, contact forces of over 100 g were recorded in 79% of patients with a high degree of inter- and intra-operator variability [57]. Importantly, high contact forces are not only detected during ablations but also throughout these cardiac procedures, such as with catheter manipulations and the relative movement of the heart associated with contractions and/or respiration. It should be noted that extensive catheter manipulation on the left side of the heart (via a transseptal puncture) also increases the risk for formation of iatrogenic atrial septal defects [58]. Additionally, transseptal punctures account for some portion of cardiac tamponade cases, so diagnostic and ablation catheters are not its only cause. Furthermore, high contact forces also increase the risk for either elicitation of steam pops and/or thrombus formation [59,60]. This underlies the need for force sensing catheter technologies, along with greater physician awareness of acceptable contact forces. It is important to note that

average contact forces below 10 g have been reported to result in higher incidences of AF recurrence, while contact forces above 20 g lowers the likelihood of such incidences [61]. This suggests that a lower bound for contact force of 20 g exists, thus facilitating successful ablation procedures. Defining the upper boundaries of applied ablative contact forces will be a step forward in reducing related complications like cardiac tamponade. Note again the minimum forces for perforation of human tissue (37 and 57 g for ablated and healthy atrium respectively) and the average forces to perforate (386 and 545 g for ablated and healthy atrium). Hence we suggest that contact forces below 50 g should greatly reduce the occurrence of cardiac perforations and/or tamponade. Perhaps a "sweet spot" of 20-50 g would be the ideal contact force range that physicians should aim to apply in order to achieve successful procedures that do not result in recurrences while ensuring minimal risk of cardiac perforations.

Minimal human heart availability, the in vitro nature of experiment, and the inability to measure tissue temperatures were the major study limitations. Measurement of tissue temperatures in this experimental paradigm would have compromised the biomechanical properties of the cardiac tissue. However, transmural tissue temperatures would allow for a more accurate analysis of the interplay between ablations, temperatures, and biomechanical properties of the cardiac specimens. In addition, conducting an in vivo assessment of perforation forces would aid in the clinical applicability, but add in cofounding factors the authors desired to remove, such as variations due to the operator. The use of non-irrigated ablation catheters and inability to measure the compressive force during tissue anchoring are also important limitations to note. Furthermore, several of the human specimens were stored in saline for up to 24 hours as immediate testing was unfeasible. It is important to consider that these punctures were performed in non-beating tissue and not in intact hearts. Also, limited human heart availability for research was anticipated, so swine hearts were used instead to approximate the biomechanical properties of cardiac tissue. The available human tissue included only one individual with a history of AF, which restricts the ability to elucidate significant findings for AF patients. Unfortunately, the swine hearts lack thinner atrial walls like the typical AF

patient, so a direct translational comparison to the patient population of interest is restricted in nature. This highlights the need for further studies on human tissue with a history of AF.

Conclusion

Importantly, cryoablation did not result in statistically significant reductions in the contact forces required to perforate atrial tissues. In contrast, applied RF ablations elicited reductions in the forces required to perforate these tissues. This is the first study to investigate perforation forces during RF ablations and following RF or cryothermal ablation, as well as the impact of catheter size. We consider that the data presented here should be of substantial interest to clinicians, as it may help define an ideal contact force range for minimizing the occurrences of cardiac tamponade while still promoting transmural lesion generation.

Clinical Perspective

The aim of this study was to define the contact forces required to elicit perforations of the cardiac atrial walls during and following RF and cryothermal ablations. Subsequently, the authors propose that contact force ranging between 20-50 g be applied during ablations to minimize AF recurrences and limit the incidences of cardiac perforations. Furthermore, following RF ablations perforations were induced at lower contact forces when compared to non-ablated tissues. In contrast, the application of cryoablation did not reduce the required perforation forces. The selection of catheter size was also identified as a principal factor altering required contact forces to elicit perforations after transmural lesions were induced: interestingly smaller catheters increased the risks for perforations. Translational investigations of contact forces to induce perforation following RF or cryothermal ablation and the effect of catheter size are currently absent in the literature. Nevertheless during clinical procedures, physicians often exceed the minimum thresholds of contact force to cause perforations. It is considered here that increased awareness of these contact force boundaries and their implementations into clinical settings should greatly reduce the occurrences of cardiac perforations or tamponade associated with

ablation procedures. In other words, the knowledge herein and potentially the usage of force sensing catheter technologies have the potential to improve clinical outcomes during cardiac ablative procedures.

Acknowledgements:

The authors would like to express their gratitude to LifeSource as well as the organ donors and their families for the hearts used in this research. The authors would also like to thank Monica Mahre for preparation of this manuscript.

Identifying the Radiofrequency Ablation Parameters That Can Induce Steam Pops

Submitted to *Heart Rhythm*, in review.

Stephen G. Quallich, BS[1,2]; Paul A. Iaizzo, PhD[1,2]

[1] Department of Biomedical Engineering, University of Minnesota, Minneapolis, MN
[2] Department of Surgery, University of Minnesota, Minneapolis, MN

Preface

During the delivery of radiofrequency energy to tissues, overheating may occur leading to the vaporization of fluid and/or the release of air/tissue emboli. These explosive steam pops events are believed to be associated with serious complications, such as cardiac tamponade, stroke, and/or myocardial infarction. The current literature acknowledges that this phenomenon occurs, but little has been done to understand the factors facilitating their elicitation. Oftentimes in an effort to encourage transmural lesion formation, power and temperature settings are pushed to undesirable or recommended limits. In this study we investigated a variety of parameters to identify how steam pops could be avoided in future clinical setting. Power, temperature, irrigation, catheter contact angle, and/or surface area contacts of employed catheters were associated with popping events. Ultimately the findings from this investigation could aid in improving patient outcomes and procedural safety: i.e., risky ablation parameters were classified and acceptable limits were defined.

I was responsible for the design of experiments, data and statistical analyses, and composition of the draft of this manuscript. The preliminary results from this study were orally presented at the Design of Medical Device (DMD) Conference at the University of Minnesota, in April 2013.

Summary

Background: It is known that during cardiac ablative procedures excess heating can lead to the generation of steam pops. This phenomenon causes the release of energy in the form of tissue and/or air emboli as well as can attribute to the elicitation of serious complications.

Objective: Investigate the parameters thought to be associated with the elicitation of intracardiac steam pops and to visualize their relative impacts.

Methods: Employing Visible Heart methodologies, we utilized 22 reanimated swine hearts to directly visualize the occurrences of steam pops. The effects of various factors including applied power, temperature, usage of irrigation, location, repeat ablation sites, amongst others were investigated with regards to their manifestation (n=539 ablations).

Results: The elicitations of steam pops were significantly increased with power application above 40 W for both non-irrigated and irrigated ablative applications ($p<0.005$). Catheter contact angles perpendicular to the tissue as well as greater surface area contacts of a given catheter both significantly increased the occurrences of steam pops ($p<0.05$). Minimum temperatures of 52°C for non-irrigated and 40°C for irrigated procedures were required for steam pop generation, and their incidences were typically observed 30±17 seconds into a given ablation application. Interestingly, the anatomical location within atria and if a site had been previously ablated did not effect steam pop elicitation.

Conclusion: While performing radiofrequency ablations it is important to acknowledge the effects of power, temperature, irrigation, catheter contact angle, and surface area contact of the employed catheter on the potential to elicit steam pops. Accounting for these parameters improves the possibility to reduce steam pops and their associated complications.

Introduction

Radiofrequency (RF) ablations are routinely performed to treat patients with cardiac arrhythmias. Currently, atrial fibrillation (AF) make up the majority of those treated by ablations, as this disease affects over 5 million Americans [43]. The safeties and

efficacies of ablative procedures are comparable between RF and cryothermal ablations, yet complication rates as high as 4.5% were recently reported [41,62]. Noteworthy, cardiac tamponade, transient ischemic attack, and stroke have occurred in such patients at rates of 1.31%, 0.71%, and 0.23%, respectively [41]. Commonly during RF ablations, cardiac tissue must be heated to temperatures of at least 50°C to ensure transmural myocardial scar formations at the target sites [56]. Unfortunately when excessive heating occurs blood may be vaporized and steam pops can be generated. It is important to note that the catheter tip temperatures which are provided as feedback to clinicians typically vary from the actual endocardial tissue temperatures: i.e., because of convective blood flow and/or the usage of catheter irrigation. Furthermore, it has been reported that the use of irrigation allows for both the generation of larger lesions with fewer occurrences of steam pops [63]. Nevertheless, with all clinicians aiming to create transmural lesions with their radiofrequency ablation procedures and the relative disparities of resultant tissue temperatures, this will continue to create circumstances facilitating the elictitation of steam pops.

The occurrences of steam pops associated with RF ablations may be quite damaging, potentially causing perforation of the atrial wall, release of tissue fragments, release of coagulum and/or air bubble generation [64,65]. The relative portions of complications associated with RF procedures that steam pops contribute to is currently unknown: yet such may induce cardiac tamponade, stroke, and transient ischemic attack. These phenomenon may occur extremely quick, within 10 ms, and are considered difficult to observe with fluoroscopy [66]. Previously, high contact forces have been correlated with significant increases in steam pop elicitation [59]. Additionally, it has been reported that lesion depth is associated with their occurrences, which suggests that factors increasing lesion depths facilitate their generation: e.g., temperature and applied power have been correlated with incidences [67,68]. To date, some of initiators for steam pop manifestation have been documented; yet, a comprehensive assessment is still lacking. The purpose of the present investigation was to further determine the parameters thought

to be associated with the elicitation of intracardiac steam pops as well as to visualize their relative impacts.

Methods

Hearts from 7 to 9-month-old Yorkshire Cross healthy swine (n=22; animal weights of 84.5±9.8 kg) were excised and reanimated using Visible Heart® methodologies.[69] In each heart, 7 Fr RF catheters (Medtronic, Minneapolis, MN) were introduced to various locations within both the right and left atrium and ablations (n=297) were performed. Additionally, irrigated ablations were also performed (n=242), with flow rates of ~17 ml/min. Contact angles of the catheters relative to the endocardial surfaces of the atria were visually determined (Figure 21), and if the catheter tip was surrounded by over 50% of the tissue this was also noted. Additionally, applied power, catheter electrode temperatures, and if a target site had previously been ablated were also recorded. This allowed for the investigations of a large number of parameters potentially associated with an increased incidence of steam pops. Their occurrences were verified both visually and audibly: i.e., one could see the release of gaseous and tissue emboli and occasionally hear such (Figure 22).

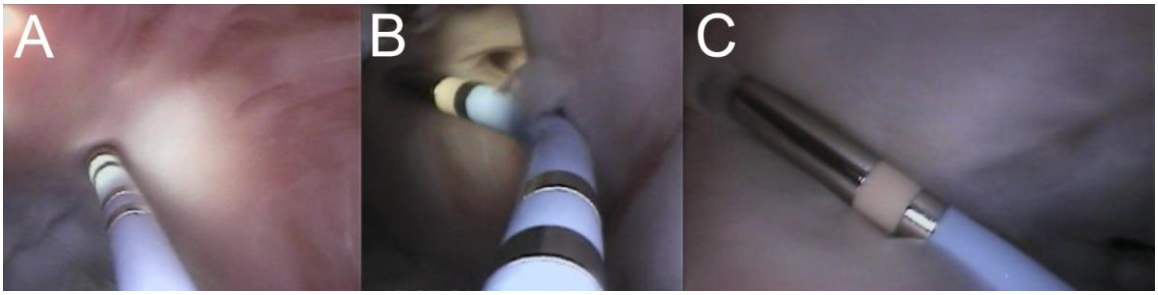

Figure 21. Different catheter contact angles relative to the atria were examined: perpendicular (A), parallel/perpendicular (B), and parallel (C).

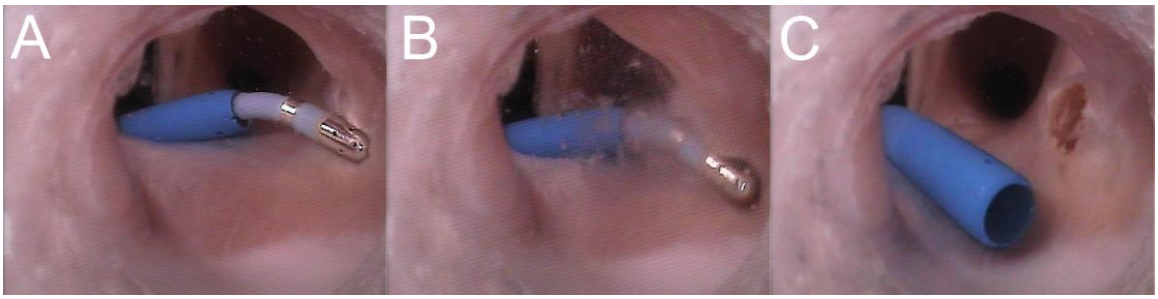

Figure 22. A 7 Fr RF catheter and 12 Fr FlexCath steerable sheath originating from the fossa ovalis are positioned near the left pulmonary vein ostia. The lesion before (A), during (B), and following (C) a steam pop may be observed as seen from an endoscope positioned within the left pulmonary vein.

The associated rates of occurrences and the related parameters were analyzed using Minitab (State College, PA). All values were reported as mean ± standard deviation. Regression analyses were initially used to identify parameters associated with steam pops and following this analysis of variance (ANOVA) was used to compare the isolated factors. P-values ≤ 0.05 were considered statistically significant.

Results

Steam pop incidence was significantly associated with power (Table 15). Only at applied powers of 40 W or greater were steam pops observed for both the applied non-irrigated and irrigated ablations. Furthermore, embedding the catheter tips in the tissue (invaginations/pectinate muscles) and/or catheter contact perpendicular to the atria were also significantly associated with steam pop initiation for the non-irrigated ablations: there was a similar trend for irrigated ablations (Table 16). In contrast, the relative location of elicited lesions and if a target sites had previously been ablated were not correlated with steam pop occurrences.

Table 15. Relationship of applied power with steam pop incidence for non-irrigated and irrigated ablations.

	Non-irrigated			
Power (W)	**Average Temperature (°C)**	**Number of Ablations**	**Steam Pop Incidence (%)**	**P-Value**
10-29	46	50	0	
30-39	50	40	0	
40-49	58	59	5	0.002
50	64	74	24	
51+	64	74	34	

	Irrigated			
10-29	44	46	0	
30-39	44	49	0	
40-49	46	51	16	<0.001
50	49	42	24	
51+	50	54	37	

Table 16. Relationship of embedded catheter tip and contact angle of the catheter with steam pop incidence for non-irrigated and irrigated ablations.

	Non-irrigated			Irrigated		
Embedded Catheter Tip	**Number of Ablations**	**Steam Pop Incidence (%)**	**P-Value**	**Number of Ablations**	**Steam Pop Incidence (%)**	**P-Value**
Yes	58	26	0.041	31	26	0.099
No	239	15		211	14	
Contact Angle of the Catheter Relative to the Atria						
Parallel	56	7		94	3	
Parallel/Perpendicular	77	13	0.022	67	19	<0.001
Perpendicular	164	22		81	27	

Steam pops typically occurred 30±17 seconds following the initiation of the ablative energies, and there were no significant timing differences of popping onset between the groups investigated. Noteworthy, a catheter tip temperature of at least 52°C for non-irrigated and 40°C for irrigated ablations were required to induce steam pops. Maximum average catheter tip temperatures were 77±14°C (non-irrigated) and 50±7°C (irrigated) during steam pop events and 60±15°C and 46±6°C respectively without them. In all cases, their occurrences were significantly correlated with temperature ($p<0.001$). Interestingly, the anatomic location of the catheter or if a site had previously been ablated had no impact on their relative formations.

Discussion

The results from this *ex vivo* experiment describe the parameters that may readily induce the formation of steam pops. We examined a large range of factors that may be associated

with the incidences of these events. It should be noted that a number of these initiators have been previously investigated: the influence of temperature, micro-bubble formation, impedance increases, and contact forces have been reported.[56,59,70] In general our data was consistent with these findings, however the aim of this study was to further examine a multitude of additional factors as they relate to steam pop formation.

Catheter contact angles relative to the atria endocardium has been associated with steam pop formation and/or cardiac tamponade: e.g., Nakagawa et al. reported that catheters perpendicular to the atrium were most likely to induce pops leading to cardiac tamponade [71]. It has also been hypothesized that steam pops that occur near the epicardial surface will more likely induce tamponade while those more directly on the endocardium may lead to the release of air and tissue emboli, potentially causing stroke or myocardial infarction [67]. Noteworthy in the present study, perpendicularly oriented catheters were more than threefold likely to generate steam pops than those positioned parallel to the endocardial surface.

Interestingly still today, the relative proportions of associated complications, such as stroke, myocardial infarction, and cardiac tamponade, that are considered in part due to steam pops remains uninvestigated. Yet, it has been reported that complications rates arising from transseptal punctures were as high as 0.79% with cardiac perforation in 0.11% of cases [7]. Furthermore, mechanical perforations with diagnostic and ablation catheters also accounts for some portion of cardiac tamponade cases. It was reported that mechanical perforation caused tamponade in 20% of cases and popping was responsible for 80% [68]. The minimum contact force required to perforate the atria is routinely exceeded during procedures with RF requiring less force than cryothermal ablations [57,72]. Nevertheless, it has been previously discussed that there remains a need for further investigations to elucidate the types and relative degrees of complications related to steam pops.

As anticipated in our study, power and temperature were significantly related to the elicitation of steam pops. Noteworthy, there appears to be a transition zone at power

levels above 40 W which significantly increased relative steam pop formations. Furthermore, Hsu et al observed that steam pop incidence was greater with higher power applications and only reported their occurrence at more than 48 W [68]. It should also be noted that high power usages have also been responsible for delayed complications like the formation of atrial-esophageal fistula [73,74]. Nevertheless, our results support the literature of a correlation between electrode temperature and steam pop incidence.[67] When considering this phenomenon from a heat transfer perspective, the effects of power and temperature produce expected reactions. As more energy is transferred to the system and as heat buildup reaches a threshold the fluid will be vaporized, and a steam pop will be elicited. Therefore, the ability to measure actual focal tissue temperatures would be of substantial benefit in reducing complications during ablation procedures while also improving efficacy.

Importantly, the application of irrigated radiofrequency ablations relative to steam pop incidence was quite similar to non-irrigated procedures, as shown in Table 15. Yet, the cooling power from irrigation was anticipated to reduce steam pop occurrences, since heat buildup in the tissue will be reduced at least on the endocardial surface. The temperature profile will be shifted, so that the point of maximum temperature will be deeper in the myocardium. In other words, irrigation was not effective at reducing steam pop incidences given similar other parameters. Although irrigation was able to reduce the catheter tip temperatures, recall again that this is not an accurate indication of tissue temperatures. Hence, irrigation may be effective at reducing the temperatures at the electrode tissue interfaces, but this does not obstruct the accumulation of energy within the tissues that may potentially be released in the formation of a steam pops. This supports the need for a better means of measuring tissue temperatures so to help ensure the creation of transmural lesions while also minimizing the manifestation of complications, such as steam pops. Interestingly, there has been recent development using acoustic signals and microwave radiometry to predict popping events and even using intracardiac echocardiography to monitor their incidence clinically [75–78].

A number of the parameters investigated here had no effects on steam pop incidences,

which may also be explained through heat transfer mechanics. For example, the authors were unable to identify literature comparing the thermal properties of the various anatomical regions of the atria. Perhaps it can be considered that the tissue types of the right and left atria are similar in nature. Thus, one would not have expected a substantial difference in their thermal properties, which would correspond with the results herein. In addition, a greater tissue surface area contact with the catheter tip should produce more efficient heat transfer, ultimately facilitating steam pop formation. When preforming a repeat ablation at a target site, heat transfer to the tissue remains unchanged. This supports the supposition that repeat ablations had little or no influence on steam pop initiations. It should however also be noted that repeat ablation sites in this study were allowed sufficient time to cool. In other words, if a repeat ablation was preformed immediately after at the same location, this finding may not hold true since there will be residual energy at the lesion site.

We consider here that it may be considered that the inability to use blood in our reanimated specimens and measure temperatures within the myocardium may be considered as study limitations. More specifically, modified Krebs-Henseleit buffer was used as a blood substitute to allow for visualizations, so direct comparisons to the clinical scenario may be somewhat reduced. However, heat transfer and fluid mechanics underlying this phenomenon remain consistent with a change of fluid. Unfortunately the use of blood would have obscured the detection of steam pops, since steam pop incidence in our study was validated with direct visualization. It should be reiterated that steam pops often create an audible pop, yet this is not always the case and may limit ones ability to detect such in other studies or in clinical situations. As noted above, measuring temperatures within the myocardium could further improve our understanding of the catheter-tissue temperature discrepancy as it relates to steam pop formation: we hope to do so in future studies, yet doing such may also modify native thermal properties. This highlights the need for clinical studies to investigate steam pops incidence and the complications that proceed them.

Conclusion

Importantly, applied radiofrequency ablative power and temperatures statistically significantly correlated with cardiac steam pop formations. Noteworthy, perpendicularly orientated catheters relative to the atria as well as catheters with greater tissue surface area contact were more likely to initiate such events. Additionally, repeat ablations at a lesion site and anatomical locations of the applied therapies in the heart were not correlated to steam pop occurrences. The use of irrigated ablation catheters were not effective at reducing steam pop generations, compared to non-irrigated procedures. We consider here that the data presented are of interest to clinicians, as it should improve awareness of factors associated with steam pop elicitation and hence aid in reducing complications associated with cardiac RF procedures.

Acknowledgements:

The authors would like to thank Monica Mahre for preparation of this manuscript.

Determination of Cryothermal Injury and Ablation Thresholds in Cardiac Tissues

Submitted to *Heart Rhythm,* in review.

Ryan P. Goff, PhD[1,2]; Stephen G. Quallich, BS[1,2];
Robert Buechler, MS[1,2]; Jeunghwan Choi, PhD[1,3];
John C. Bischof, PhD[1,3]; Paul A. Iaizzo, PhD[1,2]

[1] Department of Biomedical Engineering, University of Minnesota, Minneapolis, MN
[2] Department of Surgery, University of Minnesota, Minneapolis, MN
[3] Department of Mechanical Engineering, University of Minnesota, Minneapolis, MN

Preface

The relative tolerances of tissues to radiofrequency ablation are well established, however the effects of cryothermal therapies on the induced injury to cardiac tissues lack defined boundaries. The clinical outcomes of cardiac cryoablation have been well characterized in numerous studies, but there exists a substantial knowledge gap in the therapeutic dose responses with respect to therapeutic times, cooling profiles, and/or real-time tissue temperatures. We hypothesized that quantifying the expected viabilities and physiological responses of tissues, especially if used in conjunction with subsequently modeling efforts, would ultimately lead to more efficacious future applications, with reduced associated complications. For instance, injury to the phrenic nerves during cryoablation is a common occurrence, and the reported incidence is as high as 4% to 24%, with greater incidences for utilizations of the second-generation cryoballoon [79–86]. Therefore, this is an area where great improvements may be made: it is considered here, that the findings from this study will allow for future optimizations of cryoablation therapies, thus limiting collateral injury.

In this study Ryan Goff and I developed and ran the ablation protocols together, while I was often responsible for the subsequent staining and imaging of the tissue specimens post ablation. I also aided with significant contributions to the manuscript. Robert Bueschler was essential in developing the MATLAB code to analyze the dose, temperature, and cooling response on tissue viability. Jeunghwan Choi augmented the results of this study by performing the cell culture work. This work was also orally presented at Cryobiology in Bethesda, Maryland in July 2013. Others and I are continuing this work in the laboratory examining the effects of single, double, and triple freeze thaw cycles.

Summary

Background: Despite widespread and growing clinical use of cryoablation, there remain questions regarding dosing and treatment times, which may affect efficacy and collateral injury. The major clinical complication is phrenic nerve palsy, at rates of 4-8%.

Objective: To determine what cooling regimes lead to necrosis, injury, or recovery.

Methods: Human and swine atrial, ventricular, and lung tissue samples were ablated using two cryoablation systems with concurrent infrared thermography. Post freeze-thaw samples were cultured, then stained with triphenyltetrazolium chloride to differentiate viable and non-viable tissue. Viability staining to freeze-thaw injury was correlated, to determine thermal injury thresholds. Specifically, HL-1 cardiomyocytes were cultured and subjected to controlled freeze-thaw cycles using a cryo microscopy stage. Post thaw viability was determined using Hoechst/Propidium Iodide dye exclusion assay. Tissue data were classified as live, injured, or dead based upon staining intensity at the lesion margin.

Results: Thermal history at the transition was quantified, demonstrating that human and swine cardiac tissue injury begins at rates of ~10°C/min to 0°C with non-viable tissue, requiring cooling rates close to 100°C/min to ~-22°C for swine and significantly greater cooling to -26°C for human ($p=0.041$). At similar rates lung tissue injury began at 0°C,

with human tissue requiring significantly less cooling to ~-15°C for complete necrosis and -26°C for swine (p=0.024).

Conclusion: These experiments elucidate the myocardial tolerance of cryothermal treatments. Data presented here suggest that there are no significant differences between swine and human myocardial response, but there may be differences between swine and human lung cryothermal tolerance.

Key Words*:* Cryoablation, phrenic nerve palsy, cryothermal tolerance, atrial fibrillation

Introduction

Cardiac balloon cryoablation for the treatment of atrial fibrillation has been gaining attention as an approach for isolation of the pulmonary veins (PV) since its first reported use in 2003 [87] and in the current clinical form in 2005 [88]. Focal cryoablation has been used surgically for many years [89], with transcatheter devices becoming available in more recent decades. One benefit of cryoballoon ablation is that it is a 'single-shot' approach, which is an advantage despite the sometimes slower nature of deeper freezing compared to radiofrequency (RF) energy (i.e., freezing is not point-by-point ablation like RF). In addition, the currently available ArcticFront cryoballoon (Medtronic, Inc., Minneapolis, MN, USA) has been shown to have comparable success rates to RF ablation with low adverse events [90,91]. The recent STOP-AF trial concluded similar findings to the more observational European studies, including an acceptable safety profile and positive response from patients who failed to respond to antiarrhythmic drugs [62].

Despite widespread and growing clinical use, there are still questions regarding dosing and treatment times for cryoablation, which may affect both efficacy and collateral injury [92,93]. Parameters affecting RF ablation lesions are thoroughly characterized, and temperatures of 50°C or higher are required for the creation of myocardial scars.[8] For instance, the effects of power, ablation duration, catheter orientation, catheter size, usage of irrigation, and contact forces on lesion size have been thoroughly studied for RF

ablation [94–97]. This is particularly relevant given the release of a second generation cryoablation device with a different cooling profile that may affect operation [98]. The highest regularly detected clinical complication is phrenic nerve palsy, at rates of 4-8% [62,91]. The esophagus may be incurring even higher rates of injury, but this is not normally detectable unless specifically investigated using endoscopy [99,100]. Given that the phrenic nerve and esophagus are in intimate contact with the right PVs and posterior wall of the left atrium (LA), respectively, one can see how adjusting dosing may lead to better outcomes. It is recommended by the manufacturer that two separate four-minute ablations are applied per PV.

A survey of the literature was unable to uncover definitive data for hypothermic or cryoinjury to the myocardium and surrounding tissues impacted by ablation. This lack of data prompted the current study, which to the authors' knowledge, is the first to report these limits for cryoablation. These data will be beneficial for future numerical modeling to help guide decisions such as balloon placement, treatment times, and other patient-specific treatment planning scenarios. Such approaches could lead to optimization of treatment time and/or potentially shorter yet still effective treatments (i.e., transmural with minimal collateral injury).

Conversely, in the hyperthermic treatment area (i.e., RF, laser, HIFU), there are data regarding injury to many tissues including the myocardium [101]. For instance, work by Pearce and colleagues [102,103] exploited cardiac tissue's unique, native birefringence to detect protein denaturation after thermal ablation. Importantly, cellular protein denaturation is thought to be one of the main mechanisms leading to necrosis from hyperthermic treatments. In Pearce's study, researchers measured collagen birefringence, an extracellular matrix protein, and correlated this to tissue destruction [102]. A similar imaging technique cannot be easily implemented during or after freezing because protein denaturation is not a major mechanism of cryoinjury and has not been correlated with cellular injury after cryo therapy. More specifically, the mechanism of cellular cryoinjury is related to water phase change (i.e., intracellular ice crystal formation and cellular

dehydration) during freezing [104,105] which has been studied in numerous cell types [106–108], although less in whole tissues [101,109]. Cooling below the actual freezing point of tissue is necessary for complete destruction, as shown in studies of the kidney [89,110] and liver [111] where cooling to -15°C or below was required. Furthermore, cellular injury is known to be both end temperature and cooling rate dependent, as described in reviews on cryosurgical injury in the literature [109,112].

It is therefore the goal of this work to determine what cooling regimes lead to necrosis, injury, or recovery (i.e., have no detectable effect on myocardium). Infrared (IR) thermography was selected, instead of a thermocouple, in order to measure temperature over a large area (i.e., every pixel produces a thermal profile). Additionally, IR is a noncontact measurement technique, which is particularly beneficial given the large thermal gradients produced during cryoablation (i.e., 100°C/cm), and has been used previously for cryothermic [113] and hyperthermic [114] studies in cancer [113,115]. The drawback of IR thermography is that accuracy suffers in comparison to other techniques (i.e., ± 2°C, or 2% of total range), and that the system used is limited to detection down to -30°C. This should be sufficient since tissue injury is expected below the phase change temperature of tissue (<-.5°C), down to a range of -15 or -20°C based on previous work in liver and kidney [110,116,117]. To measure the correlative injury in cardiac tissue post cryoablation, histological and enzymatic staining were used as previously described [110]. In addition, correlative measurements of cryoinjury in a cardiac muscle cell line were performed as a function of both end temperature and cooling rate.

Methods

To benchmark this approach, a small sample of swine kidney cortex (n=6, from two animals) was obtained and ablated per the protocol described below for comparison to the literature. Kidney cortex is homogenous with a smooth, flat surface allowing ease of ablation, IR monitoring, and post cryoablation TTC (triphenyltetrazolium chloride) staining. After reproducing results from the literature with kidney, the approach was then used on cardiac tissue including myocardium and a smaller set of lung samples. Finally,

HL-1 cardiac muscle cells were also obtained from culture [118], exposed to controlled cryoinjury, and evaluated for cellular level injury for comparison with tissue data.

Sample preparation

Female Yorkshire Cross swine hearts (n=15 animals), lungs (n=5, from 2 animals), and kidneys (n=6, from 2 animals) were chilled and stored in modified Krebs-Henseleit buffer within 30 minutes post-mortem from the University of Minnesota Meat Sciences Laboratory (Minneapolis, MN, USA). Swine hearts were then transported to our laboratory within an hour. Human heart (n=3) and lung (n=3) specimens were obtained from non-viable cardiac transplant organ donors through the regional organ procurement organization, LifeSource (St. Paul, MN, USA) within 6 hours of cross-clamp time. Human and swine samples were dissected from the atria and ventricles to a nominal thickness of 5mm. Locations were selected that were relatively 'flat' with a low degree of invaginations to provide a uniform surface for IR imaging, to avoid out-of-focus effects and non-symmetrical ablation lesions. Samples were placed in individual petri dishes with room temperature phosphate buffered saline.

The prepared samples were then placed in the apparatus and imaged by an IR camera, as shown in Figure 23 (left panel). The apparatus consisted of a plastic petri dish with central ablation probe and 2mm of Sylgard (Dow Corning, Midland, MI, USA) polymer formed to the bottom. This apparatus was designed to accommodate two cryoablation probes with different cooling powers. The first was the Galil Medical SeedNet system (Arden Hills, MN, USA) designed for prostate cryoablation, using an argon refrigerant to achieve cooling rates and end temperatures of approximately 400°C/minute and -120°C at the probe surface in the absence of load. The second system was the Medtronic Cryocath system using the FreezorMAX catheter with cooling rate and end temperatures of approximately 300°C/minute and -84°C in the absence of load. The samples ablated using the Galil system were transected by the needle in the middle, whereas the samples ablated using the Medtronic system had a 2mm biopsy punch hole placed in the center of the sample through which the catheter was advanced. Using this technique approximates

a situation that is easy to model numerically, removes the variability of catheter contact pressure, and creates uniform axi-symmetric lesions (Figure 23, right panel).

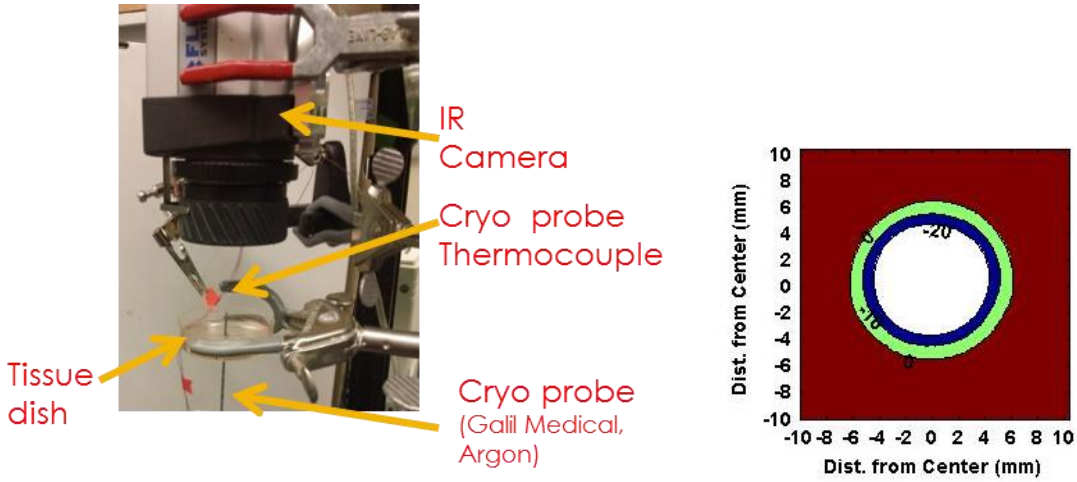

Figure 23: (Left) Infrared imaging apparatus and resultant isotherms. The samples are transected by the cryoprobe and imaged from the top down. (Right) Resultant infrared (IR) isotherm at the end of an ablation performed with the Galil system, with white indicating temperatures less than -20°C, blue -20°C to -10°C, green between -10°C to 0°C, and red greater than 0°C.

Infrared imaging and viability assessment

Prior to sample placement in the petri dish, ~5ml of ultrasound gel was distributed uniformly about the bottom of the dish. After placement of the sample, another volume of ultrasound gel was added to surround the sample. Ultrasound gel has been shown to have very similar thermal properties to myocardium [119]. By surrounding the sample with ultrasound gel, we thereby minimized variation in sample size and created a more reproducible ablation volume.

After sample placement, the emissivity and appropriate environmental parameters were input to the infrared software (ThermaCAM Researcher Pro 2.9, FLIR Systems, Inc., Boston, MA, USA). Emissivity was determined by comparison of IR temperature to a 0.040" T-type thermocouple temperature (5SRTC, Omega Engineering, Stamford, CT, USA) being read by a Fluke 51II thermometer (Everett, WA, USA). A T-type

thermocouple with data logging was affixed to the active cooling metal portion of the cryoprobe with Kapton (3M, St. Paul, MN, USA) tape for later computer modeling. Cryothermal applications (i.e., ablations) of desired durations were subsequently performed.

After ablation, samples were washed with phosphate buffered saline, incubated with 60ml of cell culture media (DMEM/F12, 10% fetal bovine serum, and 1% penicillin/streptomycin), and placed in a cell culture incubator. Myocardium samples were incubated for 22-24 hours to allow full cryoinjury to manifest. Incubation of only 4 hours was sufficient for lung and kidney samples. The effect of shrinkage or swelling was examined on a subset of ten samples by measurement of the distance between two distinct points pre-incubation and post-incubation. The average change and standard deviation was found to be an increase of 0.2±1.1mm.

Samples were then stained with 1% TTC in Trizma buffer (7.4 pH) at 37°C for 1 hour, similar to previous work [110]. TTC functions by reduction of the compound (i.e., electron donation from NADH oxidation from metabolism) and forms a red formazan derivative when in contact with viable tissue [120]. Non-viable tissue turns pale or white after incubation, as shown in Figure 24. This stain has been validated and widely used for identification of infarct regions in artery occlusion models [121,122]. The discrepancy in incubation time between tissues is believed to be due to the higher mitochondrial content (i.e., more metabolic enzymes remaining active for longer periods) of cardiac tissues.

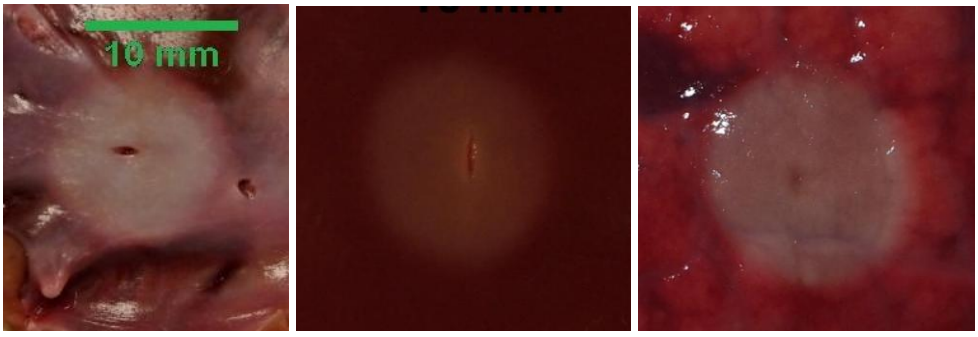

Figure 24: Examples of TTC stained myocardium (left), kidney (center), and lung (right) with central ablation lesions. Scale bar for all is 10mm.

The first six samples for this study had a .040” gauge T-type thermocouple placed in a 1mm superficial slit on the surface of the sample just under the endocardium. The IR thermographic data and thermal profiles were compared to ensure environmental and sample parameters were being appropriately captured in the IR software. The measured difference between IR thermography and thermocouple data was within the manufacturer published specification (i.e., less than ±2°C or 2% of measurement).

Data analysis

After incubation, the samples were digitally photographed under reproducible lighting with a ruler for calibration. The photographs were then analyzed using MATLAB (MathWorks, Natick, MA, USA) to determine the radial distance from cryoprobe to where the lesion ended and a zone of injured and live tissue began by plotting the gray values from the cryoprobe edge outward radially and then normalizing these values to demarcate live and dead tissue areas. This yielded a sigmoid-like curve from 0 to 1 (i.e., dead to live tissue, Figure 25). A single operator then selected two critical points on the curve where the transition from dead, injured, and live tissue occurred, as determined by TTC intensity. Samples that did not yield clear sigmoid curves, indicating non-axisymmetric lesions, were removed from analysis. This was necessary as the injury analysis algorithm relies on the symmetric nature of the lesion to obtain and compare all data at a given radius from the probe to obtain an average and standard deviation for a given temperature, T(r,t). This approach also maximized the amount of data available from a given lesion (i.e., multiple points per sample) to obtain the highest fidelity in reading injury for a given radius (and thus thermal history).

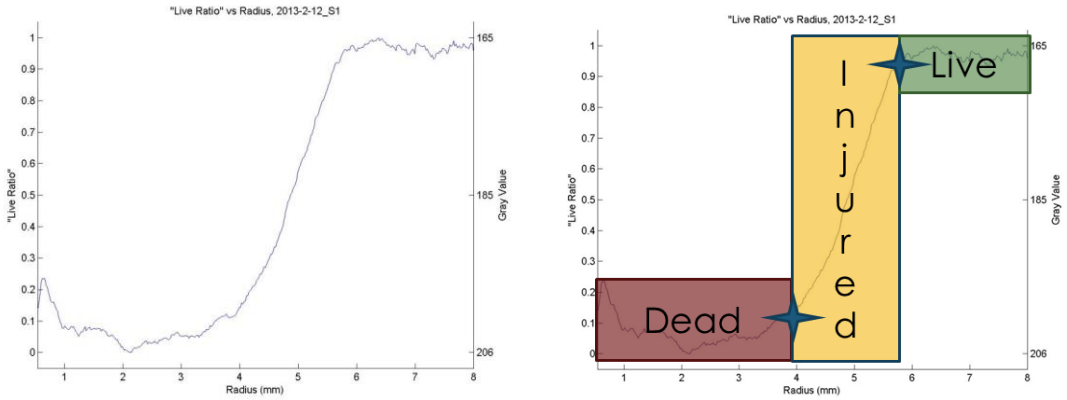

Figure 25: (Left) A plot of the normalized gray values of a TTC stained image plotted radially outward from the cryoprobe. (Right) Classification of data after selecting the two critical points (blue stars) on the sigmoid curve.

The raw IR data were analyzed with a MATLAB program that extracted temperature at a particular radial distance. This was then compared to sigmoidal staining intensity curves at the same radial distance (Figure 25). Eventually a full database of thermal profiles and another database of staining profiles as a function of radius were obtained for a given tissue tested. Finally, by comparing these databases, it was possible to determine the thermal history (i.e., cooling rates and nadir temperatures) that resulted in dead tissue, injured tissue, and live tissue in the test.

Cell culture and freeze–thaw

HL-1s cell lines, murine cardiac muscle cell lines with differentiated cardiac morphological, biochemical, and electrophysiological properties, were cultured as described in Claycomb et al [118]. Briefly, the cells were allowed to proliferate in 75cm^2 tissue culture flasks coated with gelatin/fibronectin. The cells were grown in a 5% CO_2, 37°C incubator with Claycomb media further supplemented with 10% Fetal Bovine Serum, Noreprinephrine,L-Ascorbic Acid, and L-Glutamine (SAFC Biosciences, Lenexa, KS, USA). The cultured cells were trypsinized (0.05% trypsin, Life Technologies, NY, USA) and harvested as suspensions for freeze-thaw experiments.

5-10uL of cell suspensions were placed on a quartz crucible which, in turn, was placed on a cryostage (Linkam BCS196, Surrey, UK) for controlled freeze-thaw [108]. All samples were pre-nucleated at -2°C by bringing the outer edge in contact with a chilled needle. The partially frozen samples were allowed to melt almost completely by bringing the temperature back up to -0.6°C. Thus with a small number of ice crystals present at the onset of the process, the samples were cooled down at varied rates (0.5 to 130°C/min) to varied end temperatures (-5 to -60°C) and held for 0 to 3 minutes. The cells were then rapidly thawed at a rate of 130°C/min to room temperature, then incubated (5% CO_2, 37°C) for 15 minutes prior to the subsequent viability assay. Post thaw viability was determined using a Hoechst/Propidium Iodide (PI) assay[108] (Sigma-Aldrich, St. Louis, MO, USA) where a minimum of 100 cells were counted from multiple fields of view using a fluorescence inverted microscope (Olympus IX51, Center Valley, PA, USA).

Results & Discussion

The resultant categorical tissue response (i.e., live, injured or transition zone, dead) to the thermal ablation was plotted against the cooling rate and minimum temperature reached. The swine kidney results shown in Figure 26 were found to agree with previously published data on thermal injury. Comparing the right and left panels of Figure 27, one can see that similar patterns arise in both the atria and the ventricles. Furthermore, human myocardium responses are shown in Figure 28. The effect of cooling rate on post thaw survival of HL-1 cells is shown in Figure 29 (left panel), while the effect of the lowest end temperature reached during the cooling process is shown in Figure 29 (right panel).

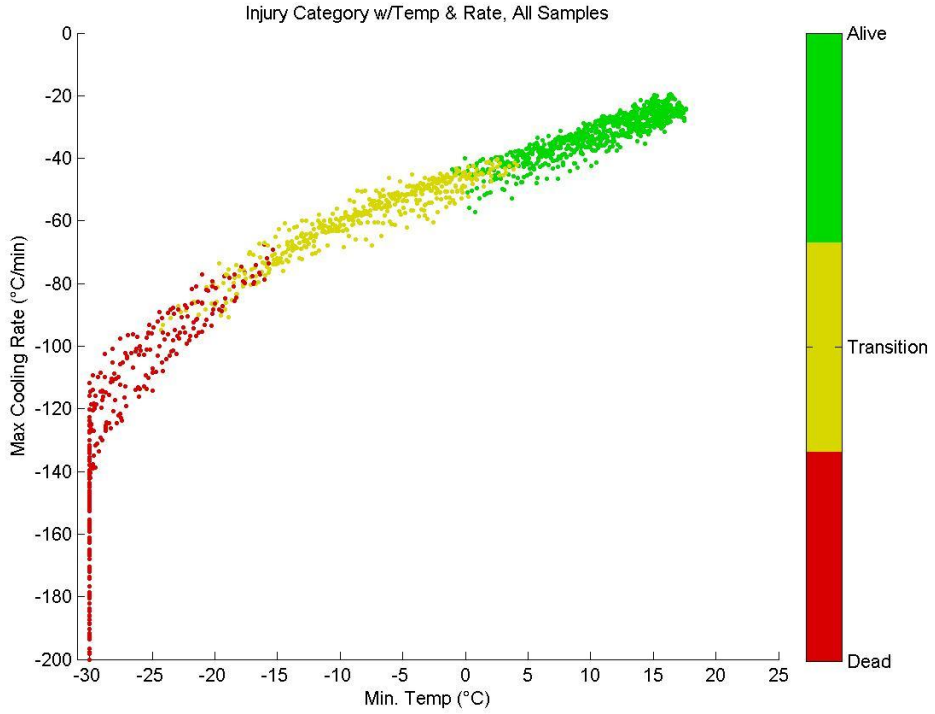

Figure 26: Swine kidney tissue viability response to ablation with Galil Seednet probe (n=6).

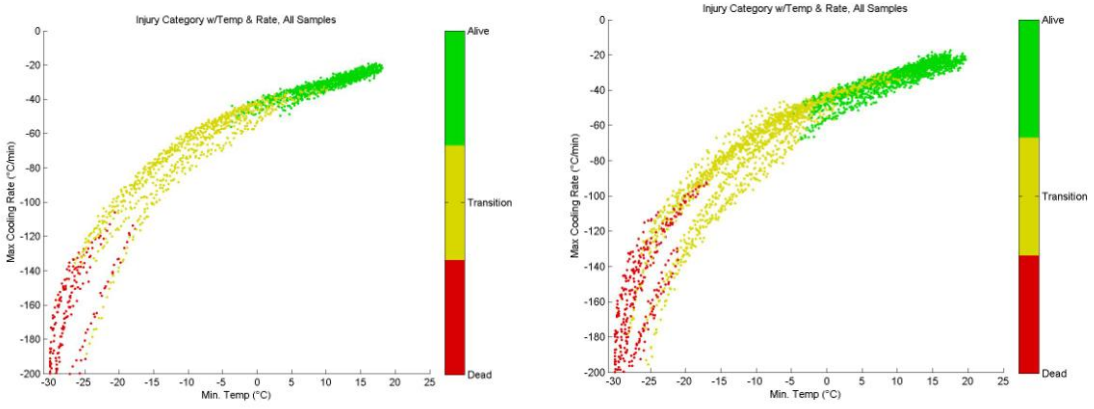

Figure 27: Swine atrium (Left; n=8) and swine ventricle (Right; n=14) tissue viability response to ablation with Medtronic FreezorMax.

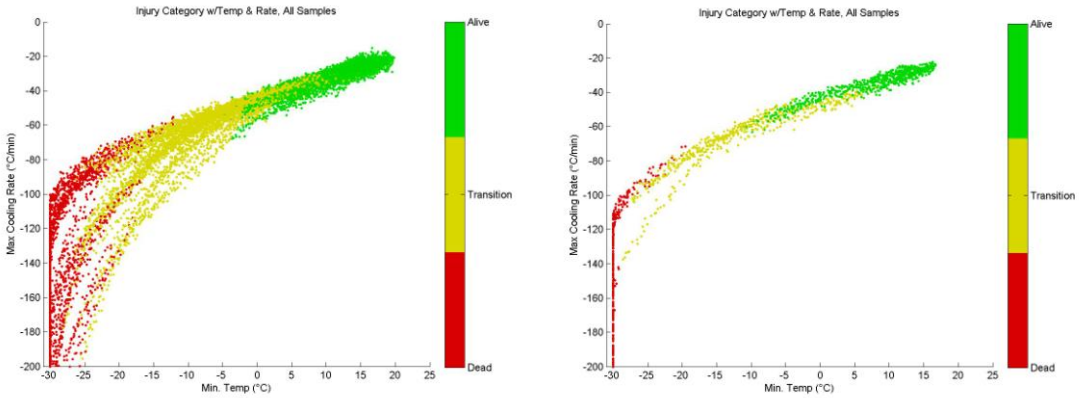

Figure 28: Resultant viability curves for swine ventricular and atrial samples (Left;, n=39) and human myocardium (Right; n=6).

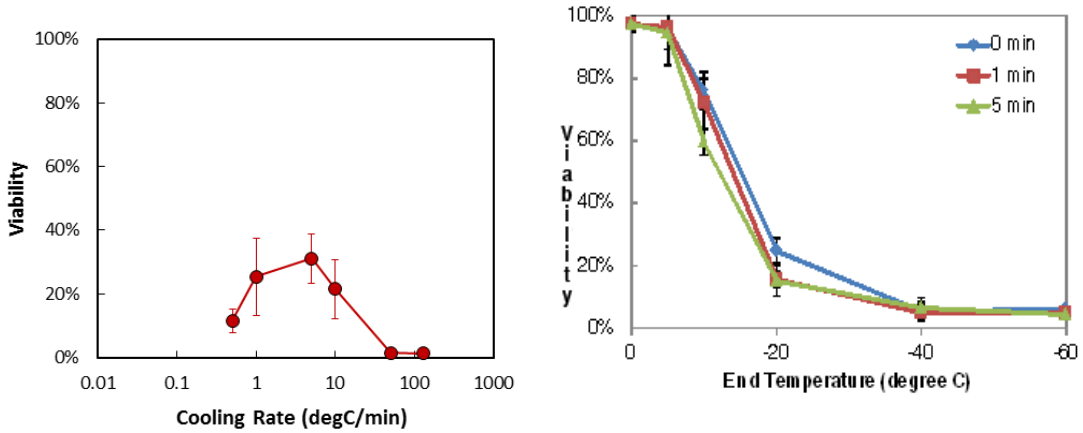

Figure 29: (Left) Effect of cooling rate on HL-1 cell post freeze thaw viability as determined by Hoechst/Propidium Iodide dye exclusion assay. All samples were pre-nucleated then cooled at rates shown to an end temperature of -20°C. Samples were held at -20°C for 1 minute prior to subsequent rapid thawing (n=6). (Right) Effect of end temperature on HL-1 cell post freeze thaw viability as determined by Hoechst/Propidium Iodide dye exclusion assay. All samples were pre-nucleated then cooled at 5°C/min to end temperatures shown. Legend indicates time duration held at end temperatures prior to subsequent rapid thawing (n=6).

This study reports on cardiac tissue cryothermic tolerance. This approach can be adapted to other tissue types, as shown here and in previous literature on heat and cryo lesions in human and animal tissues [110,123]. This methodology may also be used to study the

effects of multiple freeze-thaw cycles or complex cooling regimes. Pooling human and swine myocardial data suggests that it needs to be cooled to at least -22±3°C for the atria and -22±4°C for ventricular tissue to obtain complete necrosis at rates of -105±33°C/min and -112±39°C/min, respectively. The cooling regime contains variable cooling (and thawing) rates and hold times in addition to end temperature, which can all affect viability. Thus the authors suggest cautious and conservative use of these numbers.

Data presented here suggest that kidney tissue needs to be cooled to -19±4°C at cooling rates of -82°C/min to obtain complete necrosis (Table 17). These data agree with previously published data on kidney cryothermal tolerance [110,116,117]. Benchmarking the system against previous research data on kidney tissue demonstrates the ability of the system to determine injury thresholds accurately.

Table 17. Necrotic thermal injury thresholds summarized by tissue type and probe treatment

Tissue	Cryoprobe	Injured to Dead Transition (average)	
		End Temperature [C]	Cooling Rate [C/min]
Human myocardium	Pooled (n=6)	-26±4 †	-102±23
Human lung	Pooled	-15±8 ‡	-78±23
Swine atrium	FreezorMAX (n=8)	-24±3 †	-134±26
	Galil (n=8)	-21±4 †	-80±8
Swine ventricle	FreezorMAX (n=14)	-23±3 †	-136±35
	Galil (n=9)	-20±4 †	-81±13
Swine lung	Pooled (n=5)	-26±5 ‡	-104±20
Swine kidney	Galil (n=6)	-19±4	-78±12

*Statistical differences were detected by use of a T-test between end temperatures and cooling rates. † Human myocardium compared to pooled swine myocardium (p=0.041); ‡ Human lung compared to swine lung (p=0.041).

Interestingly, the lung data suggest that there may be significant differences between swine and human cryothermal tolerance. The human data indicate that cooling to -15±8°C at cooling rates of -78°C/min may be required for complete lesions (Table 17). The temperature necessary to destroy healthy swine lung tissue is lower than for human tissue. Specifically, temperatures of -26±5°C at -104°C/min (Table 17) were required for complete lung lesions which are approaching the limit of the current infrared camera (i.e., -30°C). The discrepancy may be due to age, disease state, species variation, and/or pre-procurement sample treatment (e.g., human samples were transported at near 0º temperatures for up to several hours before experiments). Nevertheless, these rare human specimens provide unique and translational insight to cryothermic injury thresholds of the lung.

This work is not without limitations, as is the case with any in vitro animal tissue-based model. The effect of the tissue being perfused is not fully understood. However, work by other groups on the kidney [110,116,117] have found similar temperatures are necessary for complete necrosis in experimental groups that were perfused or non-perfused. The TTC stain is an indicator of metabolic activity and therefore not truly a direct indicator of live versus dead tissue. It was considered in this experiment as an acceptable surrogate for viability based upon the wealth of previously published literature using cardiac tissues (e.g., left anterior descending artery occlusion models).

The results with HL-1 cells allow us to gain further insight into some of the possible mechanisms that affect tissue-level destruction. The left panel of Figure 7 shows that while a significant subpopulation (>30%) of cells will survive at an end temperature of -20°C if cooled at a rate of 5°C/min, complete destruction can be attained at the same end temperature if cooling rates greater than 50°C/min are employed. Likewise, the right

panel of Figure 7 suggests that even with a cooling rate of 5°C/min (an apparent optimal rate for cell survival), complete destruction can be achieved at an end temperature somewhere between -20 and -40°C. These results with HL-1 cells are similar to results for myocardium, in which complete lesions are observed in regions where the minimum temperature reached was around -22°C and where the maximum cooling rate was greater than 60°C/min.

Conclusions

Here we report tissue-level experiments to elucidate the myocardial tolerance of cryothermic treatments. The data suggest minimal differences between swine and human myocardial response, although there may be a difference between swine and human lung cryothermal tolerance. This thermal injury assessment approach may be used in future experiments on multiple tissue types to study the viability response to simple or complex cooling regimes.

Clinical Perspective

This work further elucidates the degree of cooling required to create cryothermal lesions in both human and swine cardiac tissues. It also demonstrates that human lung tissues may be more sensitive to cryothermal energy, and therefore care should be taken when cryoablation procedures are applied near lung tissues. Furthermore, these data fill a void in knowledge relative to the transmural temperatures cardiac cryoablation should be targeting, to achieve therapeutic doses. Such data could also be employed to develop computer simulations as a means to further refine dosing protocols. This work supports the supposition that swine myocardium behaves similarly to human tissues after exposure to cryothermal energy, and thus swine may be used as an appropriate animal model for testing of these therapeutic conditions as well as for new devices and procedures. In the future, as advanced temperature monitoring capabilities become available in routine clinical practice (e.g., magnetic resonance themography), our data may be applied to determine practice limits for optimizing lesion formations.

Tensile Properties of Cardiac Tissues Relative to the Application of Radiofrequency or Cryothermal Ablative Therapies

Submitted to *IEEE Journal of Translational Engineering in Health & Medicine,* in review.

Stephen G. Quallich, BS[1,2]; Kevin, K. Kriege, BS[3]; Paul A. Iaizzo, PhD[1-3]

[1] Department of Biomedical Engineering, University of Minnesota, Minneapolis, MN
[2] Department of Surgery, University of Minnesota, Minneapolis, MN
[3] Department of Physiology, University of Minnesota, Minneapolis, MN

Preface

In general, the temperature thresholds and mechanisms of injury of radiofrequency and cryothermal ablations have been previously studies; although, the specific cardiac tissue responses to these therapies remains largely uninvestigated. Importantly, associated changes of the cardiac tissue properties may alter the heat transfer as well as facilitate the development of complications, such as pulmonary vein stenosis, atrial-esophageal fistula, and/or cardiac tamponade. For example, in one of our previous studies we have shown that ablation modalities may lower the contact force required to perforate the atria [72]. A more comprehensive understanding of the impacts ablation may have on cardiac tissues could also be beneficial in the generation of accurate computational models of such ablative therapies. In an effort to better elucidate the cardiac tissue responses to ablation modalities, this study investigated the effects of both radiofrequency and cryothermal ablations on specific cardiac biomechanical properties. It was observed that radiofrequency ablations altered the cardiac tensile strengths, Young's moduli, and strains at failure, while cryothermal treatments produce minimal biomechanical transformations. It is considered here that these results utilized in conjunction with

computational models may aid in alleviating complications associated with cardiac ablative procedures and thus improve clinical awareness of the secondary consequences of such applications.

I was primarily responsible for the study design, data and statistical analyses and the initial draft of the manuscript. Kevin Kreige was an essential contributor, aiding in the dissection of specimens and data collection of the uniaxial tissue responses. The preliminary results from this study were presented at the Biomedical Engineering Society in San Antonio, TX in October 2014. On going research is also being conducted in the laboratory.

Summary

Changes in cardiac biomechanical tissue properties following the applications of various ablation modalities may lead to the development of an array of associated complications. The applications of either radiofrequency (RF) or cryothermal ablations will alter the biomechanical properties of various cardiac tissues in a differential manor: in some case this may be attributable to increased incidences of cardiac tamponade, pulmonary vein stenoses, and/or atrial-esophageal fistula. Thus, a greater understanding of the underlying changes in tissue properties induced by ablative therapies will ultimately promote safer and more efficacious procedures. The effects of either applied RF or cryothermal energies on the biomechanical properties of pulmonary vein, left atrial or right atrial samples (n=367) were examined from fresh excised porcine (n=35) and donated human tissue (n=11). Radiofrequency ablations were found to reduce the tensile strengths of the porcine cardiac specimens ($p<0.05$), and a similar trend was noted for human samples. Cryoablations did not have a significant impact on the tissue properties compared to the untreated tissue specimens. Locational and species differences were also observed in this experimental paradigm ($p<0.001$). Incorporating these findings into cardiac device design and computational modeling should aid to reduce the risks of complications associated with tissue property changes resulting from cardiac ablative procedures.

Introduction

Atrial fibrillation (AF) continues to affect millions of individuals in the United States alone, and the incidence of this disease is expected to grow rapidly, 2.5 fold, by 2050 [44]. In general, individuals over the age of 80 elicit incidences above 10% [44,124]. Unfortunately, complications associated with catheter ablation procedures for AF occur at approximate rates of 4-6% [41,42]. A number of these complications are the secondary result of the applications of either RF or cryothermal ablative energies, such as cardiac tamponade, pulmonary vein (PV) stenosis, and/or atrial-esophageal fistula. While it is generally considered that the heating or cooling of tissues will alter their biomechanical properties, the exact therapeutic thresholds have not been identified in controlled experiments. Additionally during such RF clinical procedures, surpassing the minimum target temperature of 50°C for myocardial scar formation, is quite plausible, especially when aiming to create transmural lesions [56]. It is considered that RF energies build up within the associated tissues during RF ablations [125]. Exceeding ablations temperatures of 60-65°C has been reported to result in the denaturation of collagen, temperatures higher than 80°C causes elastin denaturation, and both of these contribute to a loss of total tissue compliance [49]. In contrast, it is considered that ice formation during cryoablations induces altered alignments of structural proteins without compromising their integrities, although there were noted modifications to their elastic moduli [50]. In other words, the applications of ablation energies, changes the biomechanical as well as the tissue properties that may play roles in the manifestations of the aforementioned complications. Thus, a greater understanding of how and why these transformations occur could ultimately reduce their elicitations relative to these cardiac treatments.

Interest in thermal tolerance tissue properties has also increased in order to improve ablation procedures. For example, characterizing the cryothermal tolerances of cardiac and adjacent tissues is essential for predicting and minimizing phrenic nerve injury, amongst other complications as well. Phrenic nerve injury has been reported to occur at rates of 2-11% and was also considered to be a more prominent in the early uses of second-generation cryoballoon [62,79,126]. Also, during freezing it was reported that

thermal conductivities increase while specific heats decrease [127]. Perhaps such knowledge may explain why phrenic nerve injury occurs more readily with cryoablation compared to RF ablation. In addition, resultant protein denaturation and water vaporization reduces the thermal conductivities and specific heats of cardiac tissues, changing the thermal profile during heating and their responses to secondary energy applications [128]. Furthermore, accounting for all such tissue alterations is essential if one hopes to generation accurate computational models of ablative therapies; e.g., in order to attenuate the incidences of phrenic nerve injuries, amongst other complications.

The biomechanical characterizations of various myocardial structures within the heart as a whole are currently underway. For instance, the biomechanical properties of the fossa ovalis have been investigated in an effort to reduce iatrogenic atrial septal defect formations [58]. Additionally, our laboratory has studied the relative contact forces required to cause perforations and the associated relationships with various ablation modalities [72]. Furthermore, interest in engineered heart tissues as well as rapid utilizations of transcatheter valves has led to the study of both valves and chordae tendineae properties so to better mimic their native behavior [129,130]. Therefore, a detailed understanding of the biomechanical as well as biothermal tissue properties associated with ablative therapies remains an intense area of interest. Further, as cardiovascular technologies continue to advance, computational modeling's role in both device development and personalized medicine will likely become readily available and increasingly important [131].

Methods

Human heart specimens (n=11) were acquired from non-viable organ transplant donors through LifeSource (St. Paul, MN) as well as the University of Minnesota Bequest Program (Table 18). Also, Yorkshire cross swine (n=35) cardiac tissue was also obtained from both the University of Minnesota Meat Sciences Lab and our laboratory. Fresh atrial and ostial PV's (n=367) were carefully dissected into dog-bone shape tissue bundles and 2-0 silk sutures (Surgical Specialties Corp., Reading, PA) were tied to both ends (Figure

30). This dog-bone orientation allows for repeatable failures of these tissues near their midpoint: evulsions occurred at the tissue regions with the smallest cross sectional area. All tissue samples dimensions were measured with calipers to allow for subsequent data normalizations. All swine samples were tested within 24 hours post-explantion; some human specimens were tested beyond this timeframe, but within 48 hours. Samples were stored in saline at 4°C prior to uniaxial testing. The prepared samples were randomized to the following study groups: 1) no treatment (NT), 2) RF ablation for 1 minute at 30 W, with a 65°C temperature limit, or 3) focal cryoablation for 2 minutes. Specimens were then pulled uniaxially until failure at a rate of 100 mm/min with a mechanical force tester (Chatillon, Largo, FL).

Table 18. Human heart demographics.

Heart #	Age (Yr)	Weight (kg)	Gender	COD	Cardiac History
1	45	96	M	CVA	Hypertension, Alcoholism
2	34	86	M	CVA	None
3	62	73	F	CVA	Hypothyroidism, Hyperlipidemia
4	52	74	F	CVA	None
5	81	75	F	Natural	AF, Mitral regurgitation
6	67	82	M	Bladder cancer	None
7	69	77	M	COPD	None
8	68	137	M	CVA	Hypertension, Hyperlipidemia, CABG
9	58	93	F	Head Trauma	Hypertension
10	52	94	M	Drug overdose	None
11	57	106	M	CVA	None

*Cerebrovascular accident

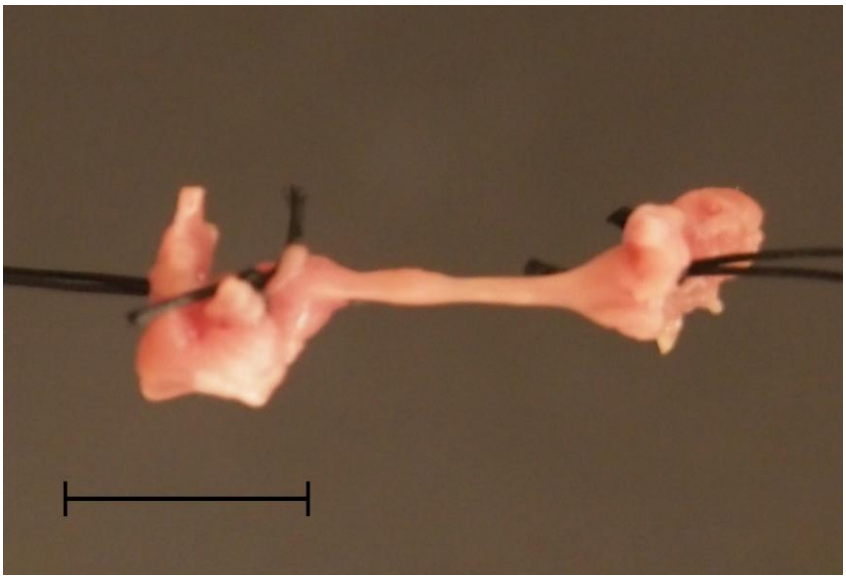

Figure 30. A typical example of a prepared dog-bone shaped specimen, which was then mounted in the mechanical force tester using sutures. The scale bar depicts 1 cm.

Data Analyses

Ultimate tensile strengths, strains at failure, and Young's moduli were calculated and analyzed with Matlab (MathWorks, Natick, MA) and Minitab (State College, PA). All determined values are presented as means ± standard deviations. Analysis of variance (ANOVA) for groups of 3 or more were used to compare normally distributed data. P-values ≤0.05 were considered as significant.

Results

The relative tensile strengths, strains at failure, and derived Young's moduli for a given tissue studied, were found to be significantly different: i.e, between the right/left atrial and PV specimens as shown in Table 19 ($p<0.001$). Furthermore, there were significant differences between species, with human hearts having greater ultimate tensile strengths and Young's moduli, but lower strains at failure: as provided in Table 20 ($p<0.001$).

Table 19. Comparisons of porcine biomechanical properties sorted by tissue type.

	Location			P-value
	RA	**LA**	**PV**	
Ultimate Tensile Strength (MPa)	0.69±0.35	1.04±0.76	1.64±0.95	<0.001
Strain at Failure (%)	87±33	117±39	153±68	<0.001

Young's Modulus (kPa)	15±8	19±10	31±23	<0.001
Number	33	23	39	

Table 20. Comparisons of pulmonary vein biomechanical properties sorted by species: human versus swine.

	Species		P-Value
	Human	Swine	
Ultimate Tensile Strength (MPa)	5.90±5.22	1.64±0.95	<0.001
Strain at Failure (%)	58±28	153±68	<0.001
Young's Modulus (kPa)	224±219	31±23	<0.001
Number	29	39	

The applied ablation modality and therapeutic application site within these hearts were both shown to be factors influencing the resultant biomechanical properties. Following therapeutic applications, the relative tensile strengths for both the porcine pulmonary veins and left atrial tissue specimens were significantly different; as shown in Table 21 ($p<0.05$). Note, that post-treatment responses of the porcine right atrial and human PV samples followed the same trends, but these effects did not achieve significance (Table 22). Further, the applications of RF energies reduced the tensile strengths of all investigated tissues; typically this resulted in reduced evulsion forces by approximately one third following RF ablations. In contrast, cryoablative therapies elicited no statistical impacts on the ultimate tensile strengths regardless of the tissue tested.

Table 21. Comparisons of the biomechanical properties of porcine pulmonary veins, right atrium, and left atrium in each treatment group: controls (NT), radiofrequency (RF) therapy or cryothermal therapy (Cryo).

	Ablation Modality			P-value
Pulmonary Vein	**NT**	**RF**	**Cryo**	
Ultimate Tensile Strength (MPa)	1.64±0.95	1.09±0.59	1.41±0.49	0.012
Strain at Failure (%)	153±68	128±62	147±72	ns
Young's Modulus (kPa)	31±23	21±13	27±18	ns
Number	39	27	32	
Left Atrium				
Ultimate Tensile Strength (MPa)	1.04±0.76	0.64±0.30	0.83±0.49	0.044

Strain at Failure (%)	117±39	90±33	85±21	0.001
Young's Modulus (kPa)	19±10	15±10	21±12	ns
Number	23	25	29	
Right Atrium				
Ultimate Tensile Strength (MPa)	0.69±0.35	0.54±0.40	0.63±0.30	ns
Strain at Failure (%)	87±33	69±36	84±32	ns
Young's Modulus (kPa)	15±8	14±8	15±9	ns
Number	33	37	40	

Table 22. Comparisons of human pulmonary vein biomechanical properties associated with treatment group: controls (NT), radiofrequency (RF) therapy or cryothermal therapy (Cryo).

	Ablation Modality			P-value
	NT	RF	Cryo	
Ultimate Tensile Strength (MPa)	5.90±5.22	3.85±2.62	6.69±5.91	ns
Strain at Failure (%)	58±28	55±21	64±25	ns
Young's Modulus (kPa)	224±219	144±108	219±225	ns
Number	29	30	25	

Discussion

The observed biomechanical properties of cardiac tissues studied here were identified to be similar to those reported in the literature. For instance, studies examining the biomechanical properties of porcine peripheral and coronary arteries observed ultimate tensile strengths and Young's modulus in agreement with this study [53,132]. It should be noted, that there were to be expected differences between arteries and the venous/cardiac tissues used in this experiment. Also, Venkatasubramanian et al reported a shift in Young's modulus of the physiological region of the frozen samples so that they acted stiffer [53]. Similar behavior was observed in this study during cryoablation with a shift of Young's modulus (data not shown). Furthermore, it was reported that RF energy applications caused a loss of pulmonary vein compliances, which were exacerbated with temperature increases beyond 60-65°C [49]. Note that a temperature limit of 65°C was utilized in our experiments, and although there was a reduction in compliance, inversely related to Young's moduli, no significant changes were observed. In other words, in the current study approach, since this temperature threshold was only approached without being exceeded for relatively short periods of time, this transformation may be masked by

the large variability in biological specimens. Additionally, similar effects of ablations were exhibited for the esophagus with RF significantly reducing the ultimate tensile strength, and cryoablation having no noticeable impact [133]. In general, the effects of RF and cryothermal ablation seen in this study are in agreement with those manifested in a variety of other tissue types including veins and esophagus.

The biophysical disruption of the structural integrity of tissues in relation to heating has been characterized numerous times [49,134–137]. As temperatures exceed 65°C collagen denaturation occurs and at temperatures above 80°C elastin denaturation is incited [49]. In this experimental paradigm a temperature limit of 65°C was used, which allowed for collagen breakdown in these tissues following the application of RF therapeutic ablations. Therefore, reduced structural integrities were expected and were found to be agreement with our presented results. In contrast, cryoablative therapy is considered to have minimal affects on the integrities of structural proteins, so reductions in ultimate tensile strengths would not be anticipated and were not observed in this study. Yet, the relative induced changes that RF and cryothermal ablative energies had on the structural proteins were associated with the tissue and species specific biomechanical responses.

Although we identified significant difference between the swine and human biomechanical properties, there are a number of other factors one needs to consider. The tissue samples studied here were from 6-9 month old swine, while samples from human donors ranged between the ages of 34-81 years. Aging processes will alter biomechanical properties: e.g., studies examining the chordae tendineae reported that with age the collagen orientations becomes more disorganized along with alterations in the collagen wave structure [138]. More specifically, the large ranges in both the sample ages and their associated disease state of the donor human specimens studied here, may have contributed to the observed variabilities and the differences when compared to the swine samples. Note that some of the donors had cardiac conditions, which may have altered their anatomy and biomechanical properties of the tissue. Also, given the relatively small sample size for human tissue, additional testing would aid in validating these findings.

Nevertheless, swine hearts were used as a translational model to approximate tissue biomechanics following ablation

The biomechanical properties assessed in our investigations of both the human and swine tissues should be of interest to scientist, engineers, as well as electrophysiologists utilizing these therapies to treat patients. We consider here that this is one of the first studies to examine the effects of ablative energies on the biomechanical properties of various cardiac tissues. Greater awareness of the resultant differences RF and cryothermal ablation applications have on tissues, may influence future iterations of such delivery devices and/or be used to fine tune clinical procedures, so to minimize circumstances leading to the development of associated complications. For instance, the knowledge that RF weakens the ultimate tensile strength of various tissues could be advantageous in particular applications. For example, the Baylis RF transseptal needle takes advantage of these induce effect and uses the aid of RF energy to more readily cross the septum: i.e., as a alternative to solely applying mechanical force. Additionally, the results presented herein may have numerous implementations for device design in numerous clinical scenarios that again may aid to improve the safety and efficacy of all types of ablation procedures.

This study had some inherent limitations that need noting, which may include: 1) tissue temperatures during applied therapies were not monitored; 2) only uniaxial force responses were studied; and 3) the relative viability of the human tissues was not always optimal. Monitoring of the contact tissue temperatures would have allowed for a more accurate examination of the influence temperature has on biomechanical properties. However, we employed clinical systems for therapeutic delivery and this type of monitoring would in turn be invasive and in itself may have compromised the measured tissue properties of interest. Furthermore, samples were typically near or less than 1 mm^2 in cross sectional area, so catheter tip temperatures were expected to be quite close to maximum tissue temperature. Noted above, biomechanical properties were only examined uniaxially and these tissues likely have directional differences, since they are

not homogeneous in nature. Furthermore, some of the human tissue used was not tested within 24 hours post-explantation. Although, we did not observe significant differences between the relative properties of our obtained human samples: this may have been masked by the small sample size. Therefore, further experiments need to be conducted to investigate these potential aforementioned study limitations.

Conclusion

The effects RF and cryothermal ablations have on the biomechanical properties of cardiac tissues were investigated using a translational approach. Applied RF energies induced significant denaturation of structural proteins, ultimately leading to decreases in tensile strengths, but without associated changes in strains at failures and/or derived Young's modulus. Cryoablations did not elicit significant effects on any tissue properties compared to untreated specimens. There are tissue specific and species variations that need to be accounted for in applications interested in the biomechanical properties of cardiac tissues. Thus, special consideration should be taken when using animal models as substitutes for human tissues in device design efforts. This research highlights the need for further studies to investigate the tissue property transitions that occur during and following the application of ablation modalities, especially with respect to clinical complications.

Acknowledgements:

The authors would like to express their gratitude to LifeSource as well as the organ donors and their families for the hearts used in this research. Additionally, the authors would like to thank Monica Mahre for preparation of this manuscript.

Acute Shrinkage of the Pulmonary Vein Ensuing From Radiofrequency and Cryo- Ablations

Published in *Journal of Medical Devices,* **9**(2), p. 020904, 2015.

Stephen G. Quallich, BS[1,2]; Paul A. Iaizzo, PhD[1,2]

[1] Department of Biomedical Engineering, University of Minnesota, Minneapolis, MN
[2] Department of Surgery, University of Minnesota, Minneapolis, MN

Preface

Augmenting our investigations on the effects ablative therapies have on cardiac tissues, this study specifically targeted the relative responses of the pulmonary veins. Unfortunately, pulmonary vein stenosis is a complication that occurs at rates as high as phrenic nerve injury, up to 15.6% [139], but its development can be further masked by time. As such, it is often developed months following the ablative procedure and not impeding until the progressive effects become substantially enough; severe induced stenosis may be life threatening. To date, there have been few investigations performed relative to identifying the initiators that spur the development of such stenosis. Hence in this experimental paradigm, we investigated the development of pulmonary vein stenosis on an acute time scale as a means to better understand how such biomechanical changes may play a role. Radiofrequency and cryothermal treatments caused shrinkage of the pulmonary veins compared to untreated controls, suggesting that increased stress states may lead to a greater likelihood of stenosis development.

I was responsible for the design of experiments, data and statistical analyses, and the initial draft of this manuscript. The preliminary results of this study were presented orally

at the European Cardiac Arrhythmia Society (ECAS) in Munich, Germany in March 2014.

Introduction

Over 5 million Americans are currently affected by atrial fibrillation, and as the population continues to age the incidence is expected to rise 2.5 fold by 2050 [44]. Radiofrequency (RF) and cryoablation are routinely used to treat atrial fibrillation to hopefully be a curative treatment. Yet, development of pulmonary vein (PV) stenosis is facilitated following cardiac ablation procedures. Although it is frequently asymptomatic, it may become a potentially life threatening condition: as the degree of stenosis escalates typically the severities of symptoms increases as well.

Noteworthy in one study, 15.6% (3.4% severe, 4.4% moderate, 7.7% mild PV stenosis) of patients were reported to develop PV narrowing 3.5 months after RF ablation procedures; it was considered that PV stenosis progression subsides 3 months following ablation procedures [139]. However, it has also been reported that 2 years following RF ablation, up to 28% of patients are affected by PV stenosis and/or occlusion. Furthermore, it is important to acknowledge that distal ablations inside the PV's compared to ostial ones were associated with over a 5 fold increase in the development of stenosis [140]. In cryoablation procedures PV stenosis incidence rates were 3.1%, and it has been suggested that cryoablation is less likely to elicit stenosis compared to RF ablation [62]. Clearly, a concerning portion of AF treated patients develops PV stenoses. There have been several chronic studies examining this phenomenon. However this study aims to investigate the development of stenosis in the distal and ostial PVs on an acute time scale using translational approaches to understand and reduce its occurrence.

Methods

Fresh pulmonary vein samples from Yorkshire Cross swine (n=25) were carefully dissected into 1 cm^2 squares and the orientation relative to the PV anatomy was noted. Human tissue (n=3) acquired from non-viable organ transplant donors through our local

organ procurement organization LifeSource (St. Paul, MN) were also used. PV specimens were sorted into ostia and 1 cm distal to the ostia groups.

Four sutures were attached to each side of the pulmonary vein samples, and they were subsequently mounted in a biaxial testing machine (Figure 31). Each specimen was used as its own control in this experimental paradigm. Samples were subjected to five preconditioning cycles of 10% strain initially, stretched to 20% strain, thus mimicking changes associated with normal physiological function, and then a randomized ablation modality of RF or cryoablation was applied tangentially (Figure 32). RF ablation was applied employing a 7 Fr Marinr® catheter (Medtronic, Minneapolis, MN) using 25 W with a 65°C temperature limit for 1 minute. Cryoablation was applied with a Freezer Max catheter (Medtronic, Minneapolis, MN) for 2 minutes. The resulting stresses in the axial and circumferential directions were measured for 6 and a third minutes following the ablation.

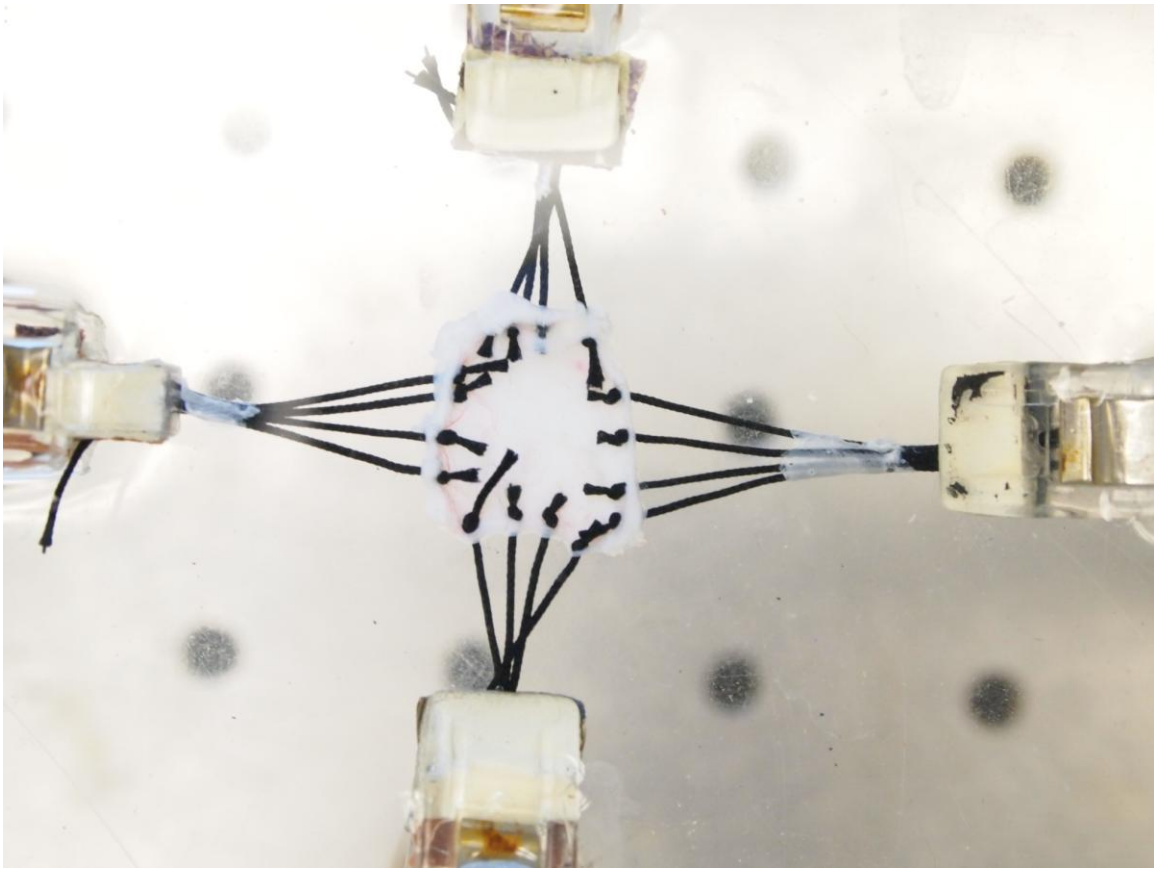

Figure 31. The pulmonary vein specimens were mounted on a biaxial testing machine using sutures in alignment with the axial and circumferential directions of a given vessel.

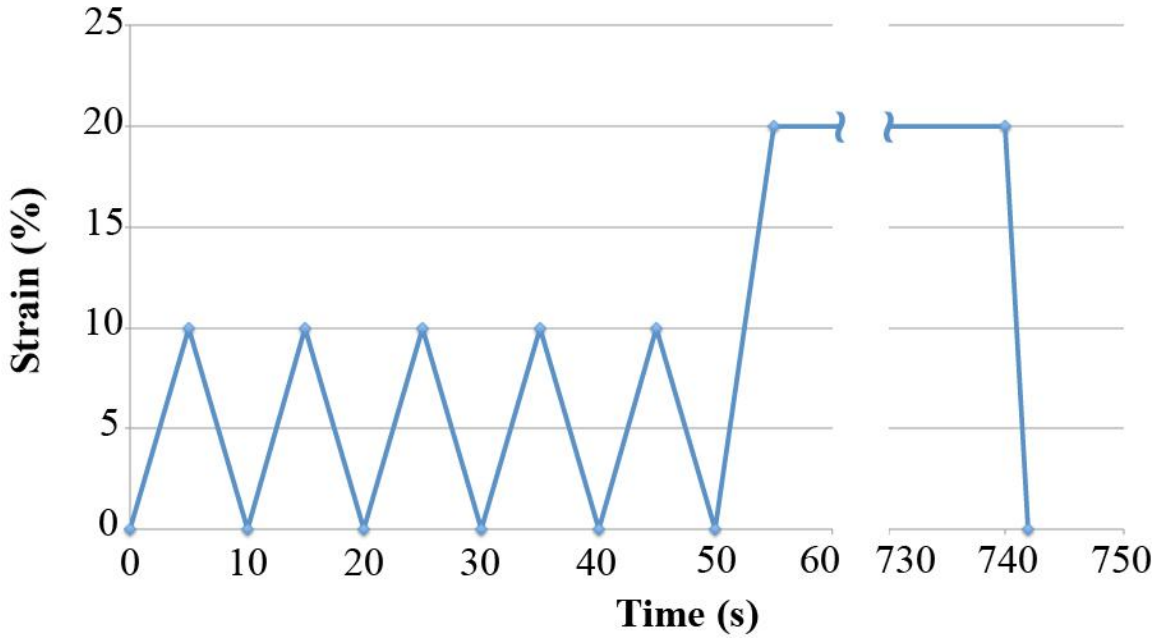

Figure 32. Graphical representation of strain imposed on the pulmonary vein sample throughout the experiment. The ablation was started at the 60-second time point.

Results

Normalized resultant circumferential stresses following the ablations were significantly different in the distal RF ablation group compared to the non-treatment controls for the porcine PV tissues as shown in Figure 33 ($p<0.05$). Cryoablation was significantly different immediately following the ablation, but this effect subsided following ice thaw. Of note, there was a trend in reduced circumferential stresses between the human RF ostia and swine RF ostia groups following ablation as shown in Figure 34 ($p=0.07$). However, significance was not achieved likely due to the limited available human samples utilized in this study. Importantly, this trend was not observed with the swine tissue. There were no noteworthy findings in the axial domain. Interestingly, a number of the results discussed herein support clinical observations and fall in agreement with similar *in-vitro* investigations.

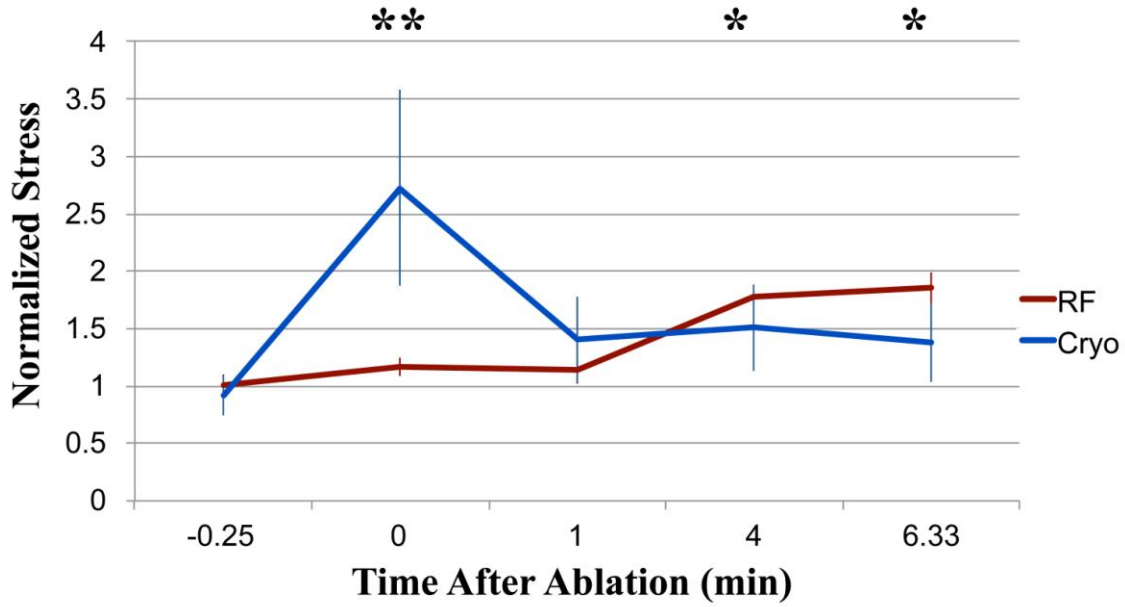

Figure 33. Normalized circumferential stresses following distal RF ablation (n=9) were significantly different compared to the non-treatment controls, while cryoablation (n=8) was only significantly different during thaw. (*p<0.05 for RF ablation, **p<0.05 for cryoablation)

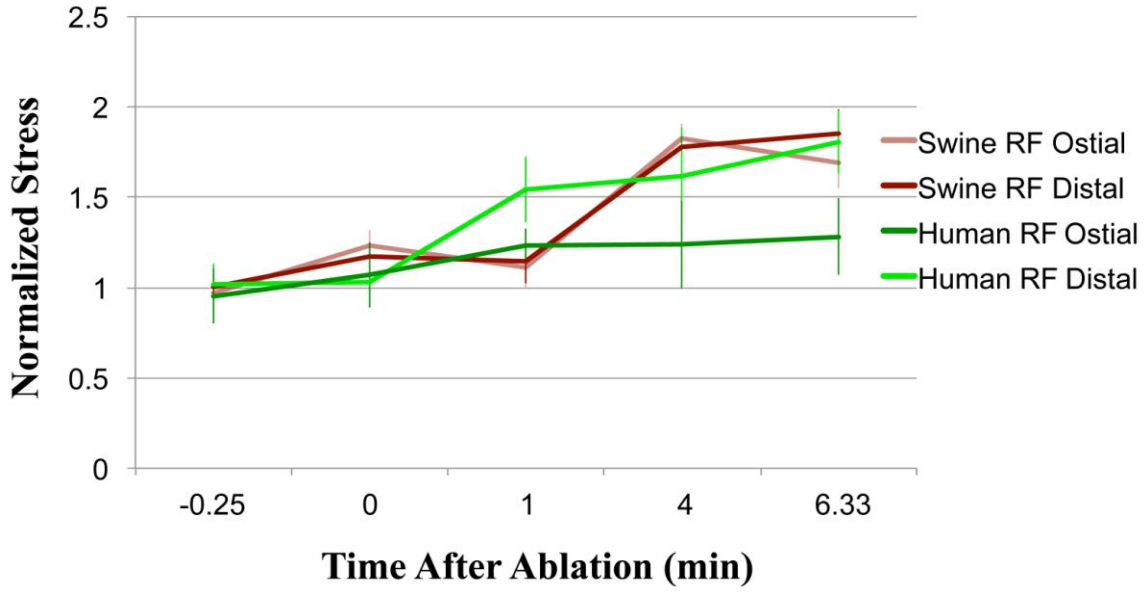

Figure 34. Performing RF ablations produced a reduction in observed circumferential stresses for only the human ostia (n=3) when compared to the swine ostia (n=8). No differences were observed between the distal human (n=3) and distal swine (n=9) groups.

Interpretation

In the circumferential direction cryo energies initially significantly increased the stresses associated with the presence of ice, but following thaw the stresses remained only somewhat elevated. It is considered that cryoablation causes the realignment of fibers, dehydration of tissues, yet leaves the extra cellular matrix intact. Also, it shifts the stress-strain relationship resulting in higher stresses in physiological ranges [53]. Our study used a strain of 20% and then we observed similar stress behaviors following cryoablation. In contrast, RF ablations induced significant increases in stresses that were sustained. RF ablation therapy is considered to: 1) denature structural proteins, 2) cause a loss of compliance, and 3) induce shifts of stress strain curve [49]. These described phenomena with RF ablation were observed in our studies for both the porcine and human tissue samples investigated.

It is suggested that such increases in induced tissue stresses and loss of PV compliances that occurs following ablations, likely initiates the development of PV stenosis in patients. Importantly, cryoablation is less likely to facilitate the development of stenoses compared to RF ablation [62,139]. We observed here, that although both ablation modalities increased circumferential stresses following treatment, only RF was significantly different compared to the non-treatment controls. These data may support the supposition that following an ablation procedure the increased stress state leads to a greater likelihood of PV stenosis development.

Here we also noted that the ostia and more distal ablations of the PV also provoked interesting insights. Minimal circumferential stress changes were induced for the swine ostia versus more distal PV tissue, however there were differences for the human tissue. In the swine model there is a distinct transition from muscular atrial to PV tissue, whereas in the human anatomy this transition lacks a clear demarcation and muscular tissue typically extended partially into the PV. In this experimental paradigm, swine tissue appeared uniform in both location groups while human tissue was not. Further studies are needed to investigate the discrepancy of the swine model as it relates to the human patient populations of interest: a translational approach is essential for investigations of underlying mechanisms. This data is particularly valuable since it

addresses anatomical differences between species and circumferential stress changes as it relates to clinical ablation complications. RF and cryoablations cause an increase in circumferential stresses that may potentially spark the developments of PV stenoses.

Section 3 Visualization of Tissue Responses to Cardiac Ablation Procedures

The ability to directly visualize the device tissue interface during cardiac ablation procedures is invaluable. The utilization of Visible Heart® methodologies has allowed for investigations of cardiac ablative procedures, specifically this procedural application and associated complications that may arise within the various cardiac chambers. For instance, the explosive steam pop phenomenon was visualized inside the atrium to demonstrate the intense release of energy and potentially damaging particulates. Furthermore, additional infrared imaging investigations on the epicardial tissue temperatures were conducted to further improve our understanding of the temperatures, which the nearby phrenic nerve may experience during a performed clinical procedure. Additionally, a typical cryoballoon ablation procedure was visualized from the transseptal puncture to the difficulty clinicians face when positioning balloon. The information gained from these investigations may provide important insights to both clinicians performing such procedures as well to device designers.

In vitro Reanimation of Isolated Human and Large Mammalian Heart-Lung Blocs

Submitted to *BMC Physiology*, in review.

Ryan P. Goff, PhD[1,2], Brian T. Howard, MS[1,2], Stephen G. Quallich, BS[1,2], Julianne H. Spencer, PhD[1,2], Tinen L. Iles, BS[2], Paul A. Iaizzo, PhD[2]

[1] Department of Biomedical Engineering, University of Minnesota, Minneapolis, MN
[2] Department of Surgery, University of Minnesota, Minneapolis, MN

Preface

Although this study does not directly examine cardiac ablation procedures, it provides the background required to generate a heart-lung bloc model that has numerous benefits for such studies. The addition of the lung(s) provides native pulmonary vein ostium that can then be invaluable for studying the device/tissue interface. This study describes the reanimation of both swine and human heart-lung blocs; the development of this methodology also allowed for the following two studies to be conducted. For example, epicardial infrared imaging to observe surface temperatures during pulmonary vein isolation would not be representative of the clinical scenario. The addition of the lungs to our reanimation procedure fabricated a more robust model that accurately represents the native anatomy and physiology, especially when performing cryoballoon ablation procedures.

I was responsible for data and statistical analysis of swine and human heart specimens. In addition, all of the contributors aided with the reanimation of these cardiac specimens. The lab is still using these techniques today, especially when representative pulmonary vein anatomy is required.

Summary

Background: In vitro isolated heart preparations are an invaluable tool for the study of cardiac anatomy, physiology, and device testing. Such preparations afford investigators a high level of control, independent of host or systemic interactions, and high throughput if desired. Here we present that isolated human and swine preparations with the lung(s) attached are particularly valuable for the study of device-tissue interaction and anatomy. Additionally we detail our laboratory's experience with developing these methodologies for heart/lung bloc studies

Methods and Results: Four human and 18 swine heart-lung preparations were procured using techniques analogous to those of cardiac transplant. Specimens were then rewarmed and reperfused using modifications of a previously developed apparatus and methodologies by our laboratory. Positive pressure mechanical ventilation was also employed, and epicardial defibrillation was applied to elicit native sinus rhythm after rewarming. Videoscopy, fluoroscopy, ultrasound, and infrared imaging were performed for anatomical and experimental study. Systolic and diastolic pressures observed for human and swine specimens, respectively, were 68/2±11/7 and 74/3±17/5 mmHg, with heart rates of 80±7 and 96±16 bpm. High resolution imaging within functioning human pulmonary vasculature was obtained among other anatomies of interest. One specimen elicited poor cardiac performance post-defibillation.

Conclusion: We report the first dynamic images of the pulmonary vasculature during cardiopulmonary function in isolated reanimated heart-lung blocs. This experimental approach provides unique in vitro opportunities for the study of medical therapeutics applied to both human and large mammalian heart-lung specimens.

Key Words: heart-lung bloc; device-tissue interaction; pulmonary vasculature; isolated heart

Introduction

In vitro isolated heart preparations have been a cornerstone of cardiac research since Langendorff's original methodology was described in the 1890s [141]. The benefits of isolated heart research are numerous and can be remarkable depending on the investigator's goal. Isolated hearts offer a high degree of control over the system including, but not limited to: perfusate selection, flow control, and pre- and after-load variability. For a thorough historic summary of these experimental models the reader is referred to a review by Hill *et al* [142]. Furthermore, numerous pharmacological studies using such approaches can help elucidate the direct action of agents on the isolated cardiac tissues, i.e., while avoiding systemic interactions of other agents or breakdown products (e.g., cardiac-nervous system, hepatic metabolism) [143].

Additionally, high-throughput cardiac perfusion systems can be designed, or now even purchased off the shelf, in which multiple small mammalian hearts can be experimented on simultaneously. Isolated heart preparations have garnered notable insights to mechanisms of arrhythmias [144] and have been reviewed elsewhere [145]. Depending upon the system configuration, a wide range of equipment and modalities are available to the investigator including: electrophysiologic monitoring and stimulus, ultrasonography, ultrasonic stimulation, fluoroscopy, infrared thermography, direct visualization via videoscopes, and anatomical mapping systems. Furthermore, the utilization of large mammalian isolated hearts allows for critical pre-clinical testing of device-tissue interactions in an environment highly similar to actual human anatomy and physiology, if the proper animal model is selected for investigation [146]. Comparative imaging of normal versus pathologic conditions, or interspecies comparisons, to determine optimal approaches, models, and designs are critical to development of novel therapeutics [147]. To the medical device designer, engineer, or clinician, these insights have proven to be of high educational value [148,149].

Despite isolated heart preparations being a valuable tool, proper anatomical relationships can be compromised when the lungs are removed. In particular, the pulmonary veins and

their native ostia are of interest in the context of pulmonary vein isolation ablation treatments for atrial fibrillation. Heart-lung preparations have been utilized previously to elucidate the release of atrial natriuretic peptide[10] and expand the pool of lung transplants to non-beating donors [150]; they have also been used in numerous pharmacologic studies. Interestingly, the first heart-lung preparations are often attributed to Knowlton and Starling [151], however their work acknowledges the methods of Martin [152] which were presented in lecture at Johns Hopkins in 1883. The first publication by Martin of his heart-lung bloc preparation was released in 1881 [153], therefore predating Langendorff's work by fourteen years. In short, this preparation cannulates in situ the superior vena cava and one of the branches coming off the aortic arch. A closed loop is created by which pressure can be monitored, a compliance chamber is incorporated, and pre- and afterloads are varied.

It is also possible for human hearts from non-viable organ donors to be successfully reanimated using an isolated experimental apparatus [142]. The Visible Heart® methodologies have been previously described by our laboratory [154], but more recently we have expanded these experimental approaches to incorporate whole large mammal heart-lung blocs, including both human and swine studies. To the authors' knowledge, this is the first description of large mammalian heart-lung blocks being used to achieve dynamic imaging in the pulmonary vasculature. The goal of the current study is to determine feasibility and characterize viability of large mammalian heart-lung preparations.

Methods

The technique developed by our laboratory has been used successfully to reanimate human and swine hearts with right, left, or both lungs attached and functioning. Swine studies were approved by the Internal Animal Care and Use Committee at the University of Minnesota. Human hearts were approved for study by the Human Subject Committee Institutional Review Board. Consent for use of the hearts for research purposes was

received from the donors' family members before explantation via LifeSource (St. Paul, MN, USA).

The detailed procurement procedure has been described previously [142,154]. Briefly, a median sternotomy was performed and an aortic root cannula implanted for delivery of cardioplegia. The inferior vena cava (IVC) was ligated and, just prior to cardioplegia delivery, the IVC for human preparations was removed with the liver if it was being recovered for transplant, and the superior vena cava (SVC) and aorta were cross-clamped. Cardioplegia was then delivered under pressure to rapidly cool and arrest the heart. The heart and lungs were then dissected and the heart-lung bloc removed by transection of the major vessels, trachea, and esophagus. The human specimens were then transported on ice to the laboratory within 6 hours of cross-clamp depending upon logistics of transportation of viable organs to recipients. The human heart-lung specimens were non-viable cardiac donors (e.g., unknown cardiac arrest period, cardiac disease). An analogous procedure was performed on swine hearts in our laboratory (mean animal weights of 84±14kg; n=18) using two liters of 4°C St. Thomas's cardioplegia for induction of cardiac arrest. We have typically performed these studies with just one lung attached, but the method has been utilized to include both lungs. Preparations with only one lung allow cannulation of the non-utilized pulmonary vein, which may be used to access the left atrium for imaging or device introduction.

Upon arrival of human (or after explantation of swine) specimens, hearts were placed in an ice slurry of modified Krebs-Henseleit buffer while cannulation of the great vessels was performed (i.e., IVC, SVC, and aorta). If a one-lung preparation was desired, the left/right pulmonary veins and artery were dissected from the left/right lung, and the lung was removed. These vessels were cannulated as well, and a hemostasis valve was fitted for access. If both lungs were desired in the preparation, the pulmonary trunk was cannulated to allow control of the buffer flow, either directing all flow through the lungs or allowing some flow to the reservoir (i.e., a parallel path through the lungs and to the reservoir). An intubation tube was placed in the trachea and connected to a ventilator to

control flow through the airway. Preparations were ventilated at a respiration rate of 11-15 per minute and a volume of 150-250 milliliters per lung.

The heart-lung blocs were then connected to the apparatus described in detail previously [154] that was adapted for such use. A schematic of this system can be found in Figure 35. The system was altered to vary the aforementioned parameters of other isolated heart research systems and functioned in either partial or four-chamber working mode. Partial working mode is similar to a Langendorff apparatus function, but fluid flow continues through an isolated lung (i.e., the right heart continues to function). The system utilized a cardiovascular bypass oxygenator and heated water jacketed fluid reservoirs to maintain the proper physiologic environment. The preparations were cradled on custom sized soft foam cushions to support the tissue. Seven to eight liters of modified Krebs-Henseleit buffer were contained in the system and buffer changes of approximately four liters were performed regularly to wash out metabolites and maintain visualization as desired.

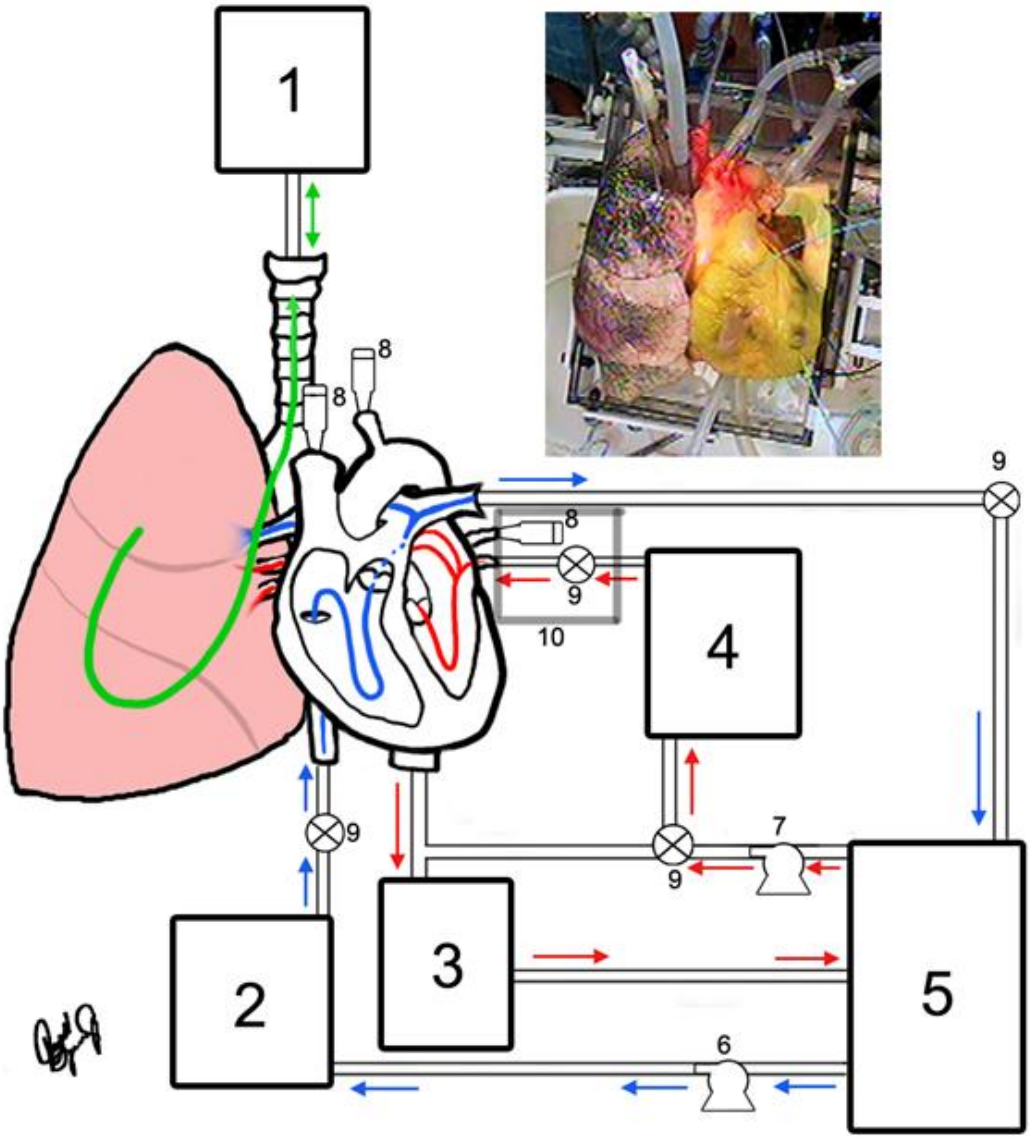

Figure 35. (Top right) External view of human heart 277 in systole and attached to the system. (Center) Flow diagram for a functional heart and lung reanimation consisting of: (1) a respirator connected to the cannulated trachea and thus attached to the lung(s), (2) a pre-load chamber for the right side of the heart, (3) an aortic after-load chamber which mimics the resistance that the left ventricle works against, (4) a left pre-load chamber employed when only one lung is present, (5) an oxygenator reservoir for pooling fluid expelled by any cannulated branch of the pulmonary artery, (6 & 7) fluid pumps to maintain the pre-load pressures, (8) hemostasis valves that allow access for delivery of cameras, instruments, and assorted devices, (9) valves that may also be used to redirect flow as physiologically appropriate, while (10) cannulation of the pulmonary vein(s) are shown here for a right lung preparation, but are absent or translated when either both lungs or the left alone respectively are used.

Once the specimen was re-warmed to 37°C, dobutamine was added to the system and the heart was defibrillated with 34 joules of energy supplied by a programmer-analyzer unit

(#88345 Medtronic, Inc., Minneapolis, MN, USA) via a pair of external patches (#6721, Medtronic, Inc.) placed epicardially above and below the ventricles. These hearts generally began beating in native sinus rhythm after a single defibrillation. It should be noted that one human heart developed heart block at two hours post-reanimation, and was then paced by a temporary pacing lead at 60 beats per minute; all specimens could be paced as desired. Hemodynamics of the left and right ventricle were recorded by Utah Medical pressure transducers (Model DPT-200, lot#1101991, Midvale, UT, USA) via water columns from venogram balloon tipped catheters (Attain 6215, Medtronic, Inc.).

High-resolution Olympus commercial endoscopes (Model 1V8200T, Model 1V8420, Center Valley, PA, USA) were then placed within these heart and/or lungs to capture functional anatomy. To our knowledge, these are the first images of the pulmonary veins and arteries within the lung of functioning human heart-lung blocs.

Results & Discussion

Using this experimental approach, eighteen swine and five human heart-lung blocs were successfully reanimated. Hemodynamic functioning of these in vitro reanimated specimens was augmented by the delivery of inotropic agents (1.5 mg doubutamine) and/or by increased dosing with extracellular calcium (3.5 mg calcium chloride). Prior to heart recovery, the mean heart rate and blood pressure for the swine were: 91±13 beats per minute and 105/56±13/9 mmHg, respectively. Table 23 provides partial cardiac medical histories for the organ donors from which the human hearts were recovered. Table 24 provides the relative hemodynamic performance data for these reanimated heart-lung preparations. These data points are calculated as 5 minute averages at the 1 hour time point post defibrillation.

Table 23. Summary of donor information and hemodynamic status prior to organ recovery

Human Specimens							
Specimen	Gender	Age (yrs)	Weight (kg)	Cause of Death	HR (bpm)	BP (mmHg)	CVP (mmHg)

HH 277	M	60	113.4	Head trauma	71	105/61	15
HH 284	F	78	54.4	CVA	103	118/70	11
HH 291	F	58	114.7	CVA	92	100/50	12
HH 295	M	34	68.0	Cardiac arrest	92	130/75	-
HH 308	F	36	53.0	CVA, previously transplanted	87	97/71	10
Average		53.2	80.7		89.0	110/65	12
Standard Dev.		18.4	31		11.6	14/10	2.2

BP=blood pressure; HR=heart rate; CVA= cerebrovascular accident; CVP=central venous pressure

Table 24. Hemodynamic performance of each reanimated heart/lung bloc specimen

Swine Specimens

Specimen	HR (bpm)	LVSP (mm Hg)	LVEDP (mm Hg)	+dLVP/dt (mm Hg/s)	-dLVP/dt (mm Hg/s)	Tau	Lung
1	95.8	91.2	12.4	982.8	-903.0	31.2	Right
2	91.0	25.0	-2.0	430.8	-343.8	36.2	Right
3	100.0	77.0	-4.0	961.0	-462.0	30.0	Right
4	81.7	73.5	2.3	772.3	-354.5	37.7	Right
5	91.8	85.7	1.3	927.0	-509.8	33.2	Right
6	99.5	62.8	11.3	574.0	-435.0	30.2	Right
7	55.8	82.0	5.7	600.2	-358.2	63.0	Right
8	90.3	79.3	-4.3	842.5	-618.0	33.5	Left
9	92.7	75.7	12.0	623.3	-771.7	32.5	Left
10	102.5	67.5	1.2	637.8	-513.2	29.7	Right

11	76.7	101.7	10.7	786.5	-501.5	39.7	Right
12	123.3	76.3	1.3	729.0	-624.5	26.0	Right
13	124.8	58.7	2.7	762.5	-532.7	24.0	Right
14	84.5	87.2	0.7	888.8	-646.0	54.0	Right
15	114.0	91.7	-2.7	922.3	-808.0	27.5	Right
16	105.0	70.8	0.0	607.7	-446.3	28.8	Right
17	101.3	56.5	3.8	529.8	-317.7	29.8	Right
18	91.2	75.7	7.0	618.3	-810.2	33.0	Right
Average	95.7	74.3	3.3	733.2	-553.1	34.4	
Standard Dev.	16.3	17	5.4	163.6	177.6	9.7	
			Human Specimens				
HH 277	85.8	65.7	-7.3	624.5	-475.5	37.2	Right
HH 284	81.2	79.5	1.7	848.2	-377.7	37.5	Right
HH 291	70.3	53.3	8.0	341.3	-273.7	45.3	Both
HH 295	81.3	72.5	4.2	415.7	-343.0	37.7	Right
HH 308	57.2	73.0	0.0	963.0	-469.8	56.2	Right
Average	75.2	68.8	1.3	638.5	-387.9	42.8	
Standard Dev.	11.6	9.9	5.7	268.1	86	8.2	

HR=heart rate; LVSP=left ventricular systolic pressure; LVEDP=left ventricular end-diastolic pressure; +dLVP/dt= maximal positive derivative of left ventricular pressure with respect to time; -dLVP/dt= maximal negative derivative of left ventricular pressure with respect to time

It should be noted that one of the early reanimated swine heart-lung specimens (#2) elicited poor hemodynamic performance from the beginning of reanimation. We suspect that injury occurred during isolation and/or that emboli caused poor coronary perfusion. Additionally, recorded data from several hearts elicited negative values for end-diastolic

pressures; we suspect that this is due to a vacuum or syphoning effect, potentially occurring in the current system modification to incorporate the lungs.

Interestingly, compared to our long-term experience with lone heart reanimation using endoscopes, a large degree of remaining particulate and blood within the lung complicated our initial imaging during certain studies. Therefore, more frequent buffer changes were required to obtain clear, high-fidelity images and video.

The main benefit of this model is the maintenance of proper pulmonary ostia and vessel anatomies. A selected anatomical image series of a videoscope being retracted from either the pulmonary arteries or veins is shown in Figure 36; a corresponding video can be accessed via supplemental materials (Supplemental Video) or online at http://www.vhlab.umn.edu/atlas. The study of cryoballoon ablation procedures motivated much of the development of this model, and a series of cryoballoon procedures have been performed, as viewed from within the vein as displayed in Figure 37, panel C. The Supplemental Video of the functioning pulmonary arteries and veins gives the reader an appreciation of the truly dynamic nature of these vessels, which are usually thought to be relatively passive structures. To the authors' knowledge, this report has provided first time dynamic images of the pulmonary vasculature during normal cardiac function in both reanimated human and swine heart-lung blocs. This model provides a unique in vitro approach for the study of medical therapeutics from both human and large mammalian heart-lung specimens.

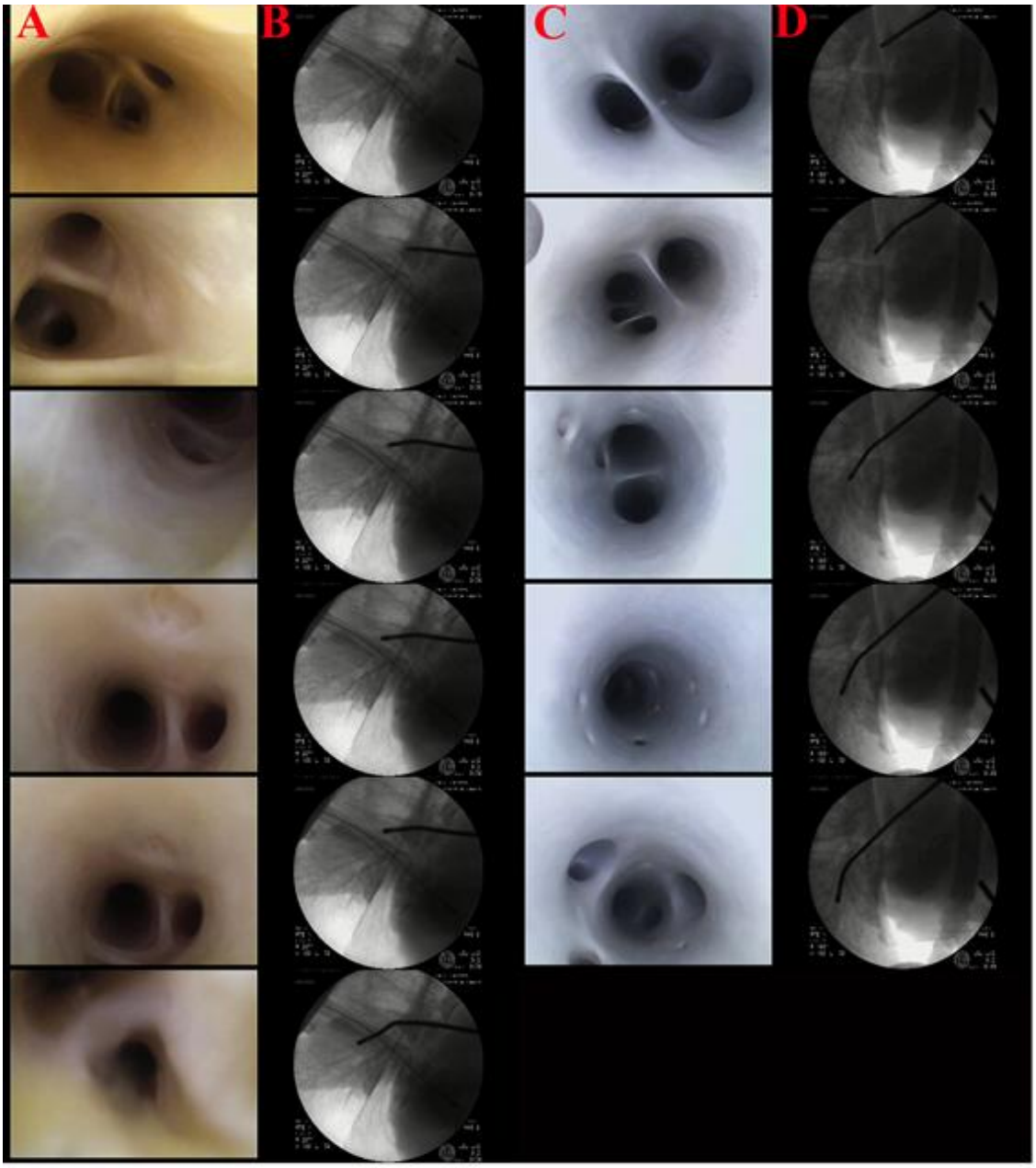

Figure 36. Image series obtained from reanimated human heart-lung bloc 284 (A,B) and 277 (C,D). Series shows the path through the distal pulmonary arteries and veins, respectively. The corresponding fluoroscopic images (B,D) in each case show the relative locations of the videoscopes (A,C). A video of the journey through the vasculature can be viewed as well (see online Supplementary Video).

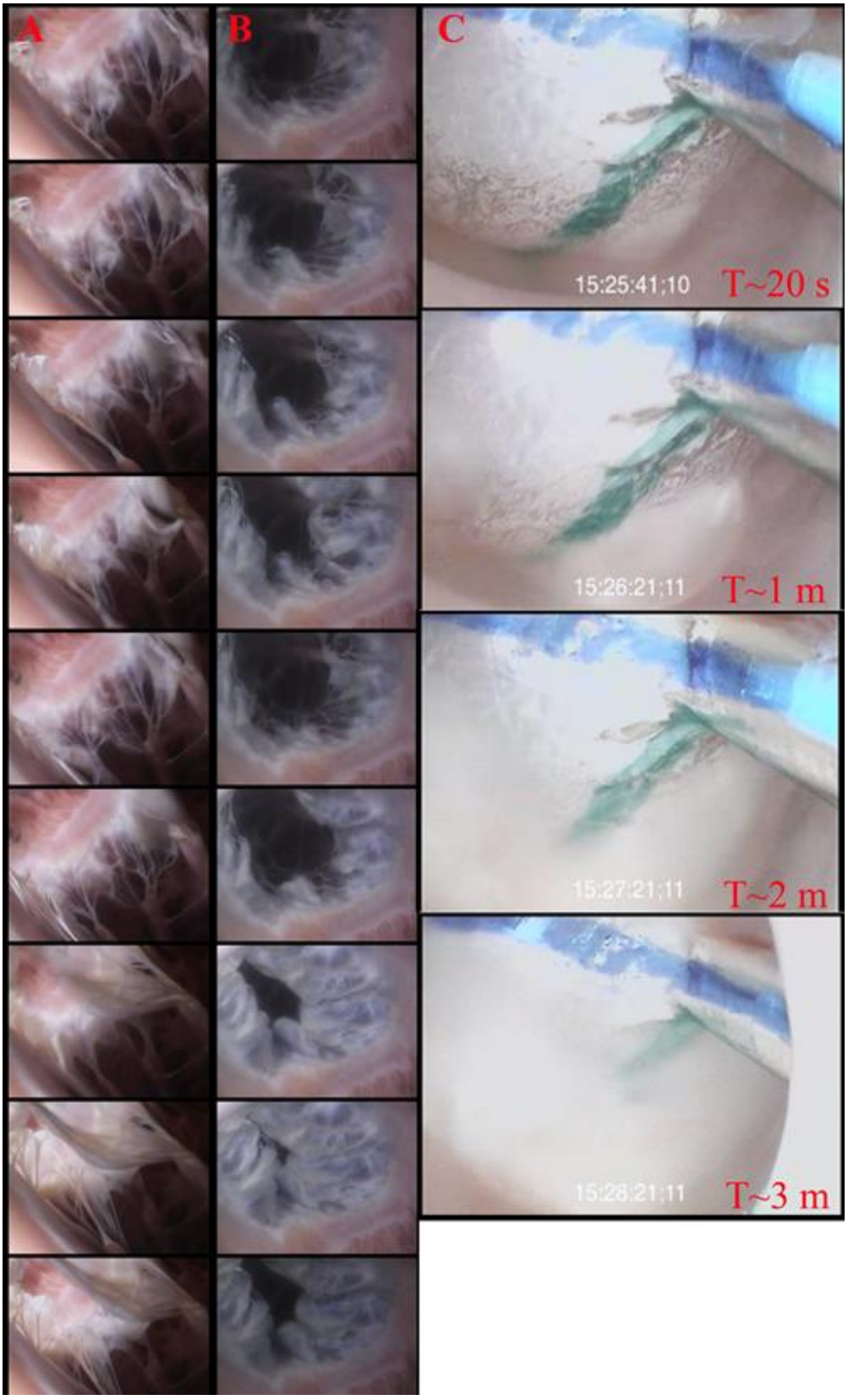
A
B
C
15:25:41;10
T~20 s
15:26:21;11
T~1 m
15:27:21;11
T~2 m
15:28:21;11
T~3 m

Figure 37. Time series of images from human heart 277. Series shows tricuspid valve closure from the right ventricle (A) and right atria (B). Images are displayed 1/15th per second apart in time. Panel C displays ice formation on the distal portion of a cryoballoon ablation catheter (Artic Front, Medtronic, Inc., Minneapolis, MN) as seen from within the pulmonary vein. The images are spaced post-ablation 30 seconds, 1, 2, and 3 minutes apart.

In a similar embodiment (i.e., without the lungs), this reanimated heart model has been utilized in numerous cardiac studies. In the electrophysiologic area, these studies have included the use of endocardial noncontact mapping, pacemakers, defibrillators, leads, and catheters [155]. The Visible Heart® model has also been employed to study the dynamic nature of valves and transcatheter valve deployment [156]. Importantly these methodological approaches also allow for use of echocardiography and fluoroscopy to guide procedures, such as for comparative imaging [157]. Most recently, this approach has proven to be quite valuable for the study of novel cardiac treatments, such as leadless pacing devices [158]. Nevertheless, the addition of a lung(s) to this paradigm still allows for any of the prior studies to be conducted, but may in turn reduce the number of hemostasis valve access points that were previously available.

Our continued use and enhancement of Visible Heart® methodology has also facilitated the creation of an open-access educational website, The Atlas of Human Cardiac Anatomy (http://www.vhlab.umn.edu/atlas) [159]. The anatomical images and videos on this website are free to download and use for presentations and teaching, however we request that proper citations be used. In other words, the images and/or comparative imaging of functional cardiac anatomies are of high value in teaching the nuances of cardiac anatomy, especially of active, complex structures such as valves. It should be noted that this website also provides instructional tutorials on cardiac anatomy and physiology, as well as full cadaveric thoracic cavity dissections. Finally, a cardiac device tutorial is also available, which has been well noted as being beneficial in explaining therapies to patients.

The model described here is not without limitations, as is true with all in vitro systems. Despite supersaturating the buffer with oxygen, there remains a significant difference in

the oxygen content of the buffer compared to blood. For this reason, the function of the heart slowly declines over time from the initial reanimation. Yet reasonable physiologic function to perform the aforementioned investigations is generally elicited for up to 4 to 8 hours, based on our previous experiences. It is possible that the addition of the lungs may extend the functionality, which we tend to believe at this point, but need more data to substantiate. Most recently, we are employing a full anesthesia suite ventilator to more closely control the ventilation parameters (e.g., provide positive end expiratory pressure, PEEP). In such experimentation, one also needs to consider that although it is also known that hypothermal transport of organs is protective, global ischemic injury still occurs to some degree. Further, our current system is designed to replicate physiologic pre- and after-loads, but there potentially are important physiological effects that are not completely replicated, such as vessel compliance. Likewise, in our studies the heart-lung blocs are cradled on soft foam sponges which may focally alter perfusion compared to the natural state. Finally, due to the nature of acquiring non-viable donor human heart-lung specimens, there are numerous differences between inherent status of the hearts that cannot be controlled. Such differences in status include, but are not limited to: method of cardiac arrest, transport time before arriving in the laboratory, inotropic support, potential air or other emboli in the coronary vasculature (potentially generated during explantation), and prior pathologies. Despite being unable to control for these parameters, the described system produced comparable pressures to other isolated human heart alone preparations [142,160]. As reviewed in Table 2, despite these variances the hemodynamic data are fairly comparable from specimen to specimen. It should be specifically noted that we are extremely grateful and privileged to obtain these donated human heart-lung preparations as gifts for research.

Conclusions

To conclude, this extension of Visible Heart® methodologies has enabled functional anatomical heart-lung anatomical visualization. Further, unique abilities to image the device-tissue interactions using this approach are unparalleled. Therefore, we consider that these obtained images are of high value to the medical device designer, educators,

and clinicians for both training and educational purposes. The lab will continue to reanimate hearts and heart-lung blocs using these methodologies and thereby enable the study of dynamic anatomies, insights into the device-tissue interface, and creation of new materials for the free-access Atlas of Human Cardiac Anatomy website.

Acknowledgements

The authors would like to thank the generous individuals and families that donated hearts for research and LifeSource for facilitation of this research. In addition, the authors would also like to thank Gary Williams for his computer assistance and Monica Mahre for preparation of this manuscript.

Disclosures: This study was funded by a Medtronic Inc. research contract, as well as the Lillehei Heart Institute and the Institute for Engineering in Medicine at the University of Minnesota. There are no relevant conflicts of interest.

Direct Visualization of Induced Steam Pops During Radiofrequency Ablations

Published in *Heart Rhythm Case Reports*, 2015, in press.

Stephen G. Quallich, BS[1,2]; Ryan P. Goff, PhD[1,2]; Paul A. Iaizzo, PhD[1-4]

[1] Department of Biomedical Engineering, University of Minnesota, Minneapolis, MN
[2] Department of Surgery, University of Minnesota, Minneapolis, MN
[3] Department of Integrative Biology and
Physiology, University of Minnesota, Minneapolis, MN
[4] Institute for Engineering in Medicine, University of Minnesota, Minneapolis, MN

Financial Support: Medtronic, Inc. research contract
Disclosures: Medtronic, Inc. research contract
Key Words: Radiofrequency ablation; steam pop; high-speed visualization

Preface

Steam pops may be associated with serious complications such as cardiac tamponade, stroke, and/or myocardial infarction. In this experiment we aimed to visualize the formation of a steam pops, as a means to observe the release of energies associated with these events. Commonly, clinicians may or may not hear pops in a surgical suite and believe it to be a mild event because of their inability to perceive them. However, a number of clinicians after seeing this publication and associated video were surprised at the damage inflicted and amount of tissue and air debris discharged from the lesion site.

I was responsible for the experimental design, data collection, and drafting of the manuscript. Ryan Goff assisted with the experimental design and data collection.

Introduction

Importantly, during clinical ablation procedures, the elicitation of elevated tissue temperatures may induce audible steam pops. Rapidly induced high endocardial tissue temperatures are considered to generate these events as a result of blood/tissue vaporizations. In addition, discrepancies between monitored catheter tip temperature and actual endocardial tissue temperature may be related to the unanticipated elicitation of steam pops. Ultimately, these induced tissue disruptions can have important clinical consequences. They even may result in perforations of the atrial wall and/or the release of tissue or air emboli from the affected tissues [65].

Case Report

A heart (427.3 g) isolated from a Yorkshire-Cross swine (87.2 kg) was reanimated using previously described Visible Heart methodologies [69]. The tricuspid valve annulus was aggressively ablated using a 7 Fr Marinr ablation catheter (Medtronic Inc, Minneapolis, MN). The occurrence of a steam pop was recorded using an intracardiac endoscope (IplexFX, Olympus Corp, Tokyo, Japan) and a high-speed camera (MotionXtra N4, Olympus Corp) equipped with a borescope (88370AX, Karl Storz, Tuttlingen, Germany) (Figure 38). Of note, formation of focal microbubbles at the ablation site was observed before steam pop initiation. The application of progressive ablative energies generated and further released large quantities of explosive bubbles/tissue disruptions, which actually caused the catheter to fly away from the application site. The duration of the recorded steam pop was less than 10 ms, although submillimeter air emboli and tissue fractions were released for seconds after the initial burst. In this case, the endocardial damage caused by this induced “explosion” was a void 7 mm in diameter and 4 mm in depth.

Discussion

It is important to consider that the use of fluoroscopy alone as an imaging modality during such clinical procedures, limits an operator’s abilities to detect relative incidences of steam pops and other associated tissue damage. In other words, the only indication in

such cases may be a visual displacement of the catheter tip and/or a rapid change in the electrode temperatures. Interestingly, an unintended catheter repositioning, causing a loss of wall contact, results in these same observations. During our unique visualization studies of applied RF ablations, we also noted that with early application of energies, we could observe the formation of focal micro-bubbles preceding the steam pop, which if one could detect them they may act as an early indicator for more undesired events. Additionally, trying to determine one's catheter tip-tissue orientation may help ensure proper lesion formations, while importantly minimizing the potential for inducing steam pops. Furthermore, it should be noted that in our setting, these observed tissue explosions were not always audible, suggesting that recognizing their occurrence may be even more clinically challenging [67]. In summary, the unique utilization of a high-speed visualization system and Visible Heart® methodologies allowed for investigation of this phenomenon at a visually perceptible rate.

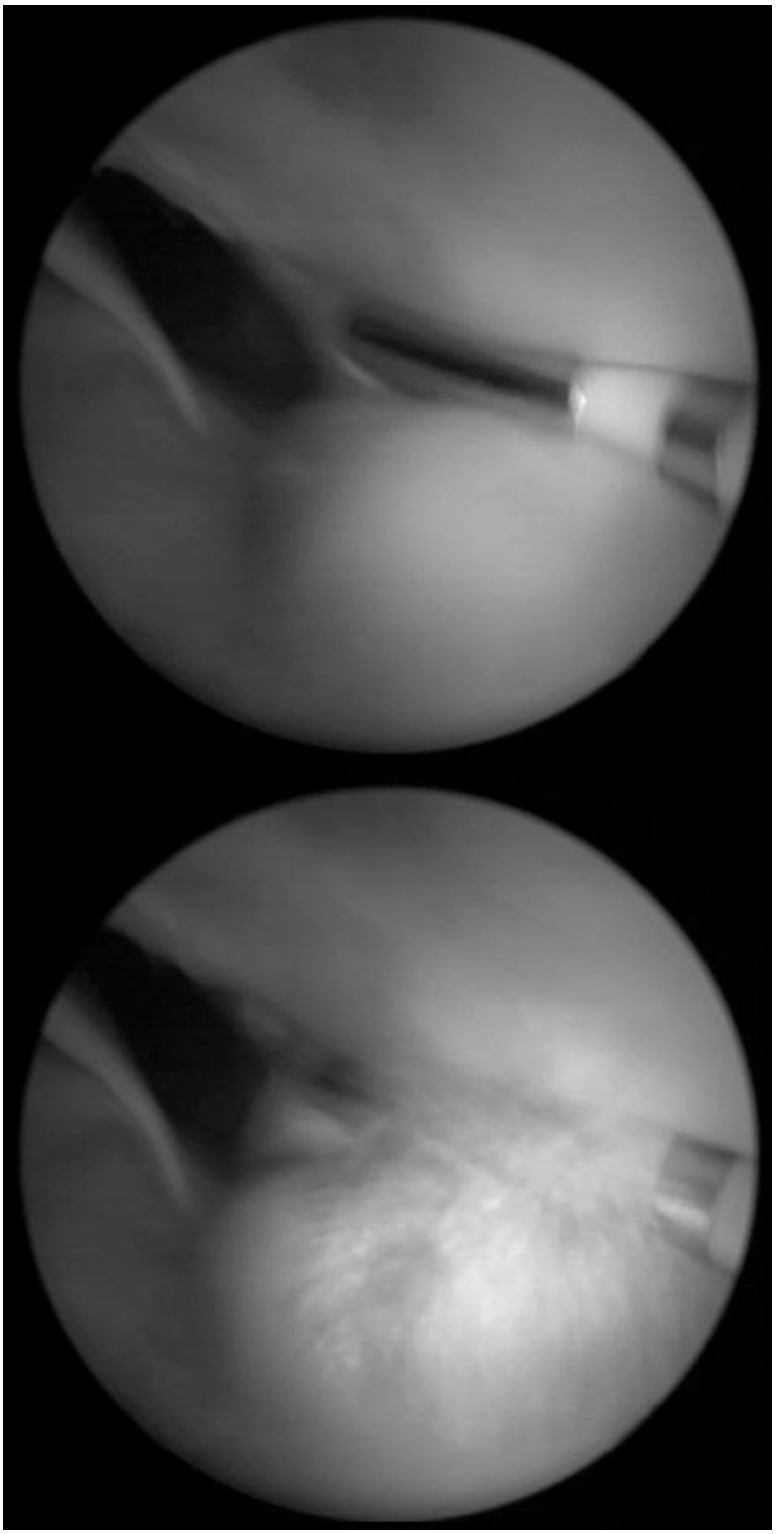

Figure 38. The explosive energy can be observed in frames 1.5 ms apart immediately prior to (Top) and during the steam pop (Bottom).

Key Teaching Points

- Cardiac ablation–induced steam pops release air/ tissue emboli that may cause myocardial infarctions or strokes. The resulting endocardial damage, if excessive, may result in perforations and/or the development of cardiac tamponade.
- Microbubbles often are released before the elicitation of steam pops. If these microbubbles could be detected, then the immediate reduction of power or halting of an ablation may reduce the occurrences of undesired steam pops.
- Identifying steam pop incidences via fluoroscopy alone may be quite challenging. Movement of the catheter during such an event, especially when there is no associated audible indicator (ie, a pop), may be misconstrued as a simple loss of wall contact.

Direct Visualization of Cryoballoon Ablation Procedures Performed within Reanimated Human Hearts

Submitted to *Heart Rhythm*, in review.

Stephen G. Quallich, BS[1]; Lars M. Mattison, BS[1];
Ryan P. Goff, PhD[1]; Paul A. Iaizzo, PhD[1,2]

[1] Department of Biomedical Engineering, University of Minnesota, Minneapolis, MN
[2] Department of Surgery, University of Minnesota, Minneapolis, MN

Preface

This experiment utilized the methods developed in our lab for reanimating heart-lung blocs. We demonstrate the typically performed clinical cryoballoon ablation procedure: i.e., with direct visualization. It cannot be stressed enough that representative pulmonary vein ostia are essential for mimicking the challenges and issues clinicians must overcome. This study visualizes the native pulmonary vein isolation from the transseptal puncture to ablation energy application. Some of the current procedural challenges were highlighted, such as the difficulties in proper balloon placements so to ensure there are no leaks: incomplete occlusions may lead to ineffective cryothermal lesions. This study also identified some of the predicaments incurred due to anatomical limitations.

Ryan Goff and I were responsible for the study design and image collection. Lars Mattison and I processed the acquired images and video. I was also responsible for the initial draft of the manuscript.

Case Report

It is considered that cryoballoon and radiofrequency ablation have comparable efficacy [161]. Optimal positioning of catheters is essential, albeit challenging due to anatomical

and morphological variations. Furthermore, respiratory and cardiac movements can cause difficulties for catheter placements [48]. Our objective was to directly visualize cryoballoon ablations to highlight procedural challenges. Human hearts deemed not viable for transplantation (n=11) were reanimated using Visible Heart® methodologies [69]. Videoscopes were placed inside the atria to visualize cryoballoon ablations with either ArticFront or ArticFront Advanced catheters (Medtronic, MN, USA). Hemodynamic monitoring and simultaneous fluoroscopy were obtained. Figure 1 illustrates the direct visualization of cryoballoon placements in four different reanimated human hearts. Videoscope views from the left atrium detected ice formation as well as the presence of ostial leaks near the pulmonary vein antrum; i.e., green dye was injected distally within the pulmonary veins. There was incomplete occlusion of the right inferior pulmonary vein in two hearts (verified using contrast fluoroscopy). These visualizations provide valuable insights into the potential challenges faced while performing cryoablation procedures of the pulmonary ostia. These images are especially valuable to clinicians, engineers, and device designers, as they accentuate anatomical and morphological differences.

A supplemental video displaying a functioning heart during the transseptal puncture, including maneuvering of the catheter to the pulmonary veins and the application of ablation in the right and left superior pulmonary veins, is also available.

Funding Source: Research contract with Medtronic, Inc. (no role in study design, data collection/analysis/interpretation, or report writing)

Evaluation of the Dose-Response Effects of Cryoballoon Ablation Therapy Applied to Reanimated Swine and Human Heart-lung Blocs Using Infrared Imaging

Ryan P. Goff, PhD[1,2]; Stephen G. Quallich, BS[1,2];
Benjamin Troness[1]; Paul A. Iaizzo, PhD[1,2]

[1] Department of Biomedical Engineering, University of Minnesota, Minneapolis, MN
[2] Department of Surgery, University of Minnesota, Minneapolis, MN

Preface

This study also relied on the unique methodologies described in our reanimated heart-lung bloc manuscript: here we investigated thermal ablation applications, specifically comparing the use of the ArticFront and ArticFront Advance catheters. In conjunction with our *in vitro* infrared cryothermal tolerances assessment, this study assessed the behavior of pulmonary vein isolation ablation systems in a setting that closely simulated such clinical situations. Identifying epicardial tissue temperatures throughout the application of cryothermal ablations should aid in better understanding the high incidences of phrenic nerve injury associated with such procedures. It was determined that the Artic Front Advances catheter appeared to be more effect in cooling larger areas of atrial tissues than the previous iteration catheter. The results from this study should also help aid in determining appropriate cryothermal dosing, as well as how to limit collateral injury to surrounding tissues such as the phrenic nerves.

Ryan Goff and I were responsible for experimental design, data collection, and statistical analyses. I also contributed to the writing of the manuscript. This work is currently ongoing in the Visible Heart® laboratory.

Introduction

Cardiac balloon cryoablation for the treatment of atrial fibrillation has been gaining attention as an approach for isolation of the pulmonary veins (PV): i.e., since its first reported use in 2003 [87] and in the current clinical form in 2005 [88]. Yet, it should be noted that focal cryoablation has been used surgically for many more years [89] with transcatheter devices becoming available in more recent decades. An advantage of cryoballoon ablation of a pulmonary vein ostium, is that it is a 'single-shot' approach, which aids in accelerating the slow nature of freezing compared to RF energy (i.e., not point-by-point ablation). Further, the currently available ArticFront (Medtronic, Minneapolis, MN) cryoballoon has been shown to have comparable success rates to radiofrequency (RF) ablation with lower adverse events [90,91]. The recent STOP-AF trial concluded similar findings to the observational European studies: that being an acceptable safety profile and superiority to antiarrhythmic drugs in those who have failed to respond to them [62].

Despite widespread and growing clinical use there are still questions regarding dosing and treatment times for optimal cryoablation therapy, which in turn may affect both efficacy and collateral tissue injury [92,93]. Conversely, parameters affecting RF ablation lesions have been investigated in numerous preclinical and clinical studies, and temperatures of 50°C or higher are required for the creation of necessary myocardial scars [56]. Additionally, although many open scientific questions remain, the effects of power, ablation durations, catheter orientations, catheter sizes, usage of irrigation, and contact forces on lesion size have been investigated for RF [94–97]. Furthermore, the release of a second generation cryoablation device with a different cooling profile merits additional research to compare to both the previous versions of theses devices and also to ablation using RF energy [98]. It should be noted, to date, the highest regularly detected clinical complication for ablation with the cryoballoon is phrenic nerve palsy with rates of 4-8% [62,91]. Yet, it remains unknown, the impact on esophageal cooling may also differ for the second generation balloon: importantly, esophageal injury is not normally detectable unless specifically searched for using endoscopy [99,100]. Reports of

hemoptysis are also reported in patient series of cryoballoon ablation, indicating the lung may be injured during these treatments as well [79,162,163]. It is currently recommended by the manufacturer that two separate four minute ablations are applied per PV: yet, several clinicians have recently suggested that only one may be adequate. In other words, given that the phrenic nerve and esophagus are in intimate contact with the right PVs and posterior wall of the LA, respectively, optimization of dosing is important to both ensure permanent isolation of the pulmonary vein tissue while minimizing the impact to these structures.

It is well accepted that in order for cardiac ablation lesions to be effective long-term, it is necessary that they are transmural. In the present study through the use of infrared (IR) imaging, the epicardial surface temperatures were monitored as well as the relative times to reach those temperatures. Due to the anatomical relation of the aforementioned collateral tissues that might be impacted during treatment, these epicardial thermal profiles should be in the range of those experienced collaterally. That is to say that since the tissues injured collaterally are in intimate contact with the epicardial surfaces, that the epicardial temperature profiles measured here are in the range of the most extreme temperatures the collateral tissues may encounter. This infrared imaging data, with additional information regarding the thermal thresholds of injury, may help guide decisions on dosing.

Methods

Isolated Heart-Lung Preparation

Swine studies were approved by the Internal Animal Care and Use Committee at the University of Minnesota. The use of human specimens for research were approved for study by Human Subjects Institutional Review Board: consent for use of the hearts for research purposes was received from the donor's closest relative(s) via LifeSource (St. Paul, MN). Note, the detailed procurement procedures have been described previously [142]. The human specimens were then transported on ice to the laboratory within 8 hours of cardiac arrest.

For isolation of the swine specimens, a median sternotomy was performed and an aortic root cannula implanted for delivery of cardioplegia. The inferior vena cava (IVC) was ligated and just prior to cardiolpegia delivery the IVC was removed with the liver and the superior vena cava (SVC) and aorta were cross-clamped. Cardioplegia was then delivered under pressure to cool and arrest the heart/lung blocs. The heart and one or both lungs were then dissected and the bloc then removed by transection of the major vessels, trachea, and esophagus. Note, we most commonly have performed these studies with just one lung attached, but the method has been easily adapted to have both lungs attached.

The heart-lung blocs were then connected an apparatus described in detail previously [154] that has been modified to accommodate the lung. The system can vary standard parameters of other isolated heart research systems (i.e., pre-load, after-load, perfusates, see Hill et al. [142]) and functions in either partial or four-chamber working mode. Partial working right-side mode allows fluid flow to continue through the isolated lung(s), but without added flow directed into the left atrium. Four-chamber working mode is analogous to the native function of the heart and was used during all ablation procedures and throughout the thawing phase. Hemodynamic performance of these hearts is summarized in Table 1. Note, that as best as possible, the reanimated lung(s) were ventilated at a respiration rate of 11-15 per minute and a volume of 150-250 milliliters per lung. To do so, the remaining airway (the distal main trachea) was intubated by placement of an endotracheal tube (if only one lung was isolated the other primary branch bronchus was tied off) and subsequently attached to the ventilator. Video endoscopes (IPLEX FX series, Olympus Corp., Tokyo, Japan) were employed so to observe the proper placements of the cryoballoons within the pulmonary vein. A supplemental video provided here, shows an anterior view of on specimen and then the simultaneous multimodal imaging performed during the experiments.

Infrared Imaging and Data Analysis

A FLIR SC620 (FLIR Systems, Inc., Boston, MA) infrared (IR) camera was used to capture thermographic data at a minimum rate of one hertz. The emissivity and

appropriate environmental parameters were input to the infrared software (ThermaCAM Researcher Pro 2.9, FLIR Systems, Inc., Boston, MA). Emissivity was determined by comparison of IR temperatures to a 0.040" T-type thermocouple (Omega Engineering) being read by a digital thermometer (Fluke 51II, Everett, WA). It should be noted that this IR system is only capable of measuring temperatures as low as -30 Celsius, below this level the accuracy of the measurements are reduced.

Measured parameters using FLIR software include: lowest epicardial temperature reached, epicardial area cooled to 10, 5, 0, and -5 °C, and time from start of an ablation until epicardial temperatures of 10, 5, 0, -5, and -10 °C were achieved. If required, the heart was held in a more lateral position to best view with the IR camera, the area being treated/cooled.

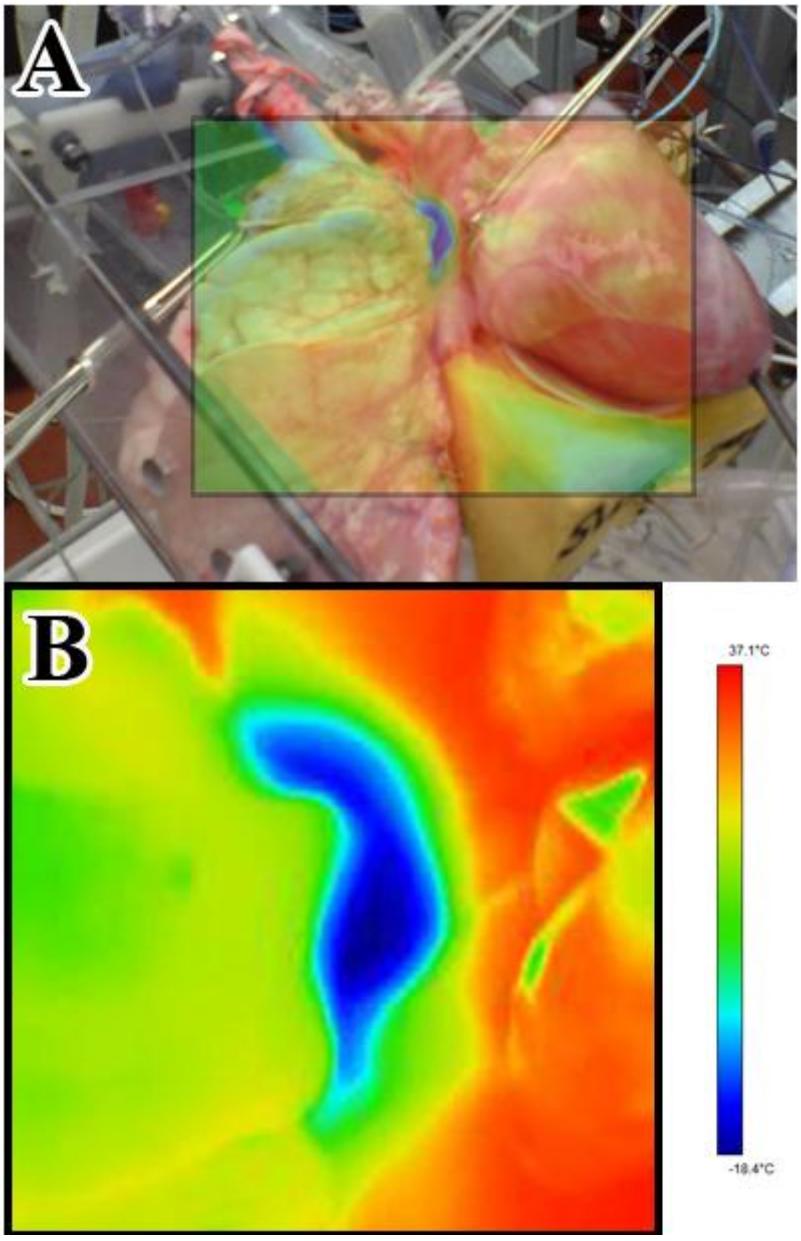

Figure 39. Shown above (A) the heart-lung bloc, with overlaid thermograph, attached to the Visible Heart ® apparatus with heart held laterally to best image area of therapy. Panel B shows a close up view of the resultant thermograph with the temperature scale ranging from -18 to 37 °C in this example.

Ablation Procedure

A steerable outer catheter (FlexCath, Medtronic, Inc.) was placed into the left atria (LA) by either a transseptal puncture via the inferior vena cava or directly via the contralateral PV cannulated with a fixture containing a hemostasis valve. Using direct endoscopic

visualization and a 0.035" guidewire (PV tracker, Medtronic, Inc.) the ablation catheter was then inserted over the wire into the LA. Once the preparation and catheter delivery sheath were in place the IR camera was setup and not moved throughout that given experimental procedure. The cryo-catheters investigated here were 28 mm ArticFront and ArticFront Advance (Medtronic, Inc.). The catheters were marked along the length of the balloon with colored fiducial markers, so to ensure that the clocking of the catheters in between exchanges or ablations were consistent (see Figure 40 and supplemental video).

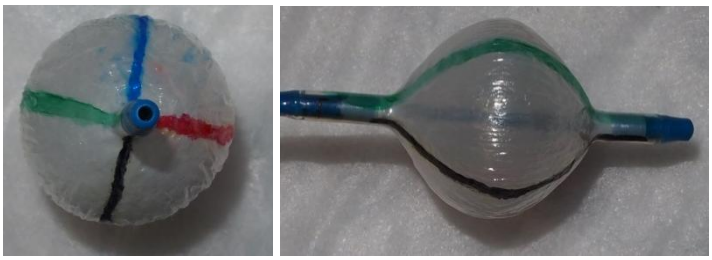

Figure 40: ArticFront 28 mm balloon cryoablation catheter with colored markings for optimizing the alignments of catheter position between ablations. The blue band corresponds to the top of the catheter handle and the red band corresponds to the left side of the handle (i.e., the operator's perspective).

Data are presented as the means ± standard deviations. These results were compared on a day by day basis using a paired T-test (α=0.05) to determine if there were statistical differences between the various parameters of interest and between the catheters employed.

Results

Swine data

Using these methods a total of 8 heart-lung blocs were reanimated and studied. In most cases, two or three ablations per catheter (ArticFront and ArticFront Advance) were performed per day; note in one instance only one ablation was performed due to technical difficulties. The daily results of the cooling measurements were averaged by catheter type. This approach was chosen to compare the differences between catheters without the influence of daily variabilities such as: camera position, atmospheric conditions,

cardiac outputs, and differing anatomies. The relative hemodynamic performances of these specimens during these applied thermal therapied were provided below in Table 25.

Table 25. Hemodynamic performance of reanimated swine heart-lung blocs.

Specimen	HR (bpm)	LVSP (mm Hg)	LVEDP (mm Hg)	+dLVP/dt (mm Hg/s)	-dLVP/dt (mm Hg/s)	Tau	Lung
1	94.0	77.8	-2.3	857.5	-553.5	32.0	Right
2	106.5	85.5	1.8	838.2	-664.2	28.3	Right
3	76.8	89.3	-1.0	893.3	-640.7	40.0	Left
4	105.2	70.7	12.0	715.8	-682.2	30.2	Left
5	108.0	79.2	1.5	683.3	-564.0	28.5	Right
6	119.7	74.0	9.0	716.5	-622.3	25.0	Right
7	90.8	96.3	5.0	853.8	-681.0	37.7	Right
8	105.0	82.0	-3.5	809.2	-662.2	31.3	Right
Average	100.8	81.9	2.8	796.0	-633.8	31.6	
Standard Dev.	13.1	8.4	5.5	79.3	50.4	5.0	
Human Specimens							
HH 277	63.7	71.8	-3.0	485.3	-428.2	50.7	Right
HH 284	104.5	83.0	0.8	836.0	-641.0	28.8	Right

The temperature area measurements were made using the time point at which the most extreme cooling had occurred. A total of 24 and 26 ablations for ArticFront and the ArticFront Advance were measured, respectively. When all the data were examined, including cases in which the ablation had not reached the indicated temperatures (i.e., an area value of zero), Figure 41 demonstrates that ArticFront Advance cooled greater areas and in most cases achieved lower temperatures. However, when the subset of data in which only ablations which reached the measured temperature were plotted in Figure 42, one can see that the differences were less pronounced.

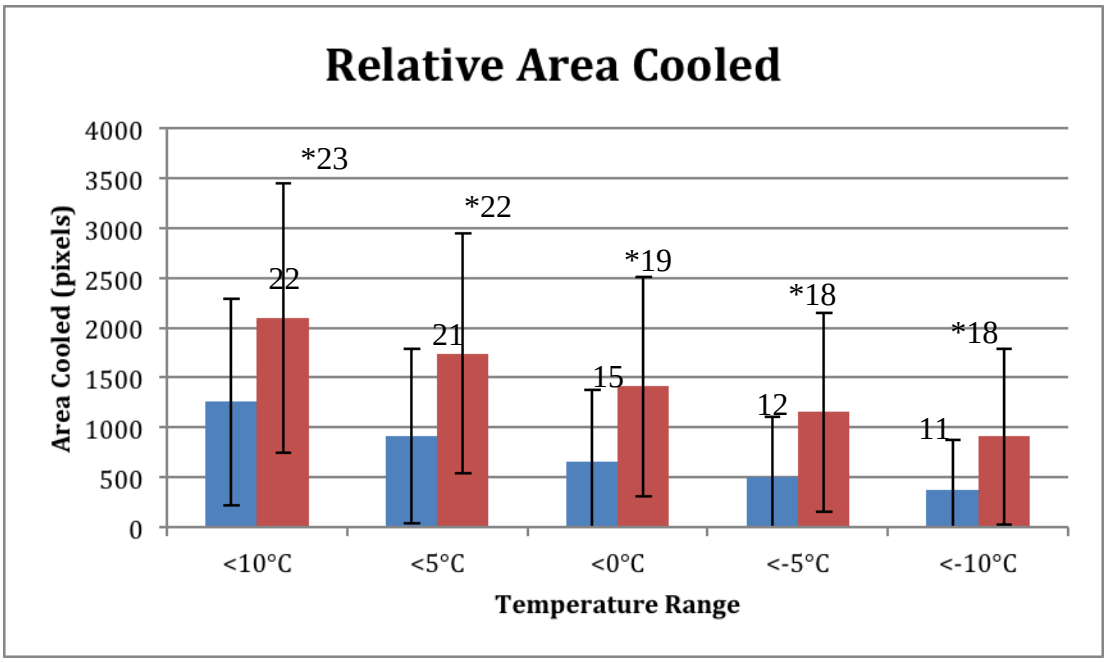

Figure 41. Relative area cooled by employing ArticFront (blue) and ArticFront Advance (red) catheters were compared. Above each bar is the number of ablations in which the indicated level of cooling was achieved. For each the ArticFront and ArticFront Advance catheters, 24 and 25 ablations were analyzed, respectively. Ablations which did not achieve cooling to the measured temperature were averaged with the other ablations performed that day as zero area cooled. (*= p<.05)

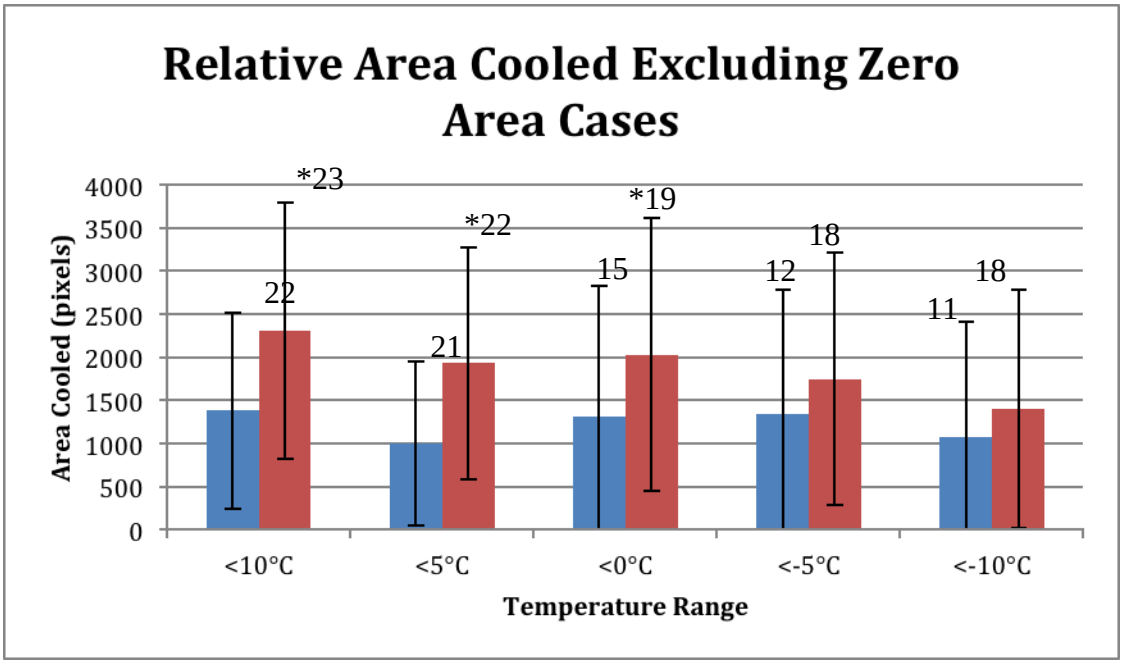

Figure 42. Relative area cooled during therapy application by ArticFront (blue) and ArticFront Advance (red) catheters excluding cases in which the measured temperature was not achieved (e.g., if

-5°C was not achieved, that ablation was not analyzed in the-5°C group). The number of ablations measured is displayed above the error bars. (*= p<.05)

The cooling time to epicardial temperatures of 10, 5, 0, -5, and -10°C were measured in 16 ablations delivered using ArticFront and 20 ablations for ArticFront Advance catheters. Note, that these Ns differ from the area measurements, due to subsequent technical problems during which the digital video recording system was damaged, thus making the syncing of multiple timed systems not possible (e.g., IR computer and CryoConsole).

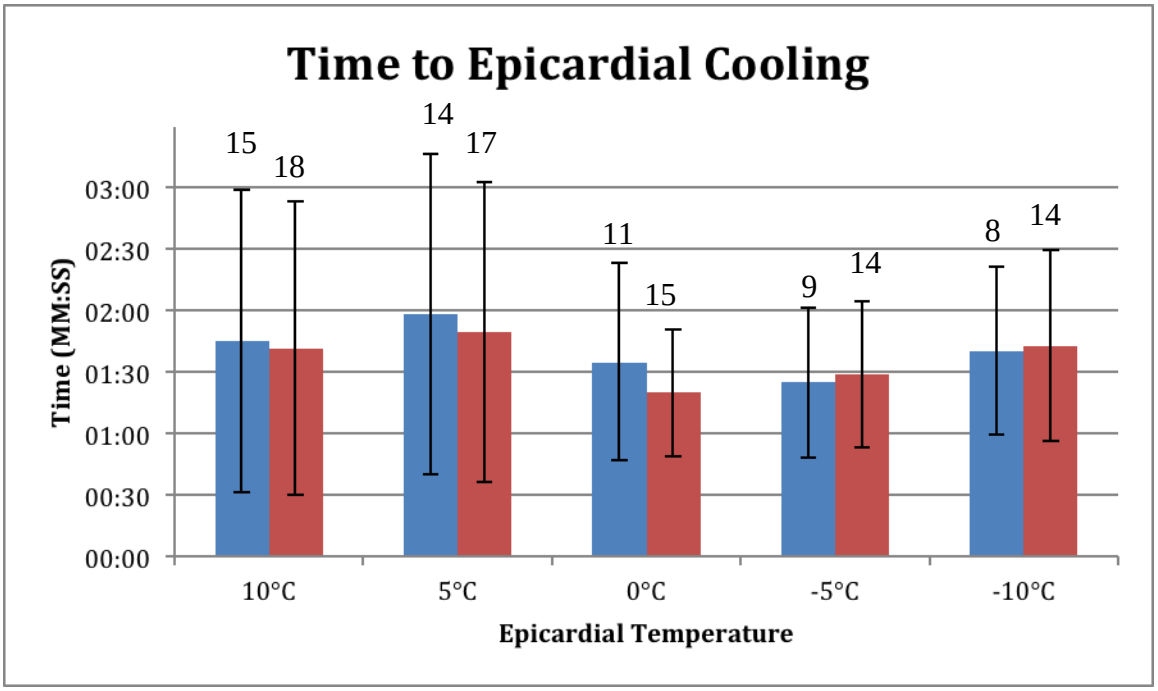

Figure 43. Time to reach indicated epicardial temperatures from beginning of ablation. Note that differences between treatments delivered with ArticFront (blue, n=16) versus ArticFront Advance (red, n=20) catheters were not found to be significant.

The lowest temperature achieved during these series of ablations were measured for each application. Again, it should be noted that the limitations of IR imaging somewhat complicated this analysis, because of the considered reduced accuracy of this specific camera for temperatures less than -30°C: therefore ablations that demonstrated very low temperatures (i.e., reading less than -40°C) were considered to be not lower than -40°C for the results shown in Figure 44 to take a conservative measurement approach. This occurred once for an ArticFront ablation and four times during ArticFront Advance

treatments, suggesting that the ArticFront Advance catheters allow for greater cooling potential. The histogram shown in Figure 45 displays the distribution of nadir temperatures: temperatures less than -30°C are denoted by an * to indicate that they may not be reliable.

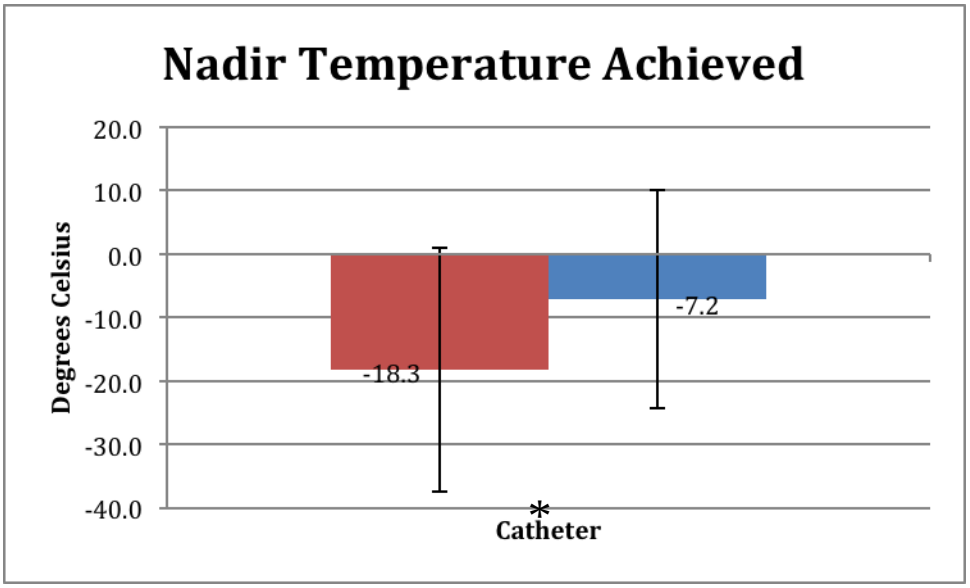

Figure 44. Minimum temperature achieved by treatment applications with ArticFront (blue) and ArticFront Advance (red) catheters (p=0.036).

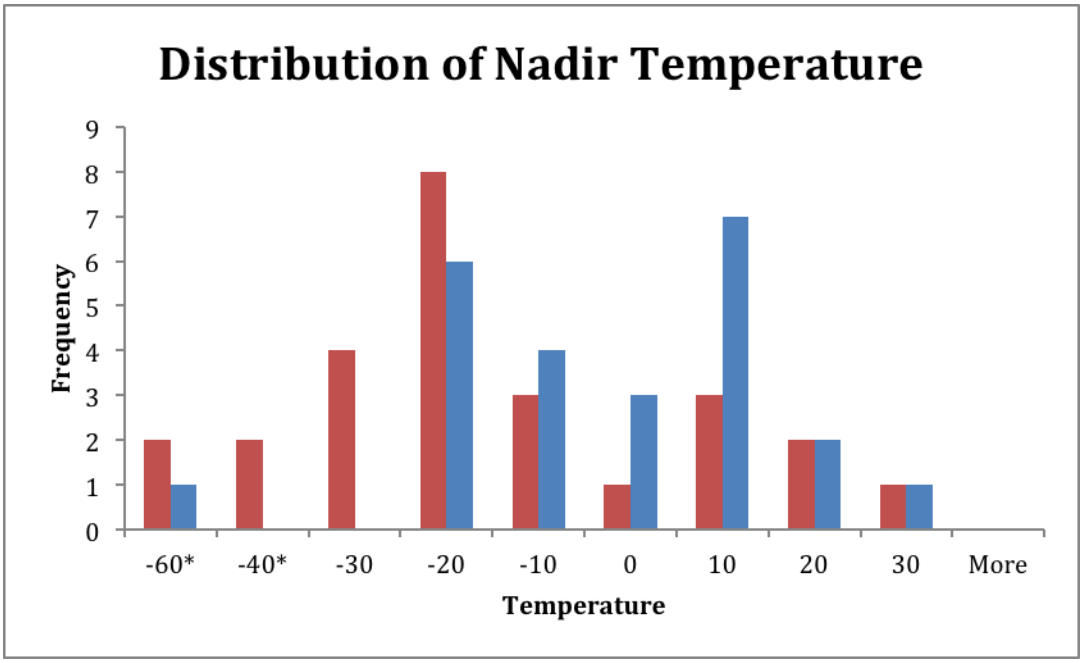

Figure 45. Distribution of nadir temperatures achieved following treatments with either catheter system: ArticFront (blue) and ArticFront Advance (red). Note, accuracy of temperatures less than -30°C may be decreased as denoted by an *. No temperatures fell within the 50°C bin and therefore it was omitted.

Human data

Data was collected from two human hearts. In each specimen two ablations with the ArticFront Advanced 23 mm catheter were performed. To compare the results of the 23 mm catheter in human versus swine, one swine experiment with six ablations using the 23 mm catheter was performed. The data is included due to the unique opportunity to study human versus swine specimens, thus making these studies of high translational value.

Since it is not feasible to compare different human samples or human to swine samples on the same day, with the same setup and anatomy, a ruler was included in the recording to scale the images. However, the ruler was not held perfectly planar to the lens by an apparatus, but was approximated. The results suggest that a smaller area is cooled in human samples as indicated by Figure 46. However, as can be seen there are very large standard deviations. Data on cooling speeds could not be calculated due to syncing technical difficulties mentioned previously. Comparing the data on the lowest temperature achieved the differences minimal, with swine achieving -17.9±18.9°C and human samples reaching 14.2±16.6°C.

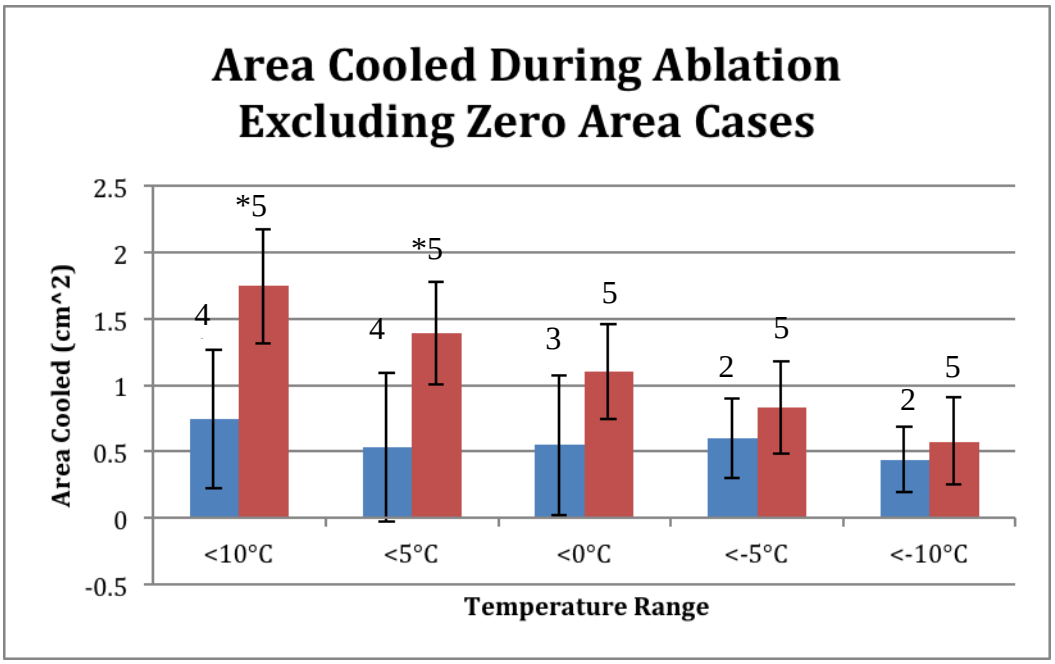

Figure 46. Area cooled by ArticFront 23 mm catheter in human (blue) and swine (red). The number of ablations measured is displayed above the error bars. (*= p<.05)

Discussion

Here we present a technically challenging study utilizing external infrared imaging data obtained during cryoablation treatments applied employing ArticFront (blue) and ArticFront Advance (red) catheters. We uniquely performed these studies employing both reanimated human and swine heart/lung blocs and believe this to be the first report of thermal ablation studies using such a method. Yet, one must also consider that the translational experimental methodology presented here, may be considered as a possible worst case scenarios or extreme cases, in the sense that the measured temperatures are expected to be colder than what would be measured in-vivo. This is due to the fact that the reanimated heart and lung(s) were surrounded by air. Note that this experimental design was required so to be able to obtain these real-time infrared measurements of the resultant tissue temperatures. Therefore, the metabolic heat generated by surrounding organs is not being transferred to the isolated block. Additionally, air is a superior insulator compared to tissues by orders of magnitude and will in effect keep the cooling within in the tissue, having very little warming effects from the air. It should be noted,

attempts by our laboratory to utilize IR imaging in-situ open chest models proved difficult to obtain direct visualization of the zone of ablation. The use of isolated hearts is already well established in cardiac research [142,154] and this methodology incorporates native sinus rhythm with physiologically relevant hemodynamics.

The results of the cooling area measurements suggest that AFA will cool a larger area and more frequently to colder temperatures. However, there may be other influencing parameters that will dictate how large an area is cooled, such as, anatomical variance and catheter pressure. This is suggested by the differences between Figure 41 and Figure 42. The time to cool the epicardium to a particular temperature did not vary much between catheters. This is expected because rate of heat transfer transmurally is most likely governed by the thermal conductivity of tissue, which should remain relatively constant between samples. The fact that it varies little between catheters may speak to the robustness of this methodology. The depth of cooling appears to be greater for AFA than AF based upon the distribution of nadir temperatures. This technique is not limited to the use of cryoablation catheters. Any thermally based ablation targeting the pulmonary veins, or even other structures, may be studied using these approaches. The authors believe that this one of the most translational methodologies available for study, especially when human heart specimens are available.

The data presented here suggests that differences exist between human and swine cryoballoon ablation cooling profiles. The differences may be due to tissue thickness, age, disease state, fibrosis, and relative mass. It should be noted that we have observed that the pulmonary veins in aged human samples that our laboratory has received are thicker than the relatively young swine. The lungs of the human samples were also larger than those of the swine. The fact that only some of the area measurements were statistically different, and the end temperatures not significantly different, suggests that the translational aspect of the swine data is valid. The human data translates to the clinical case, but as mentioned previously the temperatures are most likely colder, and/or the rate of cooling faster, than those experienced in-vivo.

Reviews of cryosurgical injury are readily available in the literature [109], and it is accepted that differing tissues and cells have varying thermal tolerance. Unfortunately, the thermal tolerance of myocardium, esophagus, and lung is not fully understood. In our lab efforts are underway to further characterize some of these tissues. However, it is accepted in the cancer field that if the vascular supply is damaged a lesion will eventually result. The vascular susceptibility to cooling also differs by tissue, but has been generally reported to be in the range of -20 to -30°C [109]. Whether or not this applies to tissues that are in contact with blood (i.e., myocardium and PV) is unclear, but may guide the community until better data is published. However, taking this into account with the aforementioned data suggests that shorter treatments may be necessary to avoid collateral injury. As a precaution, shorter treatment times are already being proposed in the literature [164].

Work done on the swine phrenic nerve is our lab suggests that cooling to mild subzero temperatures will acutely, irreversibly cease conduction [86] in most cases. This data is in agreement with previous studies [165,166]. Taken into account with the findings presented here, an operator should be particularly careful to avoid placing a cryoballoon deep within the pulmonary veins and phrenic nerve monitoring should be used, as is standard now. However, certain patients may possess atypical phrenic anatomy that is less compatible with cryoballoon and/or RF ablation of the pulmonary veins, such as: close right superior PV and superior vena cava relationship [167] or the right upper PV ostium to the right pericardiophrenic artery [168].

To the author's knowledge this is the first publication of such an experimental methodology to investigate the effects of cardiac thermal ablation. The data from these experiments may aid in the guidance of dosing. Future experiments using these methodologies could be performed to determine the characteristics of novel ablation devices and how they may impact the myocardium and surrounding tissues.

Thesis Summary

The complication rates during transcatheter cardiac ablation procedures remain concerning. The transseptal puncture procedure, the relative navigation of catheters to difficult anatomies, and the application of ablation modalities to ensure transmural lesions are all primary areas where therapeutic complications may arise. In my thesis projects, our work targeted these three areas while also specifically considering a means to reduce such complications. Specifically, iatrogenic atrial septal defect formation was investigated by assessing the biomechanical changes of the atrial septum that may occur during transseptal punctures and the further injury the septum may incur during subsequent catheter manipulations. Furthermore, the contact forces required to perforate the atria were characterized in order to determine the boundary force conditions associated with both catheter navigation and ablation energy application. In addition, the biophysical changes manifested during and following the application of ablation modalities, as well as, the parameters that facilitate the development of explosive steam pops were investigated. Finally, the cryothermal tolerances of cardiac tissues were identified to aid in reducing collateral injury and to optimize dose delivery. The insights gained from these translational studies will help define various parameters and boundary conditions that should improve both the safeties and efficacies of clinical cardiac ablation procedures. In addition to characterizing these factors, the direct visualization of such complications provides invaluable insights to engineers as well as clinicians.

References

[1] Schueler R., Öztürk C., Wedekind J. A., Werner N., Stöckigt F., Mellert F., Nickenig G., and Hammerstingl C., 2015, "Persistence of Iatrogenic Atrial Septal Defect After Interventional Mitral Valve Repair With the MitraClip System," JACC Cardiovasc. Interv., **8**(3), pp. 450–459.

[2] Braunwald E., Brockenbrough E. C., Frahm C. J., and Ross J., 1961, "Left atrial and left ventricular pressures in subjects without cardiovascular disease: observations in eighteen patients studied by transseptal left heart catheterization.," Circulation, **24**, pp. 267–269.

[3] Earley M. J., 2009, "How to perform a transseptal puncture.," Heart, **95**(1), pp. 85–92.

[4] Hahn K., Gal R., Sarnoski J., Kubota J., Schmidt D. H., and Bajwa T. K., 1995, "Transesophageal echocardiographically guided atrial transseptal catheterization in patients with normal-sized atria: incidence of complications.," Clin. Cardiol., **18**(4), pp. 217–220.

[5] Daoud E. G., 2005, "Transseptal catheterization," Hear. Rhythm, **2**(2), pp. 212–214.

[6] Kautzner J., and Peichl P., 2010, "You get what you inspect, not what you expect: Can we make the transseptal puncture safer?," Europace, **12**(10), pp. 1353–1355.

[7] De Ponti R., Cappato R., Curnis A., Della Bella P., Padeletti L., Raviele A., Santini M., and Salerno-Uriarte J. a, 2006, "Trans-septal catheterization in the electrophysiology laboratory: data from a multicenter survey spanning 12 years.," J. Am. Coll. Cardiol., **47**(5), pp. 1037–42.

[8] McGinty P. M., Smith T. W., and Rogers J. H., 2011, "Transseptal left heart catheterization and the incidence of persistent iatrogenic atrial septal defects.," J. Interv. Cardiol., **24**(3), pp. 254–63.

[9] Sy R. W., Klein G. J., Leong-Sit P., Gula L. J., Yee R., Krahn A. D., and Skanes A. C., 2011, "Troubleshooting difficult transseptal catheterization," J. Cardiovasc. Electrophysiol., **22**(6), pp. 723–727.

[10] Saitoh T., Izumo M., Furugen A., Tanaka J., Miyata-Fukuoka Y., Gurudevan S. V., Tolstrup K., Siegel R. J., Kar S., and Shiota T., 2012, "Echocardiographic evaluation of iatrogenic atrial septal defect after catheter-based mitral valve clip insertion," Am. J. Cardiol., **109**(12), pp. 1787–1791.

[11] Fitchet a, Turkie W., and Fitzpatrick a P., 1998, “Transeptal approach to ablation of left-sided arrhythmias does not lead to persisting interatrial shunt: a transesophageal echocardiographic study.,” Pacing Clin. Electrophysiol., **21**(11), pp. 2070–2072.

[12] Hammerstingl C., Lickfett L., Jeong K.-M., Troatz C., Wedekind J.-A., Tiemann K., Lüderitz B., and Lewalter T., 2006, “Persistence of iatrogenic atrial septal defect after pulmonary vein isolation--an underestimated risk?,” Am. Heart J., **152**(2), pp. 362.e1–5.

[13] Fagundes R. L., Mantica M., De Luca L., Forleo G., Pappalardo A., Avella A., Fraticelli A., Dello Russo A., Casella M., Pelargonio G., and Tondo C., 2007, “Safety of single transseptal puncture for ablation of atrial fibrillation: retrospective study from a large cohort of patients.,” J. Cardiovasc. Electrophysiol., **18**(12), pp. 1277–81.

[14] Rillig A., Meyerfeldt U., Kunze M., Birkemeyer R., Miljak T., Jäckle S., Hajredini B., Treusch F., and Jung W., 2010, “Persistent iatrogenic atrial septal defect after a single-puncture, double-transseptal approach for pulmonary vein isolation using a remote robotic navigation system: Results from a prospective study,” Europace, **12**(3), pp. 331–336.

[15] Omran H., Hardung D., Schmidt H., Hammerstingl C., and Lüderitz B., 2003, “Mechanical occlusion of the left atrial appendage.,” J. Cardiovasc. Electrophysiol., **14**(9 Suppl), pp. S56–S59.

[16] Casale P., Block P. C., O’Shea J. P., and Palacios I. F., 1990, “Atrial septal defect after percutaneous mitral balloon valvuloplasty: Immediate results and follow-up,” J. Am. Coll. Cardiol., **15**(6), pp. 1300–1304.

[17] Cope C., 1963, “Newer Techniques of Transseptal Left-Heart Catheterization,” Circulation, **27**(4), pp. 758–761.

[18] Sur J. P., Pagani F. D., and Moscucci M., 2009, “Percutaneous closure of an iatrogenic atrial septal defect,” Catheter. Cardiovasc. Interv., **73**(2), pp. 267–271.

[19] Bordacher P., Grenz N., Jais P., Ritter P., Leclercq C., Morgan J. M., Gras D., and Yang P., 2012, “Left ventricular endocardial or triventricular pacing to optimize cardiac resynchronization therapy in a chronic canine model of ischemic heart,” Am. J. Physiol. Hear. Circ. Physiol., **303**(2), pp. 207–215.

[20] Van Gelder B. M., Houthuizen P., and Bracke F. a., 2011, “Transseptal left ventricular endocardial pacing: Preliminary experience from a femoral approach with subclavian pull-through,” Europace, **13**(10), pp. 1454–1458.

[21] Himbert D., Brochet E., Radu C., Iung B., Messika-Zeitoun D., Enguerrand D., Bougoin W., Nataf P., and Vahanian A., 2011, "Transseptal implantation of a transcatheter heart valve in a mitral annuloplasty ring to treat mitral repair failure," Circ. Cardiovasc. Interv., **4**(4), pp. 396–398.

[22] Chan N. Y., Choy C. C., Lau C. L., Lo Y. K., Chu P. S., Yuen H. C., Mok N. S., Tsui P. T., and Lau S. T., 2011, "Persistent iatrogenic atrial septal defect after pulmonary vein isolation by cryoballoon: An under-recognized complication," Europace, **13**(10), pp. 1406–1410.

[23] Thiagalingam A., D'Avila A., Foley L., Fox M., Rothe C., Miller D., Malchano Z., Ruskin J. N., and Reddy V. Y., 2008, "Full-color direct visualization of the atrial septum to guide transseptal puncture," J. Cardiovasc. Electrophysiol., **19**(12), pp. 1310–1315.

[24] Elagha A. a., Kim A. H., Kocaturk O., and Lederman R. J., 2007, "Blunt atrial transseptal puncture using excimer laser in swine," Catheter. Cardiovasc. Interv., **70**(4), pp. 585–590.

[25] Dondelinger R. F., Ghysels M. P., Brisbois D., Donkers E., Snaps F. R., Saunders J., and Devière J., 1998, "Relevant radiological anatomy of the pig as a training model in interventional radiology.," Eur. Radiol., **8**(7), pp. 1254–1273.

[26] Reant P., Lafitte S., Jaïs P., Serri K., Weerasooriya R., Hocini M., Pillois X., Clementy J., Haïssaguerre M., and Roudaut R., 2005, "Reverse remodeling of the left cardiac chambers after catheter ablation after 1 year in a series of patients with isolated atrial fibrillation," Circulation, **112**(19), pp. 2896–2903.

[27] Aurigemma G. P., Gottdiener J. S., Arnold A. M., Chinali M., Hill J. C., and Kitzman D., 2009, "Left atrial volume and geometry in healthy aging the cardiovascular health study," Circ. Cardiovasc. Imaging, **2**(4), pp. 282–289.

[28] Eltchaninoff H., Prat A., Gilard M., Leguerrier A., Blanchard D., Fournial G., Iung B., Donzeau-Gouge P., Tribouilloy C., Debrux J. L., Pavie A., and Gueret P., 2011, "Transcatheter aortic valve implantation: Early results of the FRANCE (FRench Aortic National CoreValve and Edwards) registry," Eur. Heart J., **32**(2), pp. 191–197.

[29] Smith T., McGinty P., Bommer W., Low R. I., Lim S., Fail P., and Rogers J. H., 2012, "Prevalence and echocardiographic features of iatrogenic atrial septal defect after catheter-based mitral valve repair with the MitraClip system.," Catheter. Cardiovasc. Interv., **80**(4), pp. 678–85.

[30] Hara H., Virmani R., Ladich E., Mackey-Bojack S., Titus J., Reisman M., Gray W., Nakamura M., Mooney M., Poulose A., and Schwartz R. S., 2005, "Patent foramen ovale: current pathology, pathophysiology, and clinical status.," J. Am. Coll. Cardiol., **46**(9), pp. 1768–76.

[31] Howard S. a., Quallich S. G., Benscoter M. a., Holmgren B. C., Rolfes C. D., and Iaizzo P. a., 2015, "Tissue Properties of the Fossa Ovalis as They Relate to Transseptal Punctures : A Translational Approach," J. Interv. Cardiol., **28**(1), pp. 98–108.

[32] Ross J., Braunwald E., and Morrow A. G., 1959, "Transseptal left atrial puncture," Am. J. Cardiol., **3**(5), pp. 653–655.

[33] Cope C., 1959, "Technique for transseptal catheterization of the left atrium; preliminary report.," J. Thorac. Surg., **37**(4), pp. 482–486.

[34] Winkle R. a, Mead R. H., Engel G., and Patrawala R. a, 2011, "The use of a radiofrequency needle improves the safety and efficacy of transseptal puncture for atrial fibrillation ablation.," Hear. Rhythm, **8**(9), pp. 1411–5.

[35] Veldtman G. R., Wilson G. J., Peirone A., Hartley A., Estrada M., Norgard G., Leung R. K., Visram N., and Benson L. N., 2005, "Radiofrequency perforation and conventional needle percutaneous transseptal left heart access: pathological features.," Catheter. Cardiovasc. Interv., **65**(4), pp. 556–63.

[36] Crystal M. a., Mirza M. a., and Benson L. N., 2010, "A radiofrequency transseptal needle: Initial animal studies," Catheter. Cardiovasc. Interv., **76**(5), pp. 769–773.

[37] Benson L. N., Nykanen D., and Collison A., 2002, "Radiofrequency perforation in the treatment of congenital heart disease.," Catheter. Cardiovasc. Interv., **56**(1), pp. 72–82.

[38] Shimko N., Savard P., and Shah K., 2000, "Radio frequency perforation of cardiac tissue: modelling and experimental results," Med. Biol. Eng. Comput., **38**, pp. 575–582.

[39] Quallich S. G., Goff R. P., and Iaizzo P. a., 2014, "High-Speed Visualization of Steam Pops During Radiofrequency Ablation," J. Med. Device., **8**(2), p. 020903.

[40] Ilkhanoff L., Naidu S. S., Rohatgi S., Ross M. J., Silvestry F. E., and Herrmann H. C., 2005, "Transcatheter device closure of interatrial septal defects in patients with hypoxia," J. Interv. Cardiol., **18**(4), pp. 227–232.

[41] Cappato R., Calkins H., Chen S.-A., Davies W., Iesaka Y., Kalman J., Kim Y.-H., Klein G., Natale A., Packer D., Skanes A., Ambrogi F., and Biganzoli E., 2010, "Updated worldwide survey on the methods, efficacy, and safety of catheter ablation for human atrial fibrillation.," Circ. Arrhythm. Electrophysiol., **3**(1), pp. 32–8.

[42] Natale A., and Raviele A., 2011, Atrial Fibrillation Ablation, 2011 Update: The State of the Art Based on the Venicechart International Consensus Document.

[43] Go A. S., Hylek E. M., Phillips K. A., Chang Y., Henault L. E., Selby J. V., and Singer D. E., 2001, "Prevalence of diagnosed atrial fibrillation in adults: national implications for rhythm management and stroke prevention: the AnTicoagulation and Risk Factors in Atrial Fibrillation (ATRIA) Study.," JAMA J. Am. Med. Assoc., **285**(18), pp. 2370–5.

[44] Miyasaka Y., Barnes M. E., Gersh B. J., Cha S. S., Bailey K. R., Abhayaratna W. P., Seward J. B., and Tsang T. S. M., 2006, "Secular trends in incidence of atrial fibrillation in Olmsted County, Minnesota, 1980 to 2000, and implications on the projections for future prevalence.," Circulation, **114**(2), pp. 119–25.

[45] Bohnen M., Stevenson W. G., Tedrow U. B., Michaud G. F., John R. M., Epstein L. M., Albert C. M., and Koplan B. A., 2011, "Incidence and predictors of major complications from contemporary catheter ablation to treat cardiac arrhythmias," Hear. Rhythm, **8**(11), pp. 1661–1666.

[46] Chierchia G. B., Capulzini L., Droogmans S., Sorgente A., Sarkozy A., Müller-Burri A., Paparella G., de Asmundis C., Yazaki Y., Kerkhove D., Van Camp G., and Brugada P., 2010, "Pericardial effusion in atrial fibrillation ablation: a comparison between cryoballoon and radiofrequency pulmonary vein isolation.," Europace, **12**(3), pp. 337–41.

[47] Platonov P. G., Ivanov V., Ho S. Y., and Mitrofanova L., 2008, "Left atrial posterior wall thickness in patients with and without atrial fibrillation: data from 298 consecutive autopsies.," J. Cardiovasc. Electrophysiol., **19**(7), pp. 689–92.

[48] Friedman P. A., 2012, "Hitting a moving target: Catheter ablation and respiration.," Hear. Rhythm, **9**(7), pp. 1048–9.

[49] Kok L. C., Everett T. H., Akar J. G., and Haines D. E., 2003, "Effect of heating on pulmonary veins: how to avoid pulmonary vein stenosis.," J. Cardiovasc. Electrophysiol., **14**(3), pp. 250–4.

[50] Venkatasubramanian R. T., Wolkers W. F., Shenoi M. M., Barocas V. H., Lafontaine D., Soule C. L., Iaizzo P. A., and Bischof J. C., 2010, "Freeze-thaw

induced biomechanical changes in arteries: role of collagen matrix and smooth muscle cells.," Ann. Biomed. Eng., **38**(3), pp. 694–706.

[51] Shah D., Lambert H., Langenkamp A., Vanenkov Y., Leo G., Gentil-Baron P., and Walpoth B., 2011, "Catheter tip force required for mechanical perforation of porcine cardiac chambers.," Europace, **13**(2), pp. 277–83.

[52] Perna F., Heist E. K., Danik S. B., Barrett C. D., Ruskin J. N., and Mansour M., 2011, "Assessment of catheter tip contact force resulting in cardiac perforation in swine atria using force sensing technology.," Circ. Arrhythm. Electrophysiol., **4**(2), pp. 218–24.

[53] Venkatasubramanian R. T., Grassl E. D., Barocas V. H., Lafontaine D., and Bischof J. C., 2006, "Effects of freezing and cryopreservation on the mechanical properties of arteries.," Ann. Biomed. Eng., **34**(5), pp. 823–32.

[54] Litwin S., Cohen J., and Fine S., 1973, "Effects of Sterilization and Tensile Strength Preservation of Canine Aortic Tissue," J. Surigical Res., **15**, pp. 198–206.

[55] Krag S, Andreassen T., 1998, "Effect of Freezing on Lens Capsule Mechanical Behavior," Ophthalmic Res., **30**, pp. 280–285.

[56] Haines D. E., 1993, "The biophysics of radiofrequency catheter ablation in the heart: the importance of temperature monitoring.," PACE, **16**(3 Pt 2), pp. 586–91.

[57] Kuck K.-H., Reddy V. Y., Schmidt B., Natale A., Neuzil P., Saoudi N., Kautzner J., Herrera C., Hindricks G., Jaïs P., Nakagawa H., Lambert H., and Shah D. C., 2012, "A novel radiofrequency ablation catheter using contact force sensing: Toccata study.," Hear. Rhythm, **9**(1), pp. 18–23.

[58] Quallich S., Holmgren C., Howard S., and Iaizzo P., 2014, "Assessing the Biomechanical Properties of the Fossa Ovalis," European Cardiac Arrhythmia Society.

[59] Yokoyama K., Nakagawa H., Shah D. C., Lambert H., Leo G., Aeby N., Ikeda A., Pitha J. V, Sharma T., Lazzara R., and Jackman W. M., 2008, "Novel contact force sensor incorporated in irrigated radiofrequency ablation catheter predicts lesion size and incidence of steam pop and thrombus.," Circulation, **1**(5), pp. 354–62.

[60] Thiagalingam A., D'Avila A., Foley L., Guerrero J. L., Lambert H., Leo G., Ruskin J. N., and Reddy V. Y., 2010, "Importance of catheter contact force during irrigated radiofrequency ablation: evaluation in a porcine ex vivo model using a force-sensing catheter.," J. Cardiovasc. Electrophysiol., **21**(7), pp. 806–11.

[61] Reddy V. Y., Shah D., Kautzner J., Schmidt B., Saoudi N., Herrera C., Jaïs P., Hindricks G., Peichl P., Yulzari A., Lambert H., Neuzil P., Natale A., and Kuck K.-H., 2012, "The relationship between contact force and clinical outcome during radiofrequency catheter ablation of atrial fibrillation in the TOCCATA study.," Hear. Rhythm, **9**(11), pp. 1789–95.

[62] Packer D. L., Kowal R. C., Wheelan K. R., Irwin J. M., Champagne J., Guerra P. G., Dubuc M., Reddy V., Nelson L., Holcomb R. G., Lehmann J. W., and Ruskin J. N., 2013, "Cryoballoon ablation of pulmonary veins for paroxysmal atrial fibrillation: first results of the North American Arctic Front (STOP AF) pivotal trial.," J. Am. Coll. Cardiol., **61**(16), pp. 1713–23.

[63] Skrumeda L. L., and Mehra R., 1998, "Comparison of standard and irrigated radiofrequency ablation in the canine ventricle.," J. Cardiovasc. Electrophysiol., **9**(11), pp. 1196–1205.

[64] Tokuda M., Tedrow U. B., and Stevenson W. G., 2012, "Silent steam pop detected by intracardiac echocardiography.," Hear. Rhythm, **10**(10), pp. 3–4.

[65] Juneja R., and O'Callaghan P., 2001, "Tissue rupture and bubble formation during radiofrequency catheter ablation: 'Echoes of a Pop,'" Circulation, **103**, pp. 1333–1334.

[66] Quallich S. G., Goff R. P., and Iaizzo P. a., 2015, "Direct Visualization of Induced Steam Pops during Radiofrequency Ablations," Hear. Case Reports.

[67] Cooper J. M., Sapp J. L., Tedrow U., Pellegrini C. P., Robinson D., Epstein L. M., and Stevenson W. G., 2004, "Ablation with an internally irrigated radiofrequency catheter: learning how to avoid steam pops.," Hear. Rhythm, **1**(3), pp. 329–33.

[68] Hsu L., Ja P., El M., Sanders P., Ee C. S., Sacher F., Takahashi Y., Rotter M., and Ha M., 2005, "Incidence and Prevention of Cardiac Tamponade Complicating Ablation for Atrial Fibrillation," PACE, **28**(1), pp. 106–109.

[69] Chinchoy E., Soule C. L., Houlton A. J., Gallagher W. J., Hjelle M. a, Laske T. G., Morissette J., and Iaizzo P. A., 2000, "Isolated four-chamber working swine heart model.," Ann. Thorac. Surg., **70**(5), pp. 1607–14.

[70] Thompson N., Lustgarten D., Mason B., Mueller E., Calame J., Bell S., and Spector P., 2009, "The Relationship between Surface Temperature, Tissue Temperature, Microbubble Formation, and Steam Pops," PACE, **32**(7), pp. 833–841.

[71] Nakagawa H., Imai S., Arruda M., and Schleinkofer D., 1997, “Prevention of pericardial tamponade during radiofrequency ablation of accessory pathways using a saline irrigated electrode,” PACE, pp. 1068–1070.

[72] Quallich S. G., Heel M. Van, and Iaizzo P. A., 2015, “Optimal contact forces to minimize cardiac perforations before, during, and/or after radiofrequency or cryothermal ablations,” Hear. Rhythm, **12**(2), pp. 291–296.

[73] Pappone C., Oral H., Santinelli V., Vicedomini G., Lang C. C., Manguso F., Torracca L., Benussi S., Alfieri O., Hong R., Lau W., Hirata K., Shikuma N., Hall B., and Morady F., 2004, “Atrio-esophageal fistula as a complication of percutaneous transcatheter ablation of atrial fibrillation,” Circulation, **109**, pp. 2724–2726.

[74] Siegel M. O., Parenti D. M., and Simon G. L., 2010, “Atrial-esophageal fistula after atrial radiofrequency catheter ablation.,” Clin. Infect. Dis., **51**(1), pp. 73–6.

[75] Chik W. W. B., Kosobrodov R., Bhaskaran A., Barry M. A. T., Nguyen D. T., Pouliopoulos J., Byth K., Sivagangabalan G., Thomas S. P., Ross D. L., Mcewan A., Kovoor P., and Thiagalingam A., 2015, “Acoustic Signal Emission Monitoring as a Novel Method to Predict Steam Pops During Radiofrequency Ablation: Preliminary Observations,” J. Cardiovasc. Electrophysiol., **26**(4), pp. 440–447.

[76] Koruth J. S., Dukkipati S., Gangireddy S., McCarthy J., Spencer D., Weinberg A. D., Miller M. a, D’Avila A., and Reddy V. Y., 2013, “Occurrence of steam pops during irrigated RF ablation: novel insights from microwave radiometry.,” J. Cardiovasc. Electrophysiol., **24**(11), pp. 1271–7.

[77] Tokuda M., Tedrow U. B., and Stevenson W. G., 2012, “Silent steam pop detected by intracardiac echocardiography.,” Hear. Rhythm, **10**(10), pp. 3–4.

[78] Fassini G., Conti S., Pontone G., Pepi M., Tondo C., and Dello Russo A., 2015, “Tissue characteristics and evolution after steam pop,” J. Interv. Card. Electrophysiol., **7**(3), p. 20138.

[79] Vogt J., Heintze J., Gutleben K. J., Muntean B., Horstkotte D., and Nölker G., 2013, “Long-term outcomes after cryoballoon pulmonary vein isolation: results from a prospective study in 605 patients.,” J. Am. Coll. Cardiol., **61**(16), pp. 1707–12.

[80] Jackson N., Barlow M., Leitch J., and Attia J., 2012, “Treating Atrial Fibrillation: Pulmonary Vein Isolation with the Cryoballoon Technique,” Hear. Lung Circ., **21**(8), pp. 427–432.

[81] Casado-Arroyo R., Chierchia G. B., Conte G., Levinstein M., Sieira J., Rodriguez-Mañero M., Di Giovanni G., Baltogiannis Y., Wauters K., De Asmundis C., Sarkozy A., and Brugada P., 2013, "Phrenic nerve paralysis during cryoballoon ablation for atrial fibrillation: A comparison between the first- and second-generation balloon," Hear. Rhythm, **10**(9), pp. 1318–1324.

[82] Fürnkranz A., Bordignon S., Schmidt B., Gunawardene M., Schulte-Hahn B., Urban V., Bode F., Nowak B., and Chun J. K. R., 2013, "Improved procedural efficacy of pulmonary vein isolation using the novel second-generation cryoballoon," J. Cardiovasc. Electrophysiol., **24**, pp. 492–497.

[83] Metzner A., Rausch P., Lemes C., Reissmann B., Bardyszewski A., Tilz R., Rillig A., Mathew S., Deiss S., Kamioka M., Toennis T., Lin T., Ouyang F., Kuck K. H., and Wissner E., 2014, "The incidence of phrenic nerve injury during pulmonary vein isolation using the second-generation 28 mm cryoballoon," J. Cardiovasc. Electrophysiol., **25**(5), pp. 466–470.

[84] Bordignon S., Chun K. J., Gunawardene M., Fuernkranz A., Urban V., Schulte-Hahn B., Nowak B., and Schmidt B., 2013, "Comparison of balloon catheter ablation technologies for pulmonary vein isolation: The laser versus cryo study," J. Cardiovasc. Electrophysiol., **24**(9), pp. 987–994.

[85] Sohara H., Takeda H., Ueno H., Oda T., and Satake S., 2009, "Feasibility of the radiofrequency hot balloon catheter for isolation of the posterior left atrium and pulmonary veins for the treatment of atrial fibrillation," Circ. Arrhythmia Electrophysiol., **2**(3), pp. 225–232.

[86] Goff R., and Iaizzo P., 2013, "In vitro assessment of phrenic nerve cryothermal injury," Scientific Sessesions of the American Heart Association, Dallas, TX.

[87] Avitall B., Urboniene D., Rozmus G., Lafontaine D., Helms R., and Urbonas A., 2003, "New cryotechnology for electrical isolation of the pulmonary veins.," J. Cardiovasc. Electrophysiol., **14**(3), pp. 281–286.

[88] Sarabanda A. V., Bunch T. J., Johnson S. B., Mahapatra S., Milton M. a., Leite L. R., Bruce G. K., and Packer D. L., 2005, "Efficacy and safety of circumferential pulmonary vein isolation using a novel cryothermal balloon ablation system," J. Am. Coll. Cardiol., **46**(10), pp. 1902–1912.

[89] Smith J. J., and Fraser J., 1974, "An estimation of tissue damage and thermal history in the cryolesion.," Cryobiology, **11**(2), pp. 139–147.

[90] Neumann T., Vogt J., Schumacher B., Dorszewski A., Kuniss M., Neuser H., Kurzidim K., Berkowitsch A., Koller M., Heintze J., Scholz U., Wetzel U.,

Schneider M. a E., Horstkotte D., Hamm C. W., and Pitschner H. F., 2008, "Circumferential Pulmonary Vein Isolation With the Cryoballoon Technique. Results From a Prospective 3-Center Study," J. Am. Coll. Cardiol., **52**(4), pp. 273–278.

[91] Van Belle Y., Janse P., Theuns D., Szili-Torok T., and Jordaens L., 2008, "One year follow-up after cryoballoon isolation of the pulmonary veins in patients with paroxysmal atrial fibrillation," Eur. Eur. pacing, arrhythmias, Card. Electrophysiol. J. Work. groups Card. pacing, arrhythmias, Card. Cell. Electrophysiol. Eur. Soc. Cardiol., **10**(11), pp. 1271–1276.

[92] Chun K. J., Bordignon S., Gunawardene M., Urban V., Kulikoglu M., Schulte-Hahn B., Nowak B., and Schmidt B., 2012, "Single transseptal big cryoballoon pulmonary vein isolation using an inner lumen mapping catheter," PACE - Pacing Clin. Electrophysiol., **35**(11), pp. 1304–1311.

[93] Drago F., Silvetti M. S., Santis A., Grutter G., and Andrew P., 2006, "Lengthier cryoablation and a bonus cryoapplication is associated with improved efficacy for cryothermal catheter ablation of supraventricular tachycardias in children," J. Interv. Card. Electrophysiol., **16**(3), pp. 191–198.

[94] Joseph J. P., and Rajappan K., 2012, "Radiofrequency ablation of cardiac arrhythmias: past, present and future.," QJM, **105**(4), pp. 303–14.

[95] Hashimoto K., Watanabe I., Okumura Y., Ohkubo K., Ashino S., Kofune M., Nakai T., Kunimoto S., Kasamaki Y., and Hirayama A., 2009, "Comparison of endocardial and epicardial lesion size following large-tip and extra-large-tip transcatheter cryoablation.," Circ. J., **73**(9), pp. 1619–26.

[96] Parvez B., Pathak V., Schubert C. M., and Wood M., 2008, "Comparison of lesion sizes produced by cryoablation and open irrigation radiofrequency ablation catheters.," J. Cardiovasc. Electrophysiol., **19**(5), pp. 528–34.

[97] Yokoyama K., Nakagawa H., Wittkampf F. H. M., Pitha J. V, Lazzara R., and Jackman W. M., 2006, "Comparison of electrode cooling between internal and open irrigation in radiofrequency ablation lesion depth and incidence of thrombus and steam pop," Circulation, **113**(1), pp. 11–19.

[98] Bordignon S., Fürnkranz A., Schmidt B., and Chun K. R. J., 2012, "Remaining ice cap on second-generation cryoballoon after deflation," Circ. Arrhythmia Electrophysiol., **5**(5), pp. e98–99.

[99] Ahmed H., Neuzil P., D'Avila A., Cha Y. M., Laragy M., Mares K., Brugge W. R., Forcione D. G., Ruskin J. N., Packer D. L., and Reddy V. Y., 2009, "The

esophageal effects of cryoenergy during cryoablation for atrial fibrillation," Hear. Rhythm, **6**(7), pp. 962–969.

[100] Guiot A., Savouré A., Godin B., and Anselme F., 2012, "Collateral nervous damages after cryoballoon pulmonary vein isolation.," J. Cardiovasc. Electrophysiol., **23**(4), pp. 346–51.

[101] He X., and Bischof J. C., 2003, "Quantification of temperature and injury response in thermal therapy and cryosurgery," Crit. Rev. Biomed. Eng., **31**(5-6), pp. 355–422.

[102] Pearce J., and Thomsen S., 1998, "Thermal Damage Processes in Myocardium," Conf. Proc. Annu. Int. Conf. IEEE Eng. Med. Biol. Soc., **20**(1), p. 256.

[103] Han A., and Pearce J., 1990, "Kinetic Model For Thermal Damage in the Myocardium," Adv. Meas. Comput. Temp. Biomed. Therm. Tomogr. Tech. Bio-heat Transf. Model., **147**, pp. 59–66.

[104] Mazur P., 1984, "Freezing of living cells: mechanisms and implications," Am. J. Physiol. Physiol., **247**(3), p. C125.

[105] Han B., and Bischof J. C., 2004, "Direct cell injury associated with eutectic crystallization during freezing," Cryobiology, **48**(1), pp. 8–21.

[106] Balasubramanian S. K., Bischof J. C., and Hubel A., 2006, "Water transport and IIF parameters for a connective tissue equivalent," Cryobiology, **52**(1), pp. 62–73.

[107] Balasubramanian S. K., Venkatasubramanian R. T., Menon A., and Bischof J. C., 2008, "Thermal injury prediction during cryoplasty through in vitro characterization of smooth muscle cell biophysics and viability," Ann. Biomed. Eng., **36**(1), pp. 86–101.

[108] Choi J., and Bischof J. C., 2011, "Cooling rate dependent biophysical and viability response shift with attachment state in human dermal fibroblast cells," Cryobiology, **63**(3), pp. 285–291.

[109] Hoffmann N. E., and Bischof J. C., 2002, "The cryobiology of cryosurgical injury," Urology, **60**(2), pp. 40–49.

[110] Rupp C. C., Hoffmann N. E., Schmidlin F. R., Swanlund D. J., Bischof J. C., and Coad J. E., 2002, "Cryosurgical changes in the porcine kidney: histologic analysis with thermal history correlation.," Cryobiology, **45**(2), pp. 167–82.

[111] Rivoire M. L., Voiglio E. J., Kaemmerlen P., Molina G., Treilleux I., Finzy J., Delay E., and Gory F., 1996, "Hepatic cryosurgery precision: evaluation of ultrasonography, thermometry, and impedancemetry in a pig model," J. Surg. Oncol., **61**(4), pp. 242–248.

[112] Gage A. A., and Baust J., 1998, "Mechanisms of Tissue Injury in Cryosurgery," Cryobiology, **37**(3), pp. 171–186.

[113] Goel R., Swanlund D., Coad J., Paciotti G. F., and Bischof J. C., 2007, "TNF-alpha-based accentuation in cryoinjury--dose, delivery, and response.," Mol. Cancer Ther., **6**(7), pp. 2039–47.

[114] Ogan K., Roberts W. W., Wilhelm D. M., Bonnell L., Leiner D., Lindberg G., Kavoussi L. R., and Cadeddu J. A., 2003, "Infrared thermography and thermocouple mapping of radiofrequency renal ablation to assess treatment adequacy and ablation margins," Urology, **62**(1), pp. 146–151.

[115] Shenoi M. M., Iltis I., Choi J., Koonce N. A., Metzger G. J., Griffin R. J., and Bischof J. C., 2013, "Nanoparticle Delivered Vascular Disrupting Agents (VDAs): Use of TNF-Alpha Conjugated Gold Nanoparticles for Multimodal Cancer Therapy," Mol. Pharm., **10**(5), pp. 1683–1694.

[116] Chosy S. G., Nakada S. Y., Lee F. T., and Warner T. F., 1998, "Monitoring renal cryosurgery: Predictors of tissue necrosis in swine," J. Urol., **159**(4), pp. 1370–1374.

[117] Campbell S. C., Krishnamurthi V., Chow G., Hale J., Myles J., and Novick A. C., 1998, "Renal cryosurgery: Experimental evaluation of treatment parameters," Urology, **52**(1), pp. 29–34.

[118] Claycomb W. C., 1998, "HL-1 cells: A cardiac muscle cell line that contracts and retains phenotypic characteristics of the adult cardiomyocyte," Proc. Natl. Acad. Sci., **95**(6), pp. 2979–2984.

[119] Etheridge M. L., Choi J., Ramadhyani S., and Bischof J. C., 2013, "Methods for characterizing convective cryoprobe heat transfer in ultrasound gel phantoms.," J. Biomech. Eng., **135**(2), p. 021002.

[120] Klein H. H., Puschmann S., Schaper J., and Schaper W., 1981, "The mechanism of the tetrazolium reaction in identifying experimental myocardial infarction," Virchows Arch. A, **393**(3), pp. 287–297.

[121] Sigg D. C., Coles J. A. J., Oeltgen P. R., and Iaizzo P. A., 2002, "Role of delta-opioid receptor agonists on infarct size reduction in swine," Am. J. Physiol. Heart Circ. Physiol., **282**(6), pp. H1953–1960.

[122] Fishbein M. C., Meerbaum S., Rit J., Lando U., Kanmatsuse K., Mercier J. C., Corday E., and Ganz W., 1981, "Early phase acute myocardial infarct size quantification: validation of the triphenyl tetrazolium chloride tissue enzyme staining technique," Am. Heart J., **101**(5), pp. 593–600.

[123] Bhowmick P., Coad J. E., Bhowmick S., Pryor J. L., Larson T., De La Rosette J., and Bischof J. C., 2004, "In vitro assessment of the efficacy of thermal therapy in human benign prostatic hyperplasia.," Int. J. Hyperth., **20**(4), pp. 421–439.

[124] Alonso A., Agarwal S. K., Soliman E. Z., Ambrose M., Chamberlain A. M., Prineas R. J., and Folsom A. R., 2009, "Incidence of atrial fibrillation in whites and African-Americans: the Atherosclerosis Risk in Communities (ARIC) study.," Am. Heart J., **158**(1), pp. 111–7.

[125] Yokoyama K., Nakagawa H., Wittkampf F. H. M., Pitha J. V, Lazzara R., and Jackman W. M., 2006, "Comparison of electrode cooling between internal and open irrigation in radiofrequency ablation lesion depth and incidence of thrombus and steam pop.," Circulation, **113**(1), pp. 11–9.

[126] Goff R., Bersie S., and Iaizzo P., 2014, "In Vitro Assessment of Induced Phrenic Nerve Cryothermal Injury.," Hear. Rhythm, **11**(10), pp. 1779–1784.

[127] Choi J., and Bischof J. C., 2010, "Review of biomaterial thermal property measurements in the cryogenic regime and their use for prediction of equilibrium and non-equilibrium freezing applications in cryobiology.," Cryobiology, **60**(1), pp. 52–70.

[128] Choi J., 2013, "Thermal Processing of Biological Tissue at High Temperatures: Impact of Protein Denaturation and Water Loss on the Thermal Properties of Human and Porcine Liver in the Range 25–80 °C," J. Heat Transfer, **135**(6), p. 061302.

[129] Stella J., and Sacks M., 2007, "On the biaxial mechanical properties of the layers of the aortic valve leaflet.," J. Biomech. Eng., **129**(5), pp. 757–66.

[130] Sacks M. S., Schoen F. J., and Mayer J. E., 2009, "Bioengineering challenges for heart valve tissue engineering.," Annu. Rev. Biomed. Eng., **11**(1), pp. 289–313.

[131] Nordsletten D. a, Niederer S. a, Nash M. P., Hunter P. J., and Smith N. P., 2011, "Coupling multi-physics models to cardiac mechanics.," Prog. Biophys. Mol. Biol., **104**(1-3), pp. 77–88.

[132] Lally C., Reid a J., and Prendergast P. J., 2004, "Elastic behavior of porcine coronary artery tissue under uniaxial and equibiaxial tension.," Ann. Biomed. Eng., **32**(10), pp. 1355–64.

[133] Evonich R. F., Nori D. M., and Haines D. E., 2007, "A randomized trial comparing effects of radiofrequency and cryoablation on the structural integrity of esophageal tissue.," J. Interv. Card. Electrophysiol., **19**(2), pp. 77–83.

[134] Gorisch W., and Boergen K. P., 1982, "Heat-induced contraction of blood vessels.," Lasers Surg. Med., **2**(1), pp. 1–13.

[135] Chen S. S., and Humphrey J. D., 1998, "Heat-induced changes in the mechanics of a collagenous tissue: pseudoelastic behavior at 37 degrees C.," J. Biomech., **31**(3), pp. 211–6.

[136] Vangsness C. J., and Mitchell W. I., 1997, "Collagen shortening: An experimental approach with heat," Clin Orthop Rel Res, **337**, pp. 267–271.

[137] Kang T., Resar J., and Humphrey J. D., 1995, "Heat-induced changes in the mechanical behavior of passive coronary arteries.," J. Biomech. Eng., **117**(1), pp. 86–93.

[138] Millington-Sanders C., Meir A., Lawrence L., and Stolinski C., 2014, "Structure of chordae tendineae in the left ventricle of the human heart," J. Anat., **192**(May 1998), pp. 573–581.

[139] Saad E. B., Rossillo A., Saad C. P., Martin D. O., Bhargava M., Erciyes D., Bash D., Williams-Andrews M., Beheiry S., Marrouche N. F., Adams J., Pisanò E., Fanelli R., Potenza D., Raviele A., Bonso A., Themistoclakis S., Brachmann J., Saliba W. I., Schweikert R. a, and Natale A., 2003, "Pulmonary vein stenosis after radiofrequency ablation of atrial fibrillation: functional characterization, evolution, and influence of the ablation strategy.," Circulation, **108**(25), pp. 3102–7.

[140] Arentz T., 2003, "Incidence of pulmonary vein stenosis 2 years after radiofrequency catheter ablation of refractory atrial fibrillation," Eur. Heart J., **24**(10), pp. 963–969.

[141] Langendorff O., 1895, "Untersuchungen am überlebenden säugethierherzen," Eur. J. Physiol., **61**(6), pp. 291–332.

[142] Hill A. J., Laske T. G., Coles J. A. J., Sigg D. C., Skadsberg N. D., Vincent S. A., Soule C. L., Gallagher W. J., and Iaizzo P. a, 2005, "In vitro studies of human hearts.," Ann. Thorac. Surg., **79**(1), pp. 168–77.

[143] Sigg D. C., and Iaizzo P. a., 2006, "In vivo versus in vitro comparison of swine cardiac performance: Induction of cardiodepression with halothane," Eur. J. Pharmacol., **543**(1-3), pp. 97–107.

[144] Baker L. C., London B., Choi B. R., Koren G., and Salama G., 2000, "Enhanced dispersion of repolarization and refractoriness in transgenic mouse hearts promotes reentrant ventricular tachycardia.," Circ. Res., **86**(4), pp. 396–407.

[145] Efimov I. R., Nikolski V. P., and Salama G., 2004, "Optical imaging of the heart," Circ. Res., **95**(1), pp. 21–33.

[146] Hill A. J., and Iaizzo P. A., 2009, "Handbook of Cardiac Anatomy, Physiology, and Devices," Handb. Card. Anatomy, Physiol. Devices.

[147] Bateman M. G., and Iaizzo P. a., 2011, "Comparative imaging of cardiac structures and function for the optimization of transcatheter approaches for valvular and structural heart disease," Int. J. Cardiovasc. Imaging, **27**(8), pp. 1223–1234.

[148] Eggum J. H., Howard S. a., Goff R. P., and Iaizzo P. a., 2012, "Imaging of a coronary artery stent implantation within an isolated human heart," J. Cardiovasc. Transl. Res., **5**(1), pp. 73–74.

[149] Bandschapp O., Goff R., Mallin G., Loushin M., and Iaizzo P. a., 2012, "The path of a pulmonary artery catheter visualized through a beating human heart," Am. J. Respir. Crit. Care Med., **186**(4), p. 385.

[150] Inokawa H., Sevala M., Funkhouser W. K., and Egan T. M., 2006, "Ex-Vivo Perfusion and Ventilation of Rat Lungs From Non-Heart-Beating Donors Before Transplant," Ann. Thorac. Surg., **82**(4), pp. 1219–1225.

[151] Knowlton F. P., and Starling E. H., 1912, "The influence of variations in temperature and blood-pressure on the performance of the isolated mammalian heart.," J. Physiol., **44**(3), pp. 206–219.

[152] Martin H. N., 1883, "The Direct Influence of Gradual Variations of Temperature upon the Rate of Beat of the Dog's Heart," Philos. Trans. R. Soc. London, **174**, pp. 663–688.

[153] Martin H. N., 1881, “A new method of studying the mammalian heart,” Studies from the Biological Laboratory, J. Murphy & Company, Baltimore, MD, pp. 119–130.

[154] Chinchoy E., Soule C. L., Houlton A. J., Gallagher W. J., Hjelle M. A., Laske T. G., Morissette J., and Iaizzo P. A., 2000, “Isolated four-chamber working swine heart model,” Ann. Thorac. Surg., **70**(5), pp. 1607–1614.

[155] Anderson S. E., Skadsberg N. D., Laske T. G., Benditt D. G., and Iaizzo P. a., 2007, “Variation in pacing impedance: Impact of implant site and measurement method,” PACE - Pacing Clin. Electrophysiol., **30**(9), pp. 1076–1082.

[156] Quill J. L., Laske T. G., Hill A. J., Bonhoeffer P., and Iaizzo P. a., 2007, “Direct visualization of a transcatheter pulmonary valve implantation within the visible heart: A glimpse into the future,” Circulation, **116**(22).

[157] Iaizzo P. A., Hill A. J., and Laske T. G., 2008, “Cardiac device testing enhanced by simultaneous imaging modalities: the Visible Heart, fluoroscopy and echocardiography.,” Expert Rev. Med. Devices, **5**(1), pp. 51–58.

[158] Eggen M., Bonner M., Sheldon T., Williams E., and Iaizzo P., 2013, “Implantation of a Leadless Pacemaker within Reanimated Human Hearts using Direct Visualization,” Heart Rhythm Society.

[159] Spencer J. H. J., Quill J. L. J., Bateman M. M. G., Eggen M. D. M., Howard S. A. S., Goff R. P. R., Howard B. T. B., Quallich S. G. S., and Iaizzo P. A., 2013, “The benefits of the Atlas of Human Cardiac Anatomy website for the design of cardiac devices,” Expert Rev. Med. Devices, **10**(6), pp. 729–734.

[160] Slater J. P., Lipsitz E. C., Chen J. M., Levin H. R., Oz M. C., Burkhoff D., C.Oz M., and Burkhoff D., 1995, “Use of explanted human hearts as a model for the study of cardiac pathophysiologic conditions,” J. Thorac. Cardiovasc. Surg., **110**(1), pp. 239–247.

[161] Kühne M., Suter Y., Altmann D., Ammann P., Schaer B., Osswald S., and Sticherling C., 2010, “Cryoballoon versus radiofrequency catheter ablation of paroxysmal atrial fibrillation: biomarkers of myocardial injury, recurrence rates, and pulmonary vein reconnection patterns.,” Hear. Rhythm, **7**(12), pp. 1770–6.

[162] Van Opstal J. M., Timmermans C., Blaauw Y., and Pison L., 2011, “Bronchial erosion and hemoptysis after pulmonary vein isolation by cryoballoon ablation,” Hear. Rhythm, **8**(9), p. 1459.

[163] Peyrol M., Sbragia P., Quatre A., Boccara G., Zerrouk Z., Yvorra S., Guenoun M., Lévy S., and Paganelli F., 2013, "Pulmonary vein isolation using a single size cryoballoon chosen according to transesophageal echocardiography information," Int. J. Cardiol., **168**(1), pp. 108–111.

[164] Andrade J. G., Dubuc M., Guerra P. G., Landry E., Coulombe N., Leduc H., Rivard L., MacLe L., Thibault B., Talajic M., Roy D., and Khairy P., 2013, "Pulmonary vein isolation using a second-generation cryoballoon catheter: A randomized comparison of ablation duration and method of deflation," J. Cardiovasc. Electrophysiol., **24**(6), pp. 692–698.

[165] Robicsek F., Duncan G. D., Hawes A. C., Rice H. E., Harrill S., and Robicsek S. A., 1990, "Biological thresholds of cold-induced phrenic nerve injury.," J. Thorac. Cardiovasc. Surg., **99**(1), pp. 167–170.

[166] Dureuil B., Viirès N., Pariente R., Desmonts J. M., and Aubier M., 1987, "Effects of phrenic nerve cooling on diaphragmatic function.," J. Appl. Physiol., **63**(5), pp. 1763–1769.

[167] Kühne M., Knecht S., Altmann D., Kawel N., Ammann P., Schaer B., Osswald S., and Sticherling C., 2013, "Phrenic nerve palsy during ablation of atrial fibrillation using a 28-mm cryoballoon catheter: Predictors and prevention," J. Interv. Card. Electrophysiol., **36**(1), pp. 47–54.

[168] Canpolat U., Aytemir K., Hizal M., Hazirolan T., Yorgun H., Şahiner L., Kaya E. B., and Oto A., 2014, "Imaging before cryoablation of atrial fibrillation: Is phrenic nerve palsy predictable?," Europace, **16**(4), pp. 505–510.

Appendices

Appendix A: Published Conference Abstracts

Listed in chronological order beginning with most recent.

Changes in Cardiac Tissue Properties Relative to the Applications of Radiofrequency or Cryo Ablative Therapies

Selected for poster presentation at Biomedical Engineering Society 2015, San Antonio, TX.

Stephen G. Quallich; Kevin K. Kriege; Paul A. Iaizzo

Introduction: The biomechanical characterization of the myocardial structures within the heart is currently underway. For instance, interest in tissue engineered heart valves has led to the study of valve properties to better mimic their inherent properties/behaviors. Yet, there remains a lack of research investigating the biomechanical changes associated with cardiac ablations. Further, an array of associated complications including cardiac tamponade, pulmonary vein stenosis, and atrial-esophageal fistula may result from induced changes in tissue properties during such procedures. Thus, a greater understanding of how and why these transformations occur should ultimately lead to reductions in complications relative to these cardiac treatments.

Materials and Methods: Fresh atrial and pulmonary vein tissue samples were obtained from Yorkshire Cross swine (n=43) were carefully dissected. Additionally, one human tissue specimen was also acquired with donor consent. These biopsies were subsequently prepared into a dog-bone shape samples (n=285), sutures were tied to each end, and then a therapy applied. Prior to uniaxial pulling until failure, samples were randomized to the following study groups: 1) no treatment, 2) radiofrequency (RF) ablation for 1 minute at 30 W, or 3) focal cryoablation for 2 minutes.

Results and Discussion: The ultimate tensile strengths were significantly different between applied locations and/or study groups ($p<0.01$). RF ablations decreased subsequent tensile strengths and strains at failure, while cryoablation had minimal or no effects compared to the control (Table 1). Determined Young's moduli were also reduced by RF ablation; however it was noted that this effect was not statistically significant ($p=0.15$). Additionally, RF ablation caused specimens to failure at lower strains compared to the no treatment group. Furthermore, the ultimate tensile strengths, strain at failures, and Young's moduli were significantly different depending on the tissue type ($p<0.01$). In addition, similar trends in biomechanical properties were observed with the human tissue regarding ablative therapies.

	Treatment	Ultimate Tensile Strength (g/mm^2)	Strain at Failure (%)	Young's Modulus (kPa)
Left Atrium	**None**	106±16	117±8	18±2
	RF	65±6	90±7	15±2
	Cryo	85±9	85±4	21±2
Right Atrium	**None**	70±6	87±6	15±1
	RF	55±7	69±6	14±1
	Cryo	64±5	84±5	15±1
Pulmonary Vein (Axial)	**None**	167±16	153±11	31±4
	RF	111±12	128±12	21±3
	Cryo	144±9	147±13	27±3

Table 1. The ultimate tensile strength, strain at failure, and Young's modulus are listed by ablation and tissue type. Values are presented as mean±standard error.

Conclusions: This is one of the first studies that we are aware of that was performed to examine the effects of ablation modalities on the biomechanical properties of cardiac tissue. Noteworthy, cryoablations elicited negligible effects on the biomechanical properties of cardiac tissues, whereas RF ablations caused reduced ultimate tensile strengths, strains at failure, and Young's moduli. Biomechanical property alterations following cardiac ablation were not previously well documented; this data will likely be particularly useful to scientists, engineers, and physicians in minimizing the related complications incurred during ablation procedures.

Assessing Iatrogenic Atrial Septal Defect Formation with Novel Transseptal Puncture Device

Selected for poster presentation at American College of Cardiology 2015, Washington, DC.

Stephen G. Quallich; Mark A. Benscoter; Megan M. Schmidt;
Lars M. Mattison; Salah J. El Haddi; Paul A. Iaizzo

Introduction: As ablation and transseptal procedures become more common due to the aging population, transseptal puncture complications become a larger concern. Iatrogenic atrial septal defects (IASDs) are typically considered to close within a year with 7% remaining at 12 months following a puncture with a 12 Fr catheter. IASDs are also attracting attention because cryoablation and MitraClip® procedures that use larger sheaths are common. The purpose of this experimental paradigm was to characterize the biomechanical properties of the fossa ovalis in an animal model commonly used for testing these procedures.

Methods: The atrial septa from Yorkshire Cross swine (n=86) were excised for experimentation. The inferior edge of the fossa ovalis was cut off for catheter tear testing. Samples were randomized to 3 groups, and the transseptal puncture was performed with a: 1) standard Brockenbrough needle, 2) Baylis RF needle, or 3) custom RF 5 Fr needle, which is unique to this study. Catheter tear testing allowed the investigation of the effects varying catheter sizes and different transseptal approaches have on inducing trauma.

Results: The type of needle used for the transseptal puncture had no statistically significant effect on tear force ($p>0.05$). This suggests that on an acute time scale how a clinician crosses the septum is one of personal preference, since no technology demonstrated an increase in tear force and thus a reduction in IASD formation.

Additionally, there were significant differences in tearing the septum between different size sheaths ($p<0.05$). Noteworthy, the forces required to initiate tearing in this study were within the range of the forces able to be generated by clinically used catheter and sheaths.

Conclusions: Tissue properties and their role in the formation of IASDs were not previously well studied. This suggests a need to improve the understanding in how septa tearing arise and a means to minimize damage created during procedures. This is the first study to investigate a novel transseptal approach in an effort to minimize IASD formation.

High-speed Visualization of Steam Pops During Radiofrequency Ablation

Selected for oral and poster presentation at Design of Medical Devices 2014, Minneapolis, MN.

Stephen G. Quallich; Ryan P. Goff; Paul A. Iaizzo

Background: Atrial fibrillation (AF) affects up to 5 million people in the United States, and as the population continues to age, the incidence is expected to further increase. The overall cost associated with treatment for AF was estimated to be in excess of $6.5 billion dollars annually [1]. Currently, radiofrequency (RF) ablation is routinely used for the treatment of cardiac arrhythmias. In RF ablation alternating current is applied to heat the myocardial tissues, inducing temperatures of 50°C or higher that lead to the creation of a myocardial scar which is hopefully therapeutic [2].

However, when excessive and/or rapid tissue heating occurs, at temperatures of greater than 50°C, cellular content may be vaporized and in some cases an audible steam pop heard. Although temperatures measured at the electrode tip may be considerably less than 50°C, steam pop generation can result from high endocardial tissue temperatures. Importantly, it should be considered that temperatures recorded from the catheter tip may

not be indicative of the tissue temperatures because convective flow of blood or irrigation cools the electrode tip. Nevertheless, these induced steam pops can be quite damaging; potentially causing perforations of the atrial wall, clot formations on the catheter which could dislodge and form emboli, and/or air bubble generation [3].

Methods: To visualize the generation of steam pops, porcine Yorkshire Cross animals (n=14) with weights of 84.5±9.8 kg were reanimated using Visible Heart® methodologies previously described by Chinchoy and colleagues [4]. The tricuspid annuli of these reanimated hearts was aggressively ablated using a 7 Fr Marinr® catheter (Medtronic, Inc., MN) introduced through the superior vena cava and guided via fluoroscopic imaging. The incidences of steam pops were then recorded using a high-speed camera (666 frames/second) and videoscopes from within these hearts.

Results: The occurrence of a steam pop causes the ablation catheter to jump away from the lesion site: i.e. due to the explosive generation of gas bubbles (Fig. 1). Interestingly, the typical duration of the pops was less than 10 milliseconds, although in the case shown in Fig. 1, air bubbles were observed to linger for a longer period of time around the lesion site. In this case, the catheter tip temperature reached 76°C before the explosion, and dropped significantly after because of the lack of wall contact: the void created during the explosion was approximately 0.7 cm in diameter and 0.4 cm deep (Fig. 2).

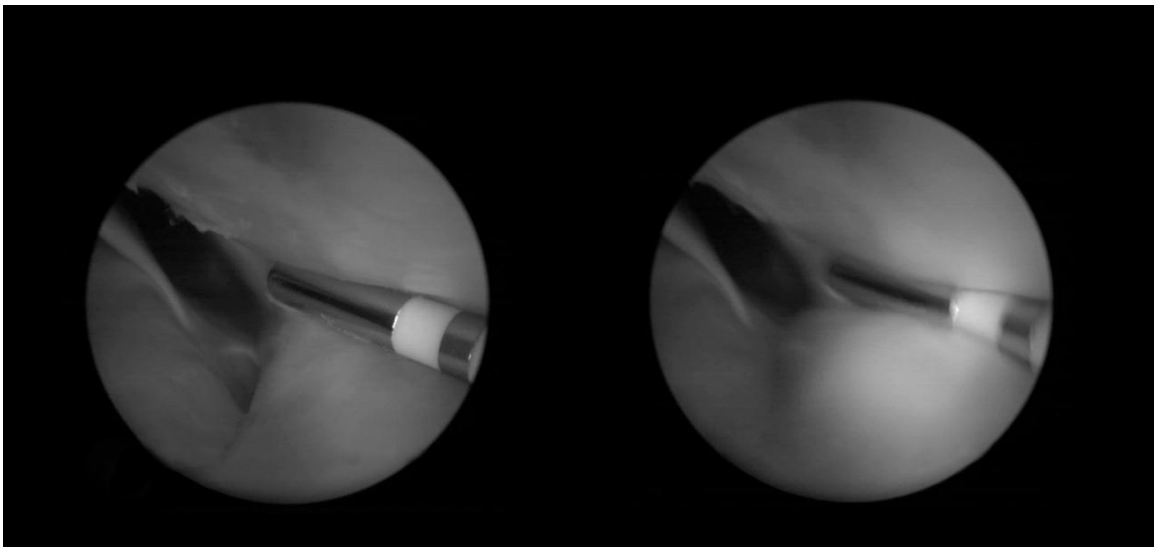

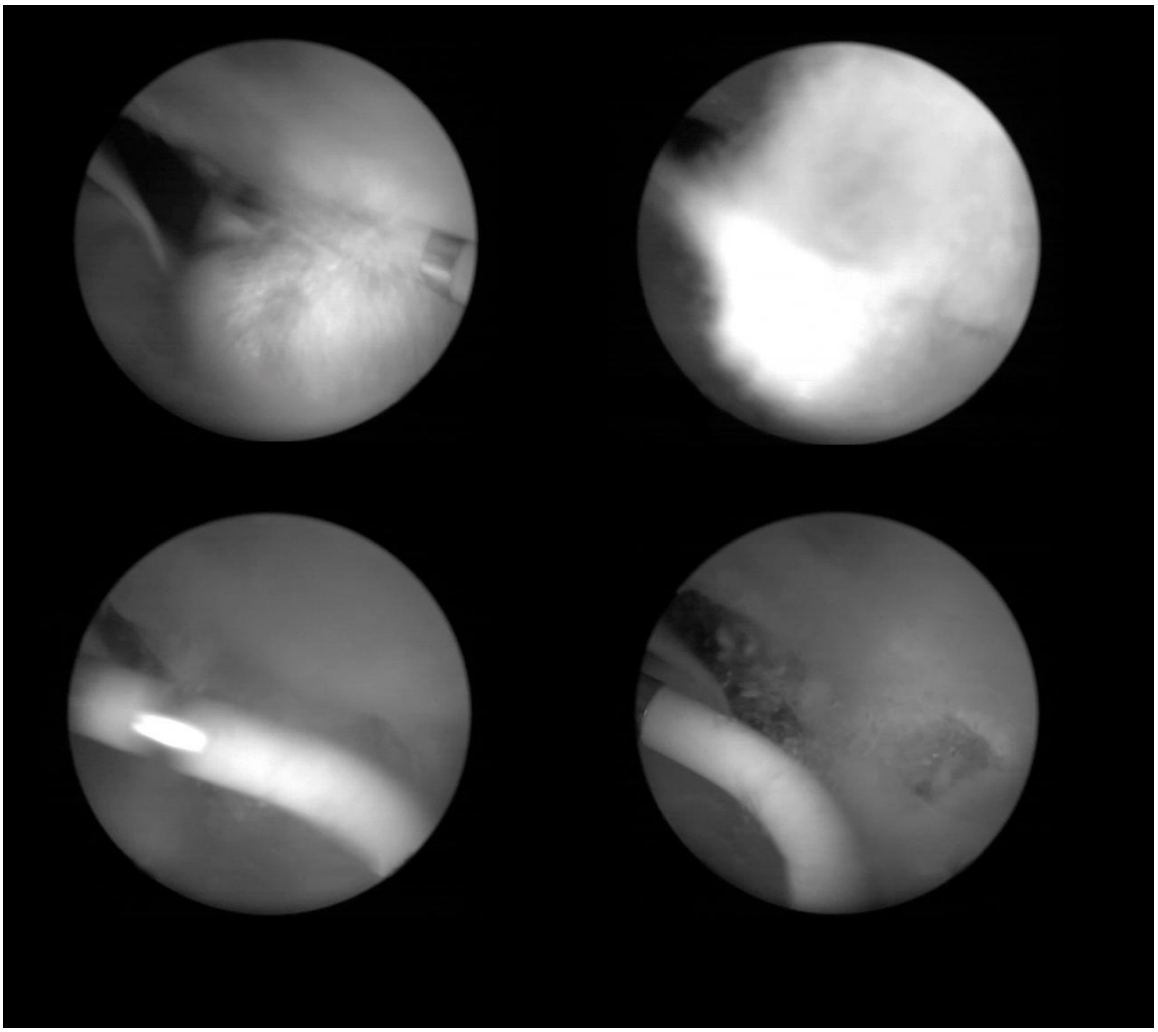

Figure 1. Frames every 1.5 ms of generated steam pop recorded with a high-speed camera as seen from within the right atrium. The explosive force produced during this event can be observed.

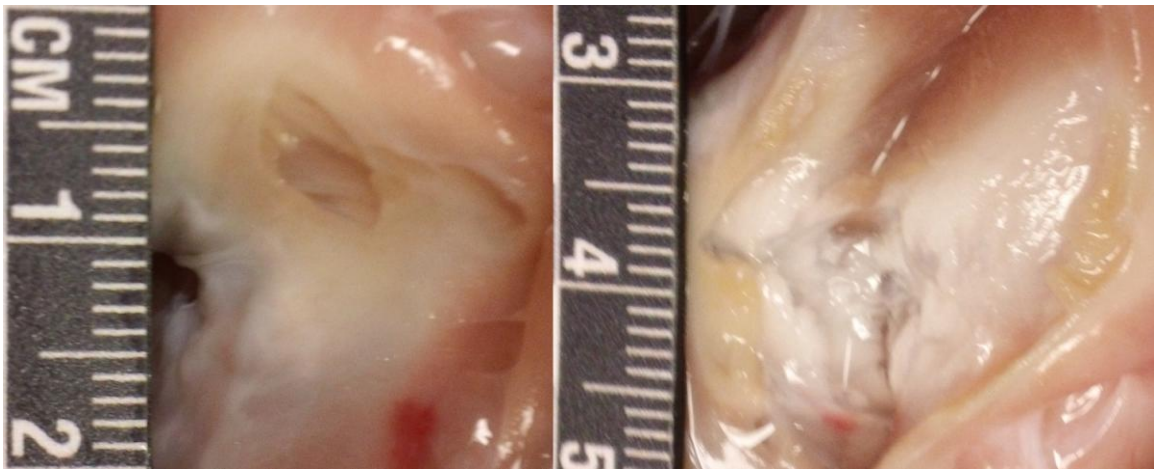

Figure 2. Photograph of post-study endocardial damage from steam pop (left) and cross-sectional view of myocardial damage (right).

In this series of studies, the relative occurrences of steam pops was 5% at energies of 40-50 W (n=59), 25% at energies of 50-60 W (n=73), and 26% at energies of 60-100 W (n=69) with average catheter tip temperatures of 52°C, 64°C, and 65°C respectively. Additionally, steam pops happened 63% of the time when power rapidly increased, at a rate of 3 W per second, from 40 W to 100 W (n=38). Applied power significantly affected steam pop generation ($p<0.01$). Steam pops occurred 33.3±17.2 seconds after the start of the ablation without any significant differences between power settings ($p>0.05$).

Interpretation:

AF is a serious health concern that affects a large number of individuals. The decrease in quality of life and cost associated with the disease are also a significant issue. One of the treatment options, RF ablation, can be accompanied by a relative risk of steam pop occurrences that can in turn cause severe damages to the myocardium. Noteworthy, there is the possibility for complete atrial rupture, which would then lead to cardiac tamponade. Additionally, released gas bubbles and tissue emboli created during the elicitation of such an event may critically lead to myocardial infarction and/or stroke if this occurs on the left side of the heart or pulmonary emboli on the right side. High-speed video was used to visualize the steam pop explosion at a visually perceptible rate.

It is important to note, that using fluoroscopy alone as an imaging modality, it is likely difficult for operators to detect the occurrences of steam pops. In other words, the only indications of these events being perhaps the visual displacement of the catheter if fluoroscopy is running at the time of the pop and/or a detected rapid reduction in tip temperatures (Fig. 3). Interestingly, the explosions are not always audible suggesting that operators may have difficulty recognizing the incidence of steam pops while using fluoroscopy alone [5]. We have shown here one example of high-speed footage of a steam pop and the resulting myocardial damage created: i.e., visualized *in vitro* using Visible Heart® methodologies. This is the first documented instance to the authors' knowledge, of visualization within a beating heart using a videoscope or high-speed camera.

We consider here, that this study highlights the difficulty physicians may encounter in recognizing steam pop incidences. In other words, these events may be occurring unnoticed: until the related complications arise. For this reason, developing a database of parameters effecting steam pop formation and a system for steam pop detection requires investigation and is underway by our laboratory. With the increasing prevalence of AF, understanding how to reduce the occurrences of steam pops may have important clinical insights.

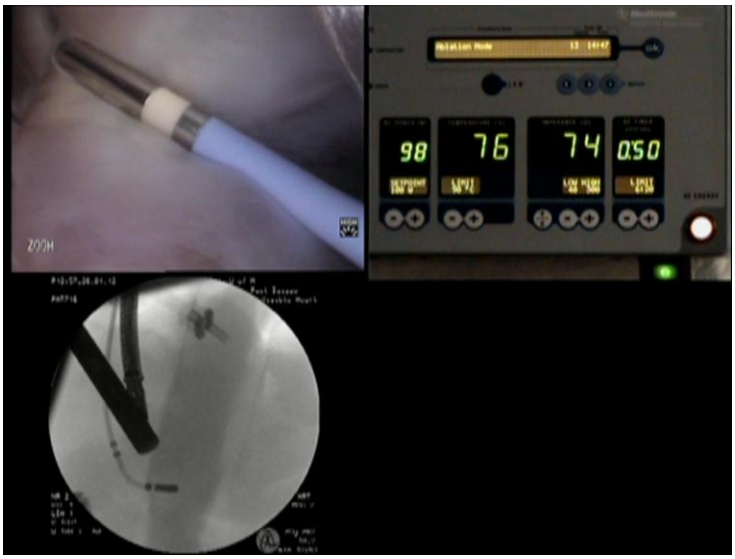

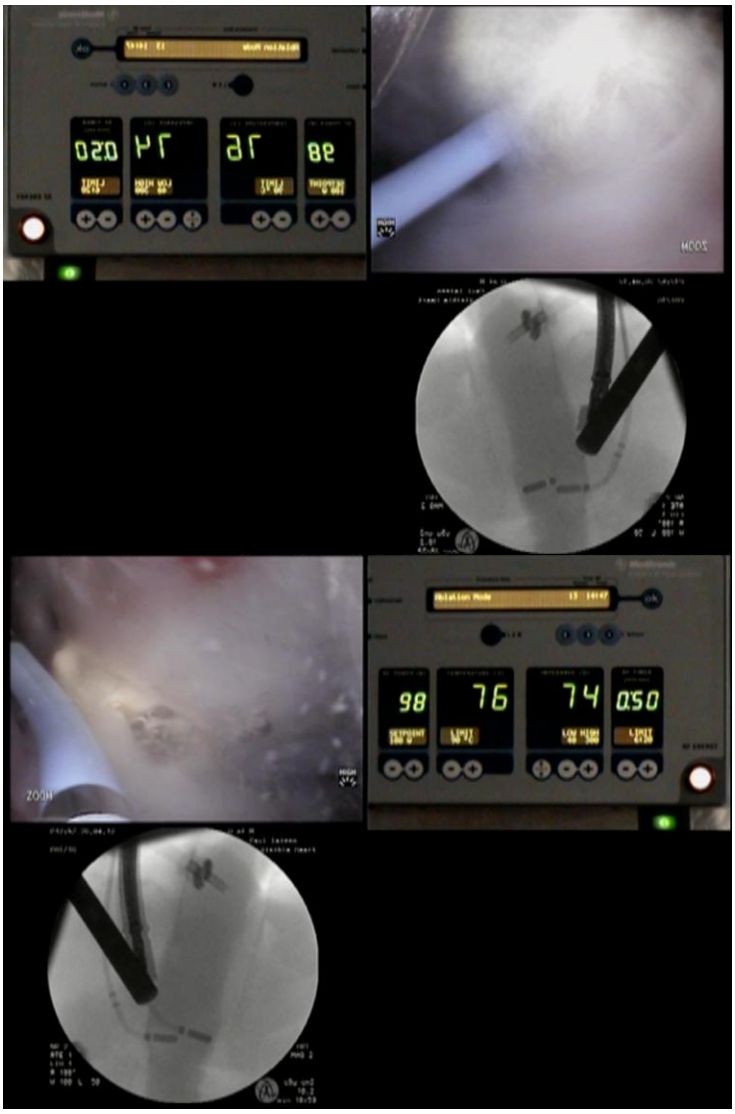

Figure 3. Frames every 17 ms of a generated steam pop from videoscope within the right atrium (top left), ablation console (top right), and fluoroscopy (bottom left). The movement artifact of the catheter is visible on fluoroscopy in this particular steam pop.

References:

[1] K. S. Coyne, C. Paramore, S. Grandy, M. Mercader, M. Reynolds, and P. Zimetbaum, "Assessing the direct costs of treating nonvalvular atrial fibrillation in the United States.," *Value Health*, vol. 9, no. 5, pp. 348–56, 2006.

[2] D. E. Haines, "The biophysics of radiofrequency catheter ablation in the heart: the importance of temperature monitoring.," *Pacing Clin. Electrophysiol.*, vol. 16, no. 3 Pt 2,

pp. 586–91, Mar. 1993.

[3] R. Juneja and P. O'Callaghan, "Tissue rupture and bubble formation during radiofrequency catheter ablation: 'Echoes of a Pop'," *Circulation*, vol. 103, pp. 1333–1334, 2001. [4] E. Chinchoy, C. L. Soule, a J. Houlton, W. J. Gallagher, M. a Hjelle, T. G. Laske, J. Morissette, and P. a Iaizzo, "Isolated four-chamber working swine heart model.," *Ann. Thorac. Surg.*, vol. 70, no. 5, pp. 1607–14, Nov. 2000.

[5] J. M. Cooper, J. L. Sapp, U. Tedrow, C. P. Pellegrini, D. Robinson, L. M. Epstein, and W. G. Stevenson, "Ablation with an internally irrigated radiofrequency catheter: learning how to avoid steam pops.," *Heart Rhythm*, vol. 1, no. 3, pp. 329–33, Sep. 2004.

Analyzing the Perforation Force of Swine and Human Atria Before, During and Following Cardiac Ablation

Selected for poster presentation at American College of Cardiology 2014, Washington, DC.

Stephen G. Quallich; Paul A. Iaizzo

Introduction: Clinical perforation of the atrial wall may lead to pericardial effusions and/or life-threatening cardiac tamponade. It is suggested that such may result from high contact forces to ensure the creation of transmural lesions. It has been reported that cardiac tamponade occurs in 1.3% of ablation procedures. It should be noted that patients with atrial fibrillation (AF) have thinner atrial walls; this likely creates circumstances for perforation to happen more readily. Therefore, better understanding the required contact forces for proper lesion formation while minimizing rupture may lead to the reduced occurrences of cardiac tamponade.

Methods: Fresh atrial samples from Yorkshire Cross swine (n=72) and humans (n=4) were carefully dissected out. Atrial samples (n=448) were randomized to the following study groups: 1) no treatment, 2) Radiofrequency (RF) ablation for 1 min at 30 W with a temperature limit of 65°C, 3) RF ablation perforating during the last 5 seconds of

ablation, or 4) focal cryoablation for 2 minutes. All samples were carefully anchored, then therapy applied, and an ablation catheter was advanced at a rate of 500 mm/min until perforation occurred.

Results: Catheter perforation forces for the left atrium (344±86 g) and right atrium (275±95 g) were significantly different for all groups ($p<0.01$). There was a significant difference in perforation force between species ($p<0.01$). Importantly, the RF ablation groups required significantly lower forces to induce perforations than the control group ($p<0.01$). Catheter size had a significant affect on perforation force ($p<0.05$).

Conclusions: Understanding the factors that may lead to atrial perforations is essential, since cardiac tamponade remains a potential complication of ablation procedures. This is the first translational study to specifically investigate relative atrial perforation forces with a variety of catheter sizes during and after the application of RF. This acquired data should be particularly useful for clinicians, engineers, and scientists to reduce the occurrence of cardiac tamponade during AF ablations, while yet ensuring the elicitation of transmural lesions.

Acute Pulmonary Vein Stenosis During and Following Ablations

Selected for oral presentation at European Cardiac Arrhythmia Society 2014, Munich, Germany.

Stephen G. Quallich; Paul A. Iaizzo

Background: Atrial fibrillation affects over 5 million Americans, and the incidence of this disease is expected to increase further as the population ages. Pulmonary vein (PV) stenosis following cardiac ablation procedures is a potentially life threatening condition. Up to 28% of patients are affected by severe PV stenosis and/or occlusion 2 years after radiofrequency (RF) ablation. It has been suggested that cryoablation is less likely to

cause pulmonary vein stenosis when compared to RF ablation. Numerous studies have examined stenosis in chronic settings, but the development of stenosis on an acute time scale lacks investigation.

Methods: Fresh pulmonary vein samples from Yorkshire Cross swine (n=22), animal weight 75-110 kg, were carefully dissected out. A human tissue specimen (n=2) was also acquired with donor consent. 4 sutures were attached to each side of the pulmonary vein sample, and they were mounted in a biaxial testing machine. Each specimen was run as its own control prior to treatment. Samples were preconditioned, stretched to 20% strain, a randomized ablation modality (RF, cryo, or no treatment) was applied, and the resulting stress was examined for up to 12 minutes.

Results: The forces in the axial and circumferential direction were significantly different between the treatment groups ($p<0.05$). Additionally, there were force differences between ostial PV tissue and PV tissue 1 cm distal to the ostia. The RF and cryoablation axial and circumferential forces compared to the no treatment group were significantly higher following ablations. This suggests that on an acute time scale these ablation modalities caused shrinkage or contraction of the tissue as seen by the increased force measurements.

Conclusion: Optimization of ablation parameters can minimize detrimental biomechanical changes, which may lead to PV stenosis. This is the first study to the authors' knowledge to report real-time force measurements during PV ablation, identify location dependent biomechanical differences, and investigate the developmental factors of PV stenosis on an acute time scale. Preliminary results suggest that RF and cryoablation are related to PV shrinkage acutely.

Assessing the Biomechanical Properties of the Porcine Fossa Ovalis

Selected for poster presentation at European Cardiac Arrhythmia Society 2014, Munich, Germany.

Stephen G. Quallich; Bryce C. Holmgren;
Stephen A. Howard; Paul A. Iaizzo

Introduction: As ablation and transseptal procedures become more common due to the aging population, transseptal puncture complications become a larger concern. Iatrogenic atrial septal defects (IASDs) are typically considered to close within a year with 7% remaining at 12 months following a puncture with a 12 Fr catheter. IASDs are also attracting attention because cryoablation and MitraClip® procedures that use larger sheaths are common. The purpose of this study was to characterize the biomechanical properties of the fossa ovalis (FO) in an animal model commonly used for testing these procedures.

Methods: The atrial septa from Yorkshire Cross swine (n=86) were excised for experimentation. Each fossa ovalis (FO) was dissected into several dog-bone shape tissue bundles for uniaxial testing (n=41), or the posterior or inferior edge of the FO was cut off for tear testing (n=70). Uniaxial testing was performed to assess the directional biomechanical properties of the FO samples. Tear testing allowed us to examine the effects of directionality and/or catheter sizes on inducing trauma.

Results: It was observed that the biomechanical properties of swine FO were dependent on directionality; stress, strain, and tearing force were significantly affected by orientation ($p<0.05$) requiring higher forces in the anterior - posterior orientations compared to that of superior - inferior. Catheter size also significantly correlated with the average and peak tearing forces of these FOs ($p<0.05$); larger catheters required greater forces to tear the FO. The measured forces required to create IASDs in this experimental paradigm were similar to the forces previously noted to generate such by catheter and sheaths employed clinically.

Conclusion: The tissue properties of the porcine FO were not previously well documented; improving the overall understanding of biomechanical properties and tearing forces is essential for expanding scientists, engineers, and physicians' view of the elicitation of IASDs. The biomechanical properties of the porcine FO exhibit a dependence on orientation. Provided here are our laboratories initial finding as to the characterization of the tissue properties of the swine FO: additional studies are ongoing.

External Infrared Visualization of an Endocardial Cryoablation: Performed on a Reanimated Swine Heart

Selected for oral presentation at the 2013 International Mechanical Engineering Conference and Expo, Houston, TX.

Ryan P. Goff; Stephen G. Quallich; Paul A. Iaizzo

Today, clinical electrophysiologists still considered cryoablation a relatively new treatment modality for cardiac arrhythmias. Interestingly, the bioheat transfer in this environment has been largely unstudied. Furthermore, during the clinical applications of cyrotherapy, adjacent tissues may become injured from the induced cooling. These facts, along with the desire to validate models of cryotherapy, to potentially increase efficacy and safety, warrants the study in reanimated large mammalian hearts where visualization of heat transfer is feasible. Specifically, cryoballoon catheters (ArticFront, Medtronic Inc.) were positioned in the superior vena cava and the clinically recommended ablation duration of four minutes was applied. Similarly, focal cryo-catheters (FreezorMax, Medtronic Inc.) were placed in the right atrial appendages and spot ablations were performed for four minutes. We believe that this novel model allows for both high spatial and temporal resolutions for the study of these treatments. More specifically, multi-modal imaging can be performed, with: intracardiac videoscopes, externally with IR and video cameras, with fluoroscopy and/or echocardiography and all while hemodynamic

monitoring of the heart (Fig. 1). Time from beginning of ablation is displayed in the top left corner and temperature scale to the right.

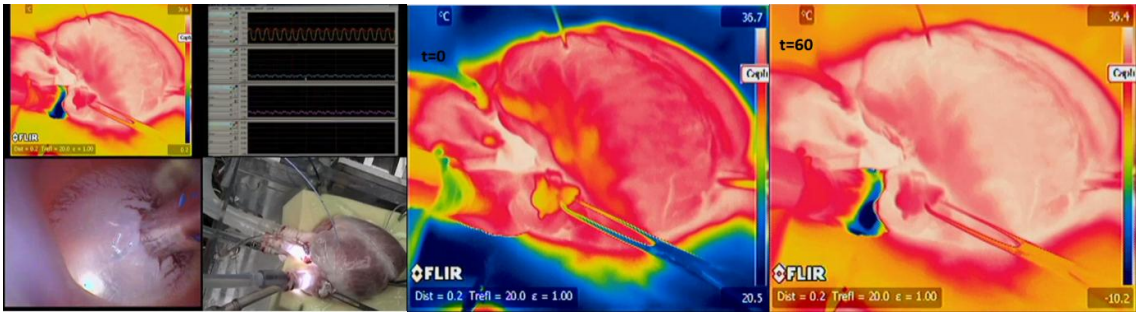

Figure 1: Quad-split of simultaneous video. Cryoballoon ablation

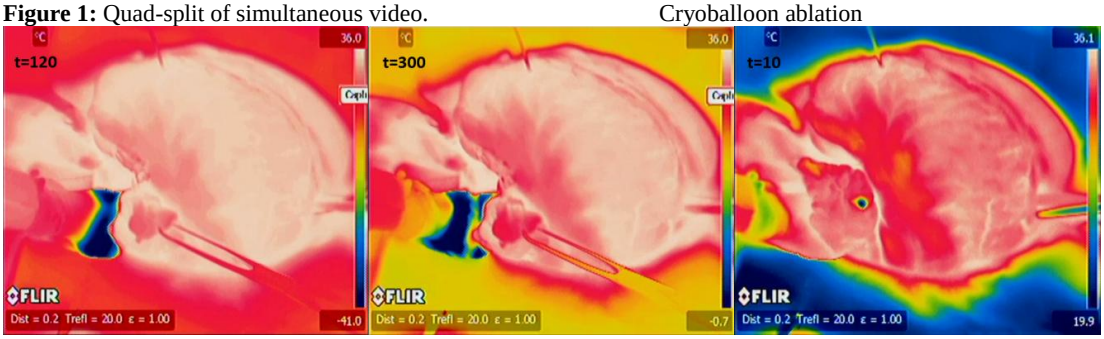

Cryoballoon ablation Focal ablation

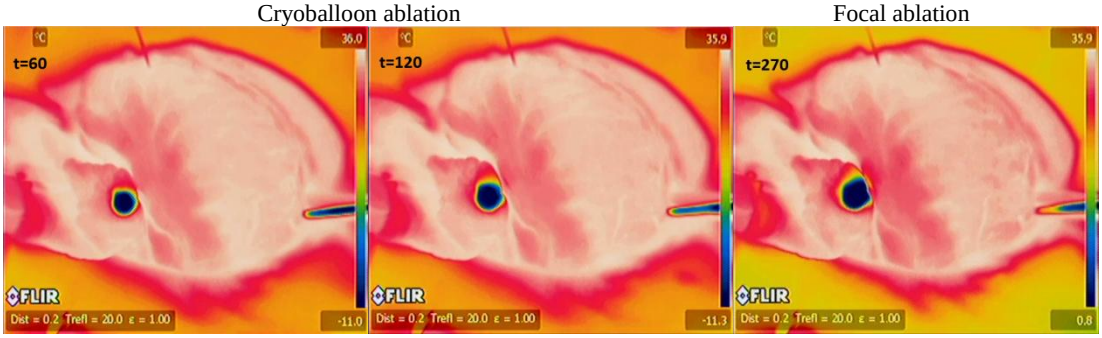

Focal ablation

In-Vitro Characterization of Myocardial Cryothermal Injury

Selected for oral presentation a Cryobiology 2013, Washington, DC.

Ryan P. Goff; Stephen G. Quallich; Robert A. Buechler;
Jeunghwan Choi; John C. Bischof; Paul A. Iaizzo

Background: Cardiac balloon and catheter cryoablations for the treatment of atrial fibrillation have been gaining attention as approaches for treating arrhythmias, in

particular for isolation of the pulmonary veins (PV). Despite widespread clinical use of cardiac cryoablation, there are still questions regarding dosing and treatment time, which may affect both efficacy and collateral injury. To date injury thresholds for therapy of cardiac tissues are largely unreported in the literature.

Methods: Slices of ventricular myocardium (n=11) and left atrial tissue (n=6) from female Yorkshire Cross swine hearts were dissected including the native endocardial surface. Samples were placed in an infrared imaging apparatus consisting of a plastic petri dish with central ablation probe (1.5 mm IceSeed, Galil Medical, Arden Hills, MN) and 2 millimeters of Sylgard polymer formed to the bottom. The tissue slices were impaled on the central cryoprobe and infrared thermography was captured using a Flir A20 looking from the top down. Subsequently, samples were cultured for 24 hours in a cell culture incubator (myocardium) at 37°C or 4 hours at room temperature (PV) for optimal lesion identification with 1% TTC in Trizma buffer for 1 hour at 37°C. Photographs of the resultant TTC staining of each sample were captured and a custom Matlab program was used to normalize staining intensity and correlate the average staining intensity with the average thermal profile at any radial distance from the cryoprobe. The relationship between the staining intensity and end temperature was fit with a sigmoidal curve. Samples with a fit of greater than $R^2 > 0.99$ were analyzed. The transition from dead to injured tissue was defined as the point on the curve fit where the staining ratio was 10% of the range between the lower and upper asymptotes of the sigmoid (i.e., 10% of the grayscale value change at the lesion margin closest to the lesion). The maximum cooling rate correlated to this ratio and end temperature was then calculated from the thermal profiles. Eight thermal profiles at different radii were averaged to obtain a characteristic thermal profile for each sample. This approach has led to the creation of a database of thermal profiles that results in either completely or partially injured tissues.

Results: Initial results suggest that cooling rates of -103±49 and -72±9 °C/min and end temperatures of approximately -21±6 and -17.2±3.2 °C are necessary for complete

necrosis of ventricular and left atrial tissue, respectively. Using a two-tailed t-test assuming equal variance the difference in end temperature and cooling rate between ventricular and left atrial tissue were non-significant ($p=0.21$, $p=0.20$ respectively).

Conclusions: Experiments are ongoing to determine cryothermal injury thresholds of tissues associated with cardiac ablation, such as: lung and esophagus. The TTC staining protocol is in the process of being validated by comparison to H&E stain. Cellular viability assays are being performed to compare to these findings.

Acknowledgment/Funding: The author's sincerely thank Dr. Jim Coad for advising on staining protocols. This work was supported by the GAANN program, the Institute for Engineering in Medicine, and a contract with Medtronic, Inc.